# Local hydroelastic response of ship structures under impact loads from water (slamming)

Alexei Bereznitski

# Local hydroelastic response of ship structures under impact loads from water (slamming)

# Local hydroelastic response of ship structures under impact loads from water (slamming)

Proefschrift

ter verkrijging van de graad van doctor
aan de Technische Universiteit Delft,
op gezag van de Rector Magnificus prof.dr.ir. J.T. Fokkema,
voorzitter van het College voor Promoties,
in het openbaar te verdedigen

op maandag 24 maart 2003 te 10.30 uur

door

*Alexei BEREZNITSKI*

Master of Science in Mechanical Engineering, Saint-Petersburg
State Marine Technical University
geboren te Saint-Petersburg, Rusland

Dit proefschrift is goedgekeurd door de promotor(en):
Prof. dr. ir. J. Pinkster

*Samenstelling promotiecommissie:*

| | |
|---|---|
| Rector Magnificus, | voorzitter |
| Prof. dr. ir. J. A. Pinkster | Technische Universiteit Delft, promotor |
| Prof. dr. V. Postnov | Saint-Petersburg State Marine Technical University, Russia |
| Prof. dr. O. M. Faltinsen | Norwegian University of Science and Technology, Norway |
| Prof. ir. B. Boon | Technische Universiteit Delft |
| Prof. dr. A.J. Hermans | Technische Universiteit Delft |
| Dr. M. Kaminski | MARIN |
| Ir. G. Hommel | Technische Universiteit Delft |
| Prof. ir. J. Klein Woud | Technische Universiteit Delft |

ISBN 90-806734-2-0

Keywords: hydroelastic response, slamming, hydrodynamic loads



Printed in SIECA REPRO, Delft.

# Local hydroelastic response of ship structures under impact loads from water (slamming)

Thesis

presented for the degree of doctor
at Delft University of Technology,
under the authority of the Vice-Chancellor, Prof. dr.ir. J.T. Fokkema,
to be defended in public in the presence of a committee,
appointed by the Board for Doctorates

on Monday March 24, 2003 at 10.30 o'clock

by

*Alexei BEREZNITSKI*

Master of Science in Mechanical Engineering, Saint-Petersburg
State Marine Technical University
born in Saint-Petersburg, Russia

To my mother and my father

# SUMMARY


## Local hydroelastic response of ship structures under impact loads from water (slamming)

Accurate prediction of representative design loads and, hence, the structural response is the key factor in performing successful design of marine structures. In most cases these design loads can be determined separately from the structural analysis and then applied to the structure in order to find the structural response. However, in some cases these loads are dependent on the structural response. In that case hydroelastic interaction takes place.

The challenge of hydroelastic problems consists of combining two areas of science: hydromechanics and structural strength. In spite of the fact that hydroelasticity has become very popular in the last years and many researches pay a lot of attention to this subject the role of hydroelasticity is not well understood in the many practical problems. The question "Should hydroelasticity be considered or can it be neglected?" still exists in many areas of science where the fluid-structure interaction takes place.

The primary goal of this thesis is achievement of better understanding of the physics of hydroelasticity for slamming problem. Expansion of knowledge in this area will lead to better prediction of the hydrodynamic loads and the structural response. This will help to improve the ship design and to make sea transportation more safe and more economically attractive. The ability to design highly optimized structures will decrease the structural weight reducing the usage of materials. The speed and load carrying capacity of ship will be improved.

A number of numerical models are discussed in this thesis incorporating different approaches and theories. The effect of hydroelasticity is studied by considering various factors that influence the slamming problem. These factors are among others structural flexibility, entrapped air, speed of impact, and deadrise angle. In order to verify the conclusions based on numerical results, available experimental data were considered. Advanced numerical models were created to simulate these experiments. Good agreement between numerical prediction and available experimental data is found.

General conclusions are drawn with respect to those factors which make the effect of hydroelasticity important. Based on detailed analysis of all numerical results the author suggests a special parameter, which can indicate the importance of hydroelasticity in each particular case. This parameter is the ratio between the duration of slamming impact and the first period of natural vibration of a dry structure. The author recommends to use this parameter in ship design.

# SAMENVATTING

## Locaal hydro-elastisch gedrag van scheepsconstructies onder impact belastingen van water (slamming)

De nauwkeurige voorspelling van representatieve ontwerpbelastingen en, dus, de respons van de constructie is een belangrijke factor om maritieme constructies te ontwerpen. In de meeste gevallen kunnen deze ontwerpbelastingen onafhankelijk worden bepaald van de sterkte en dan op de constructie worden aangebracht om de respons van de constructie te vinden. Maar is sommige gevallen zijn deze belastingen afhankelijk van de respons van de constructie. In dat geval treedt hydro-elastische interactie op.

De uitdaging van hydro-elastische problemen bestaat uit het combineren van twee gebieden in de wetenschap: hydromechanica en sterkte van de constructie. Ondanks het feit dat er in de afgelopen jaren veel aandacht is besteed aan dit onderwerp wordt hydro-elasticiteit nog niet goed begrepen in veel praktische toepassingen. De vraag "Moet hydro-elasticiteit worden meegenomen of kan het worden verwaarloosd?" bestaat nog steeds in veel takken van de wetenschap waar vloeistof-constructie interactie plaatsvindt.

Het doel van deze dissertatie is het bereiken van een beter inzicht in de fysica van hydro-elasticiteit voor slamming probleem. Uitbreiding van kennis op dit gebied zal leiden tot een betere voorspelling van de hydrodynamische belastingen en respons van de constructie. Dit zal bijdragen om het scheepsontwerp te verbeteren en om transport over zee veiliger en economisch aantrekkelijker te maken. De mogelijkheid om geoptimaliseerde constructies te ontwerpen zal leiden tot afname van het constructiegewicht van het schip en daarmee het gebruik van materialen. De snelheid en de hoeveelheid lading zullen worden verbeterd.

Een aantal numerieke modellen waarin diverse benaderingen en theorieën worden gebruikt om hydro-elasticiteit te beschrijven worden besproken in deze dissertatie. Het effect van hydro-elasticiteit wordt bestudeerd door verschillende factoren te bekijken die slamming beïnvloeden. Deze factoren zijn, onder meer, flexibiliteit van de constructie, opgesloten lucht tussen water en de constructie, impactsnelheid en vlaktilling. Om de conclusies gebaseerd op numerieke simulaties te verifiëren is experimentele data gebruikt. Een goede overeenkomst tussen numerieke voorspellingen en beschikbare experimentele data is gevonden.

Algemene conclusies worden getrokken betreffende die factoren die een belangrijk effect hebben op hydro-elasticiteit. Gebaseerd op gedetailleerde analyse van alle numerieke resultaten stelt de auteur een speciale parameter voor, die het belang van hydro-elasticiteit in ieder specifiek geval kan weergeven. Deze parameter is de verhouding tussen de duur van de slammingsimpact en de eerste periode van de eigenfrequentie van de droge constructie. De auteur beveelt aan om deze parameter te gebruiken in het scheepsontwerp.

# CONTENTS

# LIST OF SYMBOLS

$\alpha$ - deadrise angle

$\alpha_1, \alpha_2, \ldots$ - coefficients of approximation function

$\varphi$ - velocity potential

$\varphi^*$ - velocity potential (fundamental solution)

$\gamma$ - ratio of specific heat

$\rho$ - density of water

$\rho_0$ - reference density of water

$\rho^{air}$ - density of air

$a_1$ - bulk modulus

$B$ - half width of the water tank

$\{B_w\}$ - global load vector in fluid analysis

$b$ - half width of the body

$c_0$ - speed of sound in water

$E$ - modulus of elasticity

$E_{kinetic}$ - kinetic energy

$E_{potential}$ - potential energy

$e$ - specific internal energy per unit mass

$F$ - hydrodynamic force

$F_{imp}$ - force of impulse

$[G]$ - global matrix for velocity potential in the boundary element method

$\hat{G}_{ij}$ - integrals for velocity potential in the boundary element method

$H$ - water depth

$[H]$ - global matrix for velocity in the boundary element method

$\hat{H}_{ij}$ - integrals for velocity in the boundary element method

$h$ - penetration into water

$I$ - principal moment of inertia of beam cross-section about the relevant centroidal axis

$I_{imp}$ - impulse

$[K_s]$ - global stiffness matrix in structural analysis

$[K_w]$ - global stiffness matrix in fluid analysis

$[k]$ - stiffness matrix of finite element

$k_{ij}$ - coefficients of element stiffness matrix

$l$ - length of 1D fluid finite element or beam element

$l_1, l_2$ - dimensions of 2D fluid finite element

$M$ - mass of body/structure (for 1D model – per unit area; for 2D model – per unit length)

$[M_s]$ - global mass matrix in structural analysis

$[M_w]$ - global mass matrix in fluid analysis

$[m]$ - mass matrix of finite element

$m_{ij}$ - coefficients of element mass matrix

$\overline{m}$ - beam mass per unit length

$N_1, N_2, \ldots$ - shape functions

$\{P_s\}$ - global load vector in structural analysis

$p$ - water pressure

$p_0$ - atmospheric pressure

$p^{air}$ - air pressure

$p_{cav}$ - cavitation pressure

$p_{mid}$ - pressure under the middle of the panel

$\{Q\}$ - global vector specifying velocity in the boundary element method

$\{Q_s\}$ - global vector of unknown values in structural analysis

$\{Q_w\}$ - global vector of unknown values in fluid analysis

$q_1, q_2, \ldots$ - unknown values, which have to be found

$\overline{q}$ - vector of unknown values

$t$ - time

$t_{end}$ - total time of simulation

$\Delta t$ - time increment

$\Delta t_{imp}$ - duration of impulse

$\{U\}$ - global vector specifying velocity potential in the boundary element method

$V$ - velocity

$V_0$ - initial velocity

$V_{ac}$ - speed of sound in water

$V_{\text{int}}$ - interface velocity

$V_{rb}$ - rigid body velocity

$V_{str}$ - velocity of structural vibration

$W$ - displacement

$W_{\max}$ - maximum displacement

$W_{hyd.}^{\max}$ - maximum displacement (hydroelastic solution)

$W_{no\,hyd.}^{\max}$ - maximum displacement (no hydroelasticity)

# LIST OF ABBREVIATIONS

| | |
|---|---|
| ISSC | - International Ship and Offshore Structures Congress |
| SSC | - Ship Structure Committee |
| TNO | - Netherlands Organization for Applied Scientific Research |
| MARIN | - Maritime Research Institute |
| PGS | - Petroleum Geo-Services (a technologically focused oilfield service company) |
| IACS | - International Association of Classification Societies |
| ISO | - International Organization for Standardization |
| MTVV | - Maximum Transient Vibration Value |
| FPSO | - Floating Production Storage and Offloading |
| FEM (FEA) | - Finite Element Method (Finite Element Analysis) |
| FE | - Finite Element |
| BEM | - Boundary Element Method |
| BE | - Boundary Element |
| CL | - Center Line |
| COG | - Center of Gravity |

# Chapter 1

# INTRODUCTION

In spite of effort of many researchers accurate prediction of representative design loads on marine structures caused by slamming and, hence, accurate prediction of the structural response remains a great challenge [64, 65]. However without a good prediction there is no guarantee that the ship is going to be safe and the sea transportation reliable. According to ISSC'91 (International Ship and Offshore Structures Congress) [65] over the past 30 years monohull structure damages caused by slamming amount to 10-12% of total damages. Losses of complete fore bodies of ships as result of the loss of the longitudinal strength due to high longitudinal bending moment caused by slamming in combination with the wave bending moment are just some of the examples [128]. Recent accidents (1998-1999) caused by wave impacts on bows of The Varg FPSO (owned by PGS), Schiehallion and Norne FPSOs prove the necessity of improvement in prediction of hydrodynamic loads [49, 50].

The goal of this thesis is to improve knowledge of the slamming phenomenon including different aspects. One of the first priorities is given to the investigation of the effect of hydroelasticity. At the ISSC'97 the following statement was made: "Hydroelastic effects on ship structures are normally not considered for slamming. Considering structural elasticity will generally result in reduced impact loads, no matter where the impact occurs whether it is global or local. It is evident that hydroelastic effects recently are given more serious consideration." [64]. For the last decades a number of researchers have been extensively working on the slamming problem [62]. But the question "Should hydroelasticity be considered or can it be neglected?" still exists for many different problems. The correct choice of suitable models and approaches for solving water impact problems is also a great challenge.

Before discussing existing approaches, numerical models, and the experimental results a clear definition of slamming phenomena and hydroelasticity will be given.

## 1.1 Classification of slamming phenomena

A ship sailing in rough seas experiences various types of impacts from the waves. The majority of these impacts are usually called "slamming". Slamming can be defined as a transient hydrodynamic impact experienced by the ship hull. There is no strict distinction between different types of slamming. However, the SSC-385 (Ship Structure Committee) in 1995 [62] suggests the classification, which will be given in the following sections.

### 1.1.1 Slamming

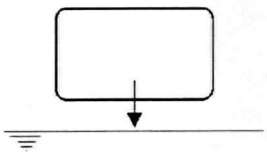

Figure 1.1. Slamming

The term Slamming describes Forward Bottom Impact. At higher sea states, when a vessel experiences large pitch and heave motions, the forefoot of a vessel rises above the water surface, the vessel re-enters the water. A water impact occurs. The hull literally slams into the water surface. The vessel receives heavy impulse pressures to the local forefoot structure, which can cause extensive local damage and high frequency stresses in the ship's structure. Moreover, this introduces subsequent whipping forces to the entire hull structure.

These slamming loads are generally associated with the short time exchange of momentum between the ship and the water. The duration of slamming pressure on the structure is in the order of milliseconds and very localized in space. Furthermore, for occurrence of this type of slamming it is required that the ship bottom is relatively flat and parallel to the water surface (this is illustrated in Figure 1.1, where a cross-section of ship hull is shown). Because of this, the high hydrodynamic pressure appears instantly within the whole area of the structure, which experiences the slamming. The loadings generated, because of their short duration, excite dynamic response of the local structure and hull girder. Damage to the local structure and support structure is the most frequent occurrence but deckhouse connections have been known to rupture and main hull girder strength failures have been initiated.

The aftbody slamming, which takes place when the bottom of the ship's stern rises above the water surface and then re-enters it again due to pitch and heave motions, also belongs to the slamming phenomenon. Here the aftship is subjected to the slamming loads. It is usually an important problem for ships with low draft aft and with relatively flat bottom in the area of the stern. The mechanism of this slamming is similar to the forward bottom impact. The aftbody slamming is quite common for modern cruise ships and ferries.

### 1.1.2 Frontal impact (Flare Slamming)

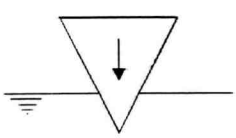

Figure 1.2. Frontal impact (Flare Slamming)

The term Frontal Impact (or the so called "Flare Slamming") describes the impact forces on the bow flare of a vessel. Due to large ship motions, an impact force is generated on the bow flare when it enters an oncoming wave.

The flare slamming is similar to bottom slamming of Section 1.1.1 except some major differences. The first difference is the duration of impact. The duration of a flare slamming impact is greater than in the case of bottom slamming. Secondly, when the bottom slamming takes place the whole area of the structure subjected to slamming loads receives almost instantly very high pressures. In case of the flare slamming the peak impulse pressure applied to the structure is less severe. Thirdly, the pressure is spread across the rapidly increasing cross-sectional area of the bow flare, potentially causing larger total forces on the structure.

### 1.1.3 Wave slap

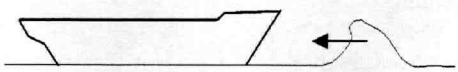

Figure 1.3. Wave slap

The term Wave Slap describes a Bow-Side Impact between a wave and a structure. In general wave slap involves a severe wave system imparting its energy to a structure. Usually for wave slap to occur, the large pitch and heave motions associated with both bottom slamming and frontal impact (flare slamming) need not be present. In addition, forefoot emergence and forward speed are not necessary to be present. An important factor of wave slap, as similar to other impact forces, is wave severity. Evidence of wave slap damage can be found at or near the operating waterline and usually affects the lighter structure at the forward end of a vessel. It is usually the least severe of the three forms of hydrodynamic impact.

### 1.1.4 Wet-deck slamming

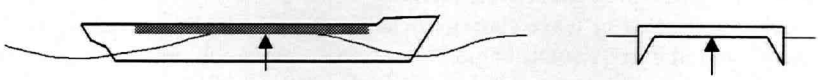

Figure 1.4. Wet-deck slamming

In addition to the classification suggested by the Ship Structure Committee [61] two more types of hydrodynamic loads can be mentioned. The first one is the so called "Wet-deck slamming". This slamming occurs when the relative heaving amplitude is larger than the height of the wet-deck of a catamaran. The physics of wet-deck slamming is quite similar with the forward bottom impact.

### 1.1.5 Green water

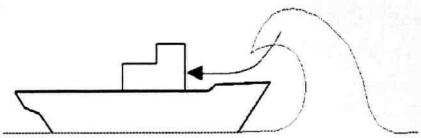

Figure 1.5. Green water

Another type of extreme hydrodynamic loads is the so called "Green water". The term Green water describes the phenomenon when the water violently flows on the ship deck. This occurs when waves exceed the freeboard of a vessel. A large amount of breaking water on the deck can cause damage of the deckhouse, hatches and other equipment located on the deck. It is not uncommon that container carriers lose their cargo because of green water. However the green water phenomenon is quite different from the other types of hydrodynamic loads discussed above. The term slamming perhaps could not be used for describing the green water.

Summarizing the classification given above it is clear that all these slamming phenomena have different nature. At the same time they do have some similarities too. With respect to the further investigation of hydroelasticity the author suggests to make a new definition of slamming phenomenon. This will be discussed in the following section.

## 1.2 Flat impact

The definitions of slamming given above describe mostly the practical meaning of this phenomenon establishing the location of impact. Based on physics of the impact a new definition of slamming can be given. The author suggests using the term slamming for any water impact wherever it occurs if it satisfies the following condition: the angle between the plane of the ship's hull subjected to water impact and the plane of the water surface is relatively small (typically 0-10 degrees). This condition can be satisfied not only for a classical case (Figure 1.6a) but also in case of bow impact if the impact occurs when the ship has a large heel (Figure 1.6b) or in case the shape of the wave corresponds to the form of the hull (Figure 1.6c). Moreover, there are some more cases such as green water impact on deckhouse fronts or wave slap on local structures, which could also satisfy the condition mentioned above. A small angle between the ship's hull and the water surface leads to the following scenario: the whole area of the hull subjected to the water impact receives high hydrodynamic pressures almost instantly. The duration of such flat impact is very short. Obviously there is no range which can be explicitly defined in seconds or milliseconds because this depends on dimensions of the structure and other factors. It is also important that the relative velocity at which the hull hits the water surface (or the wave hits the hull) plays here a secondary role.

The new definition of the slamming phenomenon is associated with an impact with much energy released and localized in time and space. This definition involves cases where the effect of hydroelasticity becomes important.

Practically the new definition of slamming combines different types of hydrodynamic impact having the same physics. This means that all these types can be treated in the same way.

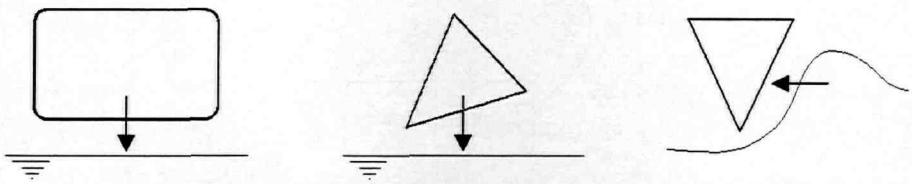

*a) Forward bottom impact* *b) Bow impact (large heel)* *c) Side wave slap on bow*

Figure 1.6. Flat impact

## 1.3 Hydroelasticity

The term hydroelasticity can be defined in a very simple way. Hydroelasticity is a two way fluid-structure interaction (Figure 1.7). This means that the system includes two parts: the water domain and the structure. During the impact the hydrodynamic pressure acts on the structure and the structure deforms. At the same time the speed of the structural deformation influences the pressure in the water. In other words the hydrodynamic pressure becomes a function of the structural response, which is again a function of the hydrodynamic pressure [48].

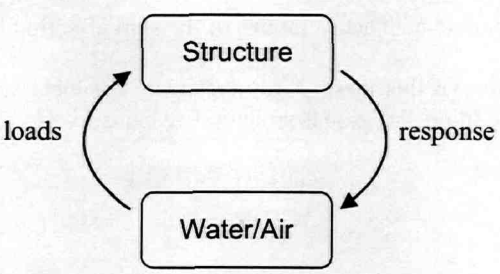


Figure 1.7. Hydroelasticity

However, traditionally a so called "2-step" approach is used. The 2-step approach considers one way interaction only and consists of two steps (Figure 1.8). First the water simulation is performed assuming that the structure is rigid. The hydrodynamic pressures are stored. At the second step the structural analysis takes place. The structural response under the hydrodynamic loads from the first step is determined. There is no feedback. The water behavior is not affected by the structural response. The 2-step approach often leads to overestimation of the hydrodynamic loads, which predicts more severe structural response. If hydroelasticity is considered it usually reduces the loads and gives more moderate structural response.
In order to investigate the effect of hydroelasticity both approaches are compared in this thesis for a number of different models.

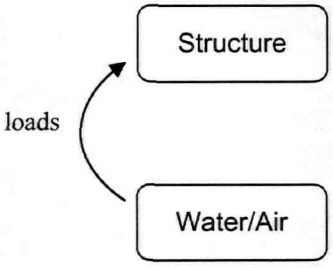


Figure 1.8. No hydroelasticity

## 1.4 Global and local effects

Slamming is a quite local phenomenon. Heavy impulse pressures occur within a quite small area of the ship structure in comparison with the dimensions of the entire ship. Slamming typically causes damage to the local and support structure. However, slamming can also have significant global effects, namely in form of 'whipping'. The term whipping refers to response of the entire hull girder due to impact with duration near the hull girder's natural period of vibration. Typically whipping assumes the two-node bending vibration of the hull girder. However in this thesis higher modes will be also referred as whipping. The whipping bending moment can be a significant addition to the global wave bending moment, creating a danger to the overall ship strength. Furthermore, the whipping can cause quite high accelerations of the ship affecting the passenger's comfort.

The primary objective of this thesis is to investigate the local structural response caused by slamming. In addition the global structural response will be discussed separately in Chapter 5.

## 1.5 Approaches

### 1.5.1 Full scale measurements, models tests and numerical research

The slamming problem can be studied by full scale measurements, model tests, and numerically. All these approaches have their advantages and disadvantages. Full scale experiments can give accurate data for a particular ship or structure. But next time when a different structure is the subject of investigation different results can be found. Full scale measurements and model tests are case sensitive. There are many factors influencing slamming like entrapped air, waves on the water surface, different structural stiffness, and speed of impact. It is extremely difficult to determine which factors are the most important and which are negligible. Unfortunately only a few measurements can usually be performed in the experiment such as data received from accelerometers, pressure and strain gauges. These measurements are limited in time and space. Often these data are not enough to understand the physics of phenomenon. A better insight is desirable. And this is

the moment when the numerical analysis helps. Contrary to experimental investigations numerical analysis can be used to study different factors influencing slamming separately. For instance if the effect of entrapped air between the structure and the water is the subject of consideration, two models are generated. The first model does not consider any air entrapment but the other one does. The results of analyses are compared and conclusions are made. Moreover numerical tools are cheaper than experimental research and full scale measurements. But how accurate are these numerical tools? Sometimes there is a debate if experimental investigation should be dominant or the numerical analysis should receive the first priority. The truth is somewhere in between. Only a combined approach based on experimental research and numerical analysis can give a good insight in the physics of this phenomenon. Numerical tools are much more flexible in comparison with experiments and full scale measurements. That is why the numerical tools can be used for a parametrical study on how different factors influence slamming. At the same time numerical tools are not reliable without experimental verification.

The author considers both experimental research and numerical models in this thesis. The discussions start with a description of slamming drop tests performed by TNO (Netherlands Organization for Applied Scientific Research). Results of these tests are used for verification of numerical tools. The numerical models are developed step by step starting with a very simple 2D analysis and ending with a quite complicated 3D model.

### 1.5.2 Strong and weak formulations in numerical analysis

With respect to the numerical approaches the following should be mentioned. The fluid-structural coupling can be carried out directly (strong formulation) or by a step by step approach (weak formulation). In the first case the governing equation for the fluid domain has to be combined with the governing equation for the structural analysis. Then this combined equation is solved giving direct coupling of fluid and structural parts of the problem. This approach, for instance, was used by Hermans [59, 58] for the analysis of a very large floating flexible platform in waves, and by Postnov and Volkov [96] in their generalized method for the fluid-structure interaction problem. In the second case the problem is solved step by step. At the first time increment the hydrodynamic pressure is found from the fluid analysis assuming the body to be undeformed. This pressure is applied to the structure in order to find the structural response. This response is the input data for the fluid analysis at the next time increment. In other words there is one-step delay since the structural response of the previous time step is used as input for the fluid analysis of the current step. This approach brings some difficulties. At the first time increment the structure is assumed rigid for the fluid simulation because the structural response is not determined yet. Quite high hydrodynamic pressures can be obtained. These pressures can cause strong structural response. This response leads to a significant reduction of pressures or even negative pressures at the second time step. This gives instabilities in the structural analysis, making the fluid simulation unstable as well. The whole analysis procedure can become divergent. This is especially critical for the incompressible water model. Contrary to the weak formulation, the strong formulation does not suffer from this problem. The solution is found accurately. The disadvantage of

the strong formulation is that this is a very case sensitive and complicated approach because changes of the model can lead to the necessity of rewriting the formulation.

The primary goal of this thesis is investigation of different factors influencing the slamming problem with the effect of hydroelasticity as the main focus of research. This required a very flexible analysis tool. The preference was given to the weak formulation because the weak formulation provides the degree of flexibility necessary for the application of different fluid and structural models. These fluid and structural models are independent from each other. A special code has been developed having two independent blocks: fluid- and structural subroutines. By means of a special interface procedure the data were exchanged between these blocks providing the hydroelastic coupling. Commercial codes used later are also based on the weak formulation [89].

## 1.6 Impact pressure and structural response

Traditionally in ship design the key parameter in the definition of slamming loads is the maximum impact pressure. Finding of this maximum pressure is quite a heavy task. Both the numerical (especially when the weak formulation is employed) and experimental approaches are still not very reliable, when slamming is the subject of consideration. The pressure trace is usually very spiky. A typical pressure trace obtained from numerical analysis is shown in Figure 1.9. The data has to be filtered. Depending on the filtering procedure significantly different results can be obtained. Furthermore, areas of the structure subjected to very high pressure are usually extremely small. This presents difficulties with regard to the experimental measurements.

But what is the objective? The objective is to make a proper design of a ship, based on the accurate prediction of the structural response. Prediction of maximum stresses plays the most important role. When the deadrise angle is small and hydroelasticity is of importance, the time scale of the occurrence of the maximum hydrodynamic pressure and the maximum stresses in the structure is different [47]. The maximum pressure occurs in the very beginning of the impact, while the maximum stresses occur later. Here it is not the maximum hydrodynamic pressure but the energy transferred to the structure during the impact and the impact impulse duration that become the key factors.

The inertia of the structure is so great that even very strong pressure oscillations, but with very short duration, do not influence the structural response. The duration of each spike in Figure 1.9 is very short. In spite of the fact that the spikes have high value of pressure, each of them does not transfer much energy. The integration of the pressure trace gives the energy, which causes the structural response.

If slamming is treated as a hydroelastic problem, the structural response analysis is performed simultaneously with the water simulation. The separate determination of impact pressures is not required any more. This is why the majority of conclusions in this thesis are based on the structural response, in particular, on the structural displacements, often omitting discussions about the pressure history plots.

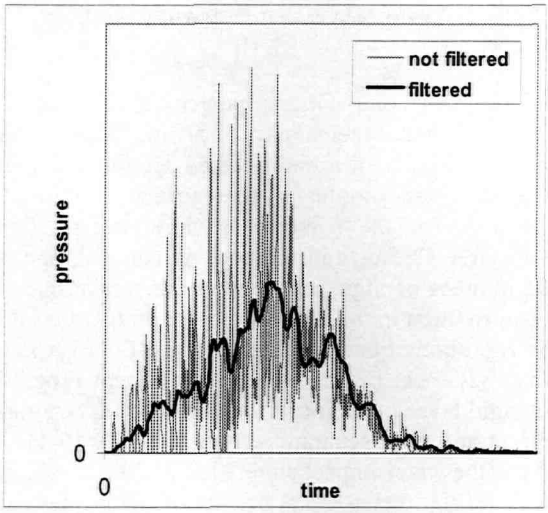


Figure 1.9. Typical pressure trace

## 1.7 Literature survey

Slamming is a strongly transient and non-linear phenomenon with random character. Furthermore, slamming is highly sensitive to the relative motion and contact angle between the ship hull and the water surface. Air entrapment between the hull and the water surface, the shape and the momentum of the structure are very important parameters of the slamming phenomenon. Moreover, slamming is ultimately caused by wave conditions, which are stochastic in nature. All these factors make the prediction of slamming loads one of the most challenging tasks in ship design. This resulted in more than 1000 publications in the last 100 years. The literature survey of this section gives just a very brief overview of the most important theories and approaches.

Beginning of fundamental investigation of slamming problems can be associated with the name of Von Karman [113] who in 1929 developed an asymptotic theory for the flat and near-flat impact problems based on linearized boundary conditions in order to predict the impact loads on seaplane floats during landing. In 1932 Wagner improved Karman's solution by considering spray during the impact. He studied a two-dimensional rigid wedge penetrating a calm water surface [116]. Since then Wagner's solution has been modified and improved many times. However, the disadvantage of Wagner's theory is that this theory predicts infinite impact pressure if the ship bottom has a zero deadrise angle. The theory developed by Watanabe illuminates this singularity. Watanabe derived a general expression for the impact pressure distribution on the flat bottom ship experiencing slamming by matched asymptotic expansion on the bases of shallow draft and the gravity free assumptions [117, 118]. The basic premise behind Wagner's work is well summarized by Dobrovol'skaya [37]. The 2D problem of water impact is also extensively studied by Howison et al [61], summarizing and extending some mathematical

results for a water-entry problem where the impacting body is nearly parallel to the undisturbed water surface.

The rapid increase of computer computational power has resulted in the development of many numerical solutions for the water impact of a rigid body. A numerical method for studying water entry of a 2D body of arbitrary cross-section was presented by Zhao and Faltinsen [129]. Here the exact nonlinear free-surface condition without gravity is satisfied. Important features of the solution are how the jet flow occurring at the intersection between the free surface and the body is handled, and how conservation of fluid mass is satisfied in areas of high curvature of the free surface. Greenhow has also made a considerable contribution in the 2D water-entry problem using the Cauchy integral theorem including the rigid body boundary and a mixed Eulerian-Lagrangian description of the free surface [51, 52]. Arai has achieved a significant progress in calculating the impact pressures on a rigid body of arbitrary shape providing accurate modeling of spray generation, gravity effect and flow separation from the body [6-11]. These are the most critical factors in making the water impact simulation more realistic. In recent years many researchers have studied 2D water-entry problems of rigid bodies. The following researchers can be listed: Armand and Cointe [12], Vorus [114], Mei et al [87], Xu et al [126, 127], Wenyang [120], Cointe [31] etc. A 3D problem was studied by Wenyang et al [121], Troesch et al [110, 111], Ann et al [4], and Maskew et al [86].

Traditionally it is assumed that the water is incompressible and the flow is irrational. One of the first extensive investigations on the effect of water compressibility was performed by Ogilvie [94]. Later Korobkin studied blunt-body water impact taking into account water compressibility [73, 74]. He showed that if the impact velocity is not very high assuming water incompressible is not a severe limitation. Similar conclusions have been drawn by Kvalsvold and Faltinsen [79, 43]. Ershov and Shahverdy [39], and Shahverdy [105] have also considered fluid compressibility for modeling of water impact problems. Iwanowski developed a numerical approach in order to investigate air entrapment between the rigid body and the water surface [66, 67]. Verhagen performed analytical and experimental studies of the impact of a flat plate on a water surface [112]. He states that, by taking into account the influence of the compressible air layer caught between the falling plate and the water surface, the experimental results can be fully explained. Falch studied the impact of a flat-bottomed two-dimensional body theoretically and numerically also taking into account air entrapment [41, 40]. He also investigated the effect of various deadrise angles.

Kaplan has expanded the investigation of the slamming problem from the local determination of impact loads [71, 70] to the creation of a general procedure incorporating the global ship motions, local slamming loads and the global structural response [69]. Ochi and Motter have developed an overall method of prediction of slamming loads and the structural response caused by these loads including stochastic approach [93, 92]. The method considers many factors including the frequency of slamming occurrence, time interval between slams, slamming pressure, extreme probability pressure, extreme pressure for design, ship speed free from slamming, slam impact force, and main hull girder response (global response). The global response caused by slamming was also studied, among others, by Lundgren et al [84], Nikolaidis and Kaplan [91], Ramos and

Soares [102], Weems et al [119], Mansour and Oliveira [85], Hansen [54], Hansen et al [55], Rassinot and Mansour [103], Soares [107], Takemoto et al [108].

The appearance of hydroelasticity theory as a branch of science can be associated with the names of Bishop and Price [26]. Their two-dimensional hydroelasticity theory has continuously been employed and has further improved the predictions of the dynamic loads on ships. In [99] and [100] Price et al use this theory for the prediction of wave induced responses, loads and stresses for different types of vessels. Aksu et al considered the transient loadings experienced by a flexible structure of arbitrary shape slamming in an irregular seaway within the framework of a three-dimensional hydroelasticity theory described in terms of generalized coordinates and forces [1]. Aksu et al have also performed a comparative study between full scale measurements and theoretical predictions in [2]. Xia et al have developed a time-domain theory of fluid-structure interaction between floating structures and the incident waves [124, 125]. Wu et al in [123] and Hermundstad et al [60] presented a method for hydroelastic analysis of high speed vessels, where the flexibility of the ship hull is taken into account by using a number of dry eigenmodes in addition to the rigid body modes. In [5] Arai has improved his own numerical method introducing a hydroelastic coupling for the problem of a water impact of cylindrical shells. In [75-77] Korobkin studied theoretically unsteady hydroelasticity of floating plates, and wetdeck slamming in particular. Kvalsvold et al have studied wetdeck slamming of a high speed catamaran in head sea waves including the effect of hydroelasticity in [78-80]. Du and Wu considered the influence of forward speed on the hydroelastic structural response in [38]. Tanizawa has developed a 2D code for a fully nonlinear time-domain simulation method for the analysis of transient hydroelastic problem with free-surface in [109].

A significant contribution to the investigation of the effect of hydroelasticity for slamming problems has been made by Faltinsen. In [43, 42, and 48] Faltinsen analyzed theoretically the effect of hydroelasticity for wetdeck slamming using a hydroelastic beam model and comparing results of computations with drop tests of elastic plates. In [46] the effect of hydroelasticity is studied for a problem of water entry of a wedge by orthotropic plate theory. In [45] full scale measurements of wetdeck slamming on the Ulstein Test Vessel are interpreted by theory, followed by systematic studies on the importance of hydroelasticity as a function of deadrise angle and impact velocity. In addition to this Faltinsen [44] studied global hydroelastic effects due to wave induced springing and whipping. A broad overview of many slamming problems in ship and ocean engineering is given by Faltinsen in [47]. Here Faltinsen emphasizes that maximum pressure can not be used to estimate maximum slamming induced stresses when the maximum pressure is large, because dynamic hydroelastic effects then become important. Furthermore, Faltinsen states that the significance of hydroelasticity increases with decreasing dead-rise angle, increasing impact velocity, and increasing the value of the highest local natural period of the structure.

In addition to the significant number of publications on theoretical and numerical investigation of the slamming problems given above, special attention should be given to the experimental work. In [82] Lacey and Edwards and in [81] Lacey and Chen present measurements obtained from the structural monitoring system installed on ARCO Marine

oil tankers. The system was designed to measure different effects of subjecting a ship to the typical loads and forces encountered at sea, including slamming pressures and global structural response. In [122] Witmer and Levis present similar measurements conducted for a BP oil tanker. Model tests and full scale measurements of bottom impact pressures on a 5.99 m high speed boat were conducted by Motora et al in [88]. In order to study the impact pressure and the structural response many researchers choose drop tests. Such experiments were conducted by Shibue and Nakayama [106] and Arai [5] for cylindrical shells, Haugen et al [56] for plates, Hayman et al [57], and Chuang [29, 30] for models of hull sections, Greenhow [51], and Radev and Beukelman [101] for wedges, Vredeveldt et al [115] for ship panels, Samuelides and Katsaounis [104] for wetdeck slamming. Okada and Sumi [95], and Lewison and Maclean [83] paid special attention to the consideration of air entrapment. Datta [36] performed some model tests studying the vertical hydrodynamic force and pressures on the bow. Results of similar tests were presented by Colwell et al in [32]. An advanced series of tests with a segmented ship model in order to measure slamming pressures on two segments was performed by Beukelman in [25].

## 1.8 Goal of the research

As it is seen from the literature survey the slamming problem, and hydroelasticity in particular, have extensively been studied by many researchers. However, the role of the effect of hydroelasticity in each particular case is still a question.

The goal of this thesis is development of a better understanding of the effect of hydroelasticity in slamming including: finding the most important factors of the slamming phenomenon, which make the effect of hydroelasticity important, and development of a practical criterion, which can answer the question "Should hydroelasticity be considered or can it be neglected" for each practical problem.

# Chapter 2

# CHOICE OF SUITABLE MODELS

The nature of the slamming problem involving hydroelasticity is very complicated. It requires consideration of both: the structural analysis and the fluid flow. Only a correct choice of suitable approaches and modelling methods can provide a reliable solution. The author decided to begin his research with studying and comparison of different numerical tools. This chapter is devoted to this research. The following sections will present several methods of modelling showing their advantages and disadvantages. But first the requirements to the numerical tools will be stated.

## 2.1 Requirements

### 2.1.1 Modelling of water, air, and structure

In order to solve a hydroelastic problem both the water simulation and the structural analysis have to be performed simultaneously. Moreover, if air entrapment plays an important role, the air domain should also be included in the model. In other words, the general model can be represented as it is shown for a 2D situation in Figure 2.1.

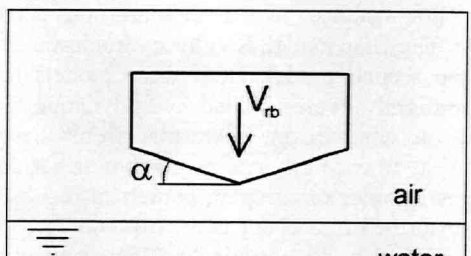


Figure 2.1. The model

There are a number of factors, which influence the fluid-structure interaction. Additionally to the entrapped air, the structural stiffness (or flexibility) is important. The shape of the ship's bottom, or the deadrise angle in a more simple case, is also very critical.

### 2.1.2 "Rigid wall" boundary condition for the water/air regions

In a real situation the ship usually sails at sea where the water depth is much larger than the breadth of the ship (the breadth of a cross-section is considered, or the ship length if the whole hull is investigated). Slamming does not occur in very shallow water except in some very special cases. A large water depth means that there is no influence of the sea bottom on the slamming loads. In the numerical analysis, however, the water region generally has to have boundaries. The reason of this is that when the finite analysis or other similar methods are used the modeling area is always limited in space having finite dimensions. Unfortunately there is no easy and reliable way of modeling the boundary condition, which is capable of describing infinite depth accurately. The most common approach is to set a "rigid wall". This means that the fluid velocity in the direction normal to the boundary is zero. This causes reflections. The pressure wave in water generated during the slam propagates to the boundary then reflects from it, coming back and hitting the ship hull again. This generally makes the impact force higher. The closer the boundary is to the structure, the higher the loads that can be expected. Application of a water volume with large dimensions can be a solution in this case, but this gives a large mesh leading to very high requirements of computer power, especially for 3D models. However a compromise can be found. If the dimensions of the water region are three or four times larger that the dimensions of the ship hull, the effect of the boundary is quite small [53]. This is the way in which the water boundaries are modeled in this thesis. It was found that if the bottom of the water area is located in distance about four times larger than the breadth of the ship, this gives an increase of the hydrodynamic force of only 5-12%. This is not so critical for the primary goal of this study, which is an investigation of the importance of different factors influencing slamming with the effect of hydroelasticity as the primary focal point. For instance, two models are considered in order to study the effect of hydroelasticity. The first model is fully hydroelastic, but no hydroelasticity is taken into account in the second model. Both these models have the same boundary conditions resulting in a slightly overestimated hydrodynamic force due to reflection of pressure waves. Based on comparison of results from these models a qualitative estimation of the effect of hydroelasticity can be given. Furthermore, some drop tests will be discussed in this thesis in order to compare numerical results with experimental data. These drop tests were performed in a water tank with concrete walls. The application of "rigid wall" boundary condition in the numerical analysis is the most accurate in this case. If air is modeled the same conclusions can be applied for modeling of boundaries of the air region.

### 2.1.3 Numerical tools

There are a number of commercial codes, which are capable of solving hydrodynamic problems quite accurately. There are also a number of commercial codes for structural analysis which are very powerful and universal. However, only a few programs can handle the fluid-structure interaction problems. This is the reason why the author started his investigation of the hydroelastic problem with development of a new code. The following sections will show the process of the code development. Subsequently some commercial codes, which have been used in this thesis, will be discussed.

## 2.2 Available experimental data

The present research work was performed in close cooperation with TNO. This gave an opportunity to use their experimental data for verification of numerical models developed and discussed in this thesis. TNO carried out three series of drop tests in the Ship Structures Laboratory of the Delft University of Technology in order to study the slamming phenomenon [34, 35, and 115]. One of the tests is shown in Figure 2.2. In each series a full scale stiffened plate panel, of moderate dimensions (2000 mm / 2500 mm), was subjected to hydrodynamic impact loads. Two steel panels with a plate thickness of 6 and 14 mm were tested. These panels are typical for a fast monohull and a container vessel respectively. The 6 mm panel is shown in Figure 2.3. The panels have three stiffeners with spacing of 650 mm each. An aluminium panel with a thickness of 6 mm was also tested in the third series of tests. All of these panels were mounted in a drop box and instrumented with accelerometers, strain gauges and pressure gauges. The panels were subjected to hydrodynamic impacts by dropping the assembly box into a water tank with the panel facing toward the water surface.

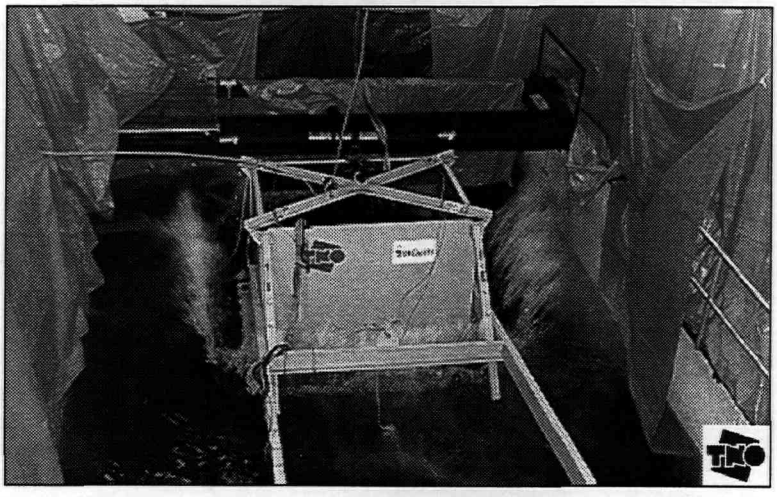


Figure 2.2. TNO test set-up

The test setup consists of a rectangular box of approximately length/width/height = 2500mm/2000mm/1200mm. The mass of the box without the panel attached is 840 kg. The basis of the drop box was a rectangular frame of tubular beams. These provided stiffness and sufficient space to mount the plate panels. On top of this frame, four vertical plates were welded so the test specimen on the support frame together with these plates became a box. To this box, two 6-meter levers were attached, which on their turn were hinged on the edge of water basin (water basin: length/width = 9.5 m / 5.6 m, water depth = 2.3 m). The box was hoisted by a crane with a slip hook. By pulling a release chord, the box drops towards the water surface. The levers are attached to the box in such a way that the entire box can be tilted. Thus the angle of impact of the panel with the water surface could be adjusted between 0 to 20 degrees. The vertical motion of the panel during impact

is considered to be small to such an extent that the rotation of the test panel at impact can be neglected. Along the levers, cables for data acquisition were led. Accelerometers were fitted on both the panels and the box. The global motion of the box was recorded by accelerometers as well. Besides accelerometers, pressure gauges were fitted.

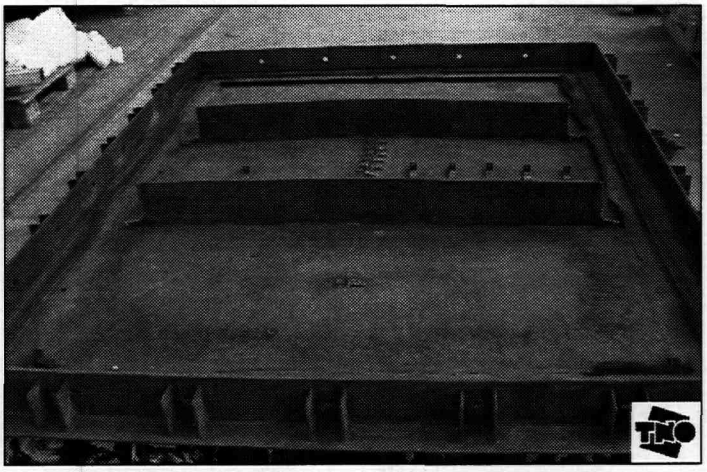

Figure 2.3. The bottom panel

## 2.3 Development of a fluid-structural coupling code

The author started working on the hydroelastic problem by considering the fluid flow. Obviously there is a large variety of different methods for the modelling of fluid flow. The goal, however, was to find an approach, which is quite simple but at the same time capable to provide a sufficient accurate description. The potential flow was chosen for this purpose. Both compressible and incompressible potential flow models were considered. Simulation of incompressible potential flow is generally more simple than compressible flow. However it was initially expected that compressibility of water would play an important role in slamming problem. This was assumed due to the fact that the hydrodynamic loads caused by slamming are impulse loads with a very short duration but large transfer of energy. This is why both compressible and incompressible flow models were developed and compared. It was found later that compressibility is not so important (Section 3.6). At the same time the compressible flow model results into much more stable solutions. This is the reason why compressible flow was used for majority of models considered.

With respect to numerical tools the following should be mentioned. Traditionally there are several ways of numerical modelling of fluids. The best known approaches are the finite difference method, the finite element method, and the boundary element method. Each method has disadvantages and advantages. The finite difference method and its variations are widely used for modeling of fluids, finding its application in the very beginning of the computer era. The finite difference method is the most suitable for large computing

domains. Moderate memory requirements of this method allow generating large meshes. However, in order to compensate for the lack of accuracy, the computing domain sometimes has to be subdivided into very small elements giving an extremely large mesh. This causes high memory requirements. The finite element method was developed later. This method gives better accuracy with limited amount of elements due to the application of highly sophisticated approximation functions within each element. Another advantage of the finite element method is the easy programming of this method. One of disadvantages of this method is its high memory requirement. The boundary element method is the most recent approach of the three. The key feature of the boundary element method is that the solution is found on the boundary of the computing domain. This reduces the dimensionality of the problem. For instance, a 3D computing domain has to be described on the boundary only. This virtually reduces the problem to a 2D case, where only the surface of the 3D domain is considered. However programming the boundary element method is more complicated than the finite element analysis. There are still a lot of discussions about advantages and disadvantages of these three methods. At the same time new approaches are being developed. At one point the author had to make his choice of which method to use. Having some experience with the finite element analysis the author decided to chose this method as the basic approach used in the self-developed code. Furthermore, the study on the choice of numerical tools was not the main subject of this thesis. The investigation of the effect of hydroelasticity reduced the time available for advanced study of numerical tools, concentrating the author on physics of the slamming phenomenon. Nevertheless, the author has also evaluated the boundary element method, which was, however, not included in the final code developed by the author.

For the structural analysis the author chose the finite element method. Usage of the finite element method for structures is the most common and reliable approach today.

The following sections show how the self-developed code was created. First, the simulation of the water domain will be discussed. Then attention will be given to the structural analysis. Subsequently the coupling procedure combining the water simulation and the structural analysis will be explained.

### 2.3.1 Finite element method for compressible fluid

*a) 1D model*

Development of a FE program for compressible water began with a 1D problem. The model is shown in Figure 2.4. The rigid body having a specific mass $M$ is dropped onto the water column with a prescribed initial velocity $V_0$. The area of the cross-section of the water column has unit value. During the interaction the velocity of rigid body $V_{rb}(t)$ can be found from the Newton low:

$$M\frac{dV_{rb}}{dt} = -p \tag{2.1}$$

Here $M$ is the mass of the rigid body per unit area of the water column cross-section, and $p$ is the pressure in the water. The positive direction of $V_{rb}(t)$ is downward. The effect of gravity is neglected.

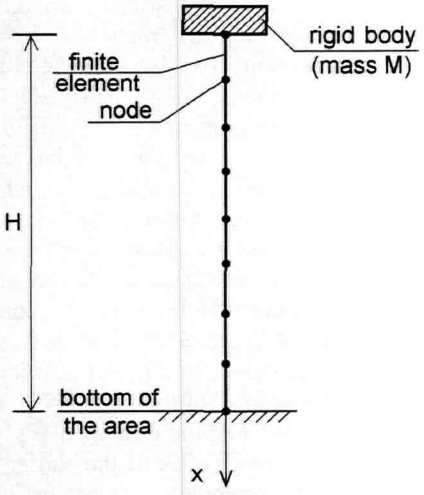


Figure 2.4. 1D model

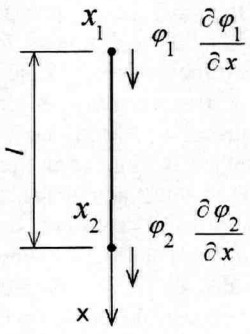


Figure 2.5. 1D finite element

The governing equation for the potential flow for a 1D case is:

$$\frac{\partial^2 \varphi}{\partial x^2} = \frac{1}{c_0^2} \cdot \frac{\partial^2 \varphi}{\partial t^2} \tag{2.2}$$

Here $c_0$ is speed of sound in water.

Finite element analysis is applied for this model. The finite element has two nodes (Figure 2.5). Each node has two degrees of freedom: the velocity potential $\varphi$ and the x-coordinate derivative $\frac{\partial \varphi}{\partial x}$, which represents the velocity in x direction. This element has a cubic approximation function, which gives a rather accurate solution. The presence of both the velocity and potential in each node makes the application of boundary conditions easier. The approximation function is:

$$\varphi(x) = \alpha_1 + \alpha_2 x + \alpha_3 x^2 + \alpha_4 x^3 \tag{2.3}$$

The following shape functions are derived [98]:

$$N_1(x) = 1 - 3\frac{x^2}{l^2} + 2\frac{x^3}{l^3}$$
$$N_2(x) = x - 2\frac{x^2}{l} + \frac{x^3}{l^2}$$
$$N_3(x) = 3\frac{x^2}{l^2} - 2\frac{x^3}{l^3} \tag{2.4}$$
$$N_4(x) = -\frac{x^2}{l} + \frac{x^3}{l^2}$$

The vector of unknown degrees of freedom is defined:

$$\overline{q} = \left[\varphi_1, \frac{\partial \varphi_1}{\partial x}, \varphi_2, \frac{\partial \varphi_2}{\partial x}\right] \tag{2.5}$$

The potential $\varphi$ can be represented as:

$$\varphi = \sum_{j=1}^{4} q_j(t) \cdot N_j \tag{2.6}$$

Then this approximation is substituted into the equation (2.2):

$$-\sum_{j=1}^{4} q_j(t) \cdot \frac{\partial^2 N_j}{\partial x^2} + \frac{1}{c_0^2} \cdot \sum_{j=1}^{4} \ddot{q}_j(t) \cdot N_j = 0 \tag{2.7}$$

Bubnov-Galerkin's procedure is applied [28]:

$$\int_0^l \left[ -\sum_{j=1}^{4} q_j(t) \cdot \frac{\partial^2 N_j}{\partial x^2} + \frac{1}{c_0^2} \cdot \sum_{j=1}^{4} \ddot{q}_j(t) \cdot N_j \right] \cdot N_i \, dx = 0 \tag{2.8}$$

Equation (2.8) can be rewritten as:

$$\sum_{j=1}^{4} \left( \ddot{q}_j \cdot m_{i,j} + q_j \cdot k_{i,j} \right) = 0 \tag{2.9}$$

Here $m_{i,j}$ and $k_{i,j}$ are coefficients of the mass and the stiffness matrices of the finite element:

$$m_{i,j} = \frac{1}{c_0^2} \int_0^l N_i \cdot N_j \, dx \tag{2.10}$$

$$k_{i,j} = -\int_0^l \frac{\partial^2 N_j}{\partial x^2} \cdot N_i \, dx \tag{2.11}$$

The global finite element equation is (here $\{B_w\}$ is the global load vector incorporating known values of potential and velocity on the boundary):

$$[M_w]\{\ddot{Q}_w\}+[K_w]\{Q_w\}=\{B_w\} \tag{2.12}$$

This equation is solved for the unknown vector $\{Q_w\}$ by application of a direct time integration procedure. This is a step by step Newmark method. The stability of integration depends on the time step $\Delta t$. The integration is stable if the following condition (Courant criterion) is satisfied: $\Delta t < l/c_0$. Here $l$ is the length of finite element. This condition is based on the minimum time for a pressure wave to cross on element.

The pressure in water is found as [105]:

$$p = p_0 - \rho_0 \frac{\partial \varphi}{\partial t} \tag{2.13}$$

Here $p_0$ is the atmospheric pressure, and $\rho_0$ is the reference density of water.
At time moment $t = 0$:

$$\varphi = 0$$

$$\frac{\partial \varphi}{\partial t} = 0 \tag{2.14}$$

$$V_{rb}(t) = V_0$$

The boundary conditions are:

$$\frac{\partial \varphi}{\partial x} = V_{rb}(t) \text{ under the rigid body}$$

$$\frac{\partial \varphi}{\partial x} = 0 \text{ at the bottom} \tag{2.15}$$

A special code was written to solve the problem in FORTRAN. A number of simulations were carried out in order to find the model sensitivity with respect to the number of finite elements, time increment etc. The results of the simulation were compared with an analytical solution, which is available for this problem. It was found that a model with a larger number of elements gives better fitting of the analytical curve. If the time increment satisfies the Courant criterion mentioned above the analysis is stable even if the water column has one element only. This analytical solution, which was used, predicts the pressure under the rigid body as a function of time (it is assumed that the height of the water column $H$ is infinite) [39]:

$$p = p_0 + \rho_0 c_0 V_0 e^{-\frac{\rho_0 c_0}{M} t} \tag{2.16}$$

Results of calculations and the analytical solution are shown in Figure 2.6 and Figure 2.7 for $M/(\rho_0 H) = 1$ and $M/(\rho_0 H) = \infty$ correspondingly. The oscillations in Figure 2.6 and Figure 2.7 occurring in the beginning of the impact in the numerical solution are caused by the time integration procedure.

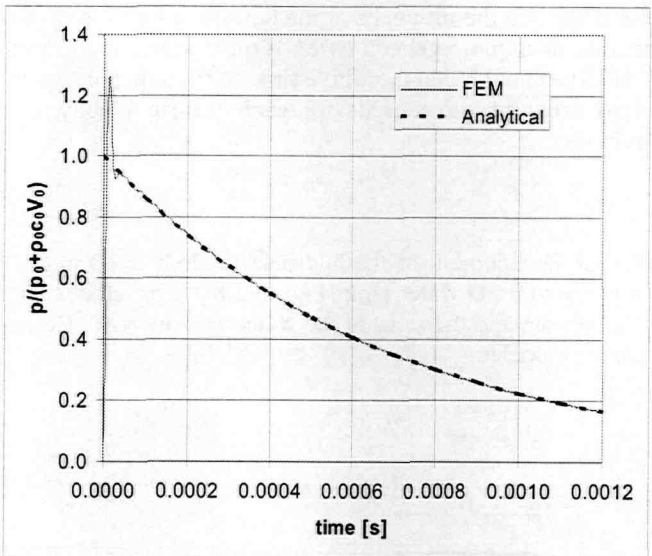


Figure 2.6. Pressure under the rigid body as a function of time ( $M/(\rho_0 H) = 1$ )

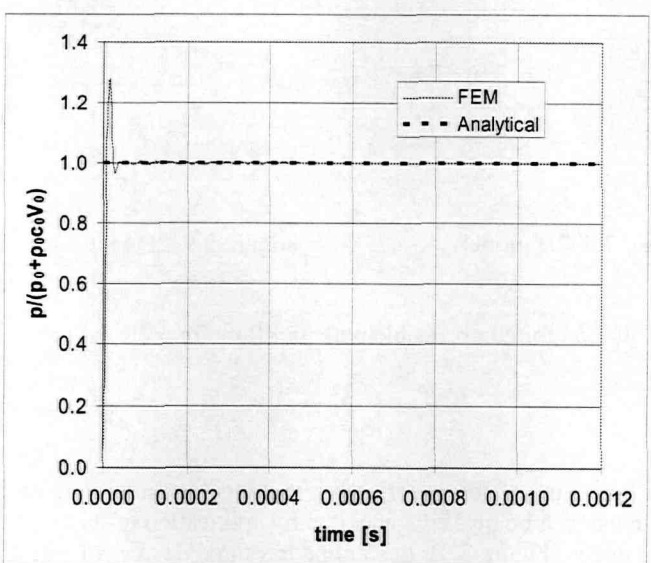


Figure 2.7. Pressure under the rigid body as a function of time ( $M/(\rho_0 H) = \infty$, which means that the velocity of the mass is constant)

The analytical solution assumes that the height of the water column is infinite. The numerical analysis is performed for a column with finite height. However the agreement between the analytical solution and the numerical results is very good for the considered time duration. This is due to the fact that the water depth is sufficiently large that the reflected pressure wave from the bottom has not arrived yet. This allows us to conclude the following with respect to the influence of the bottom of the water column (or the rigid wall boundary conditions in more general case): if the distance to the bottom (or distance to the rigid wall) is large enough that the whole time of the simulation is less than the time which the reflected pressure wave needs to reach the rigid body again, there is no influence of boundaries.

*b) 2D model*

As the second step in development of the hydroelastic code a 2D model was created. A rigid body is dropped into a 2D water tank (Figure 2.8). It penetrates into the water with constant speed. The bottom and the sides of the water area are rigid. Because of symmetry only half of the area is modeled.

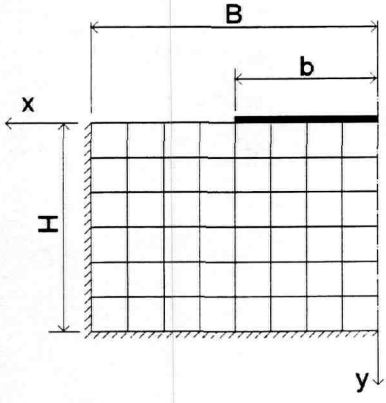


Figure 2.8. 2D model

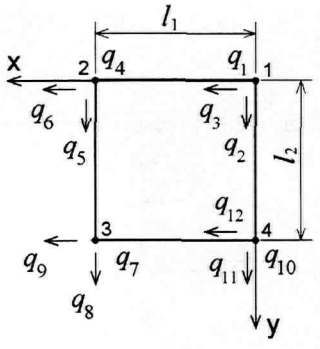


Figure 2.9. 2D rectangular finite element

The governing equation for compressible potential flow for a 2D case is:

$$\frac{\partial^2 \varphi}{\partial x^2} + \frac{\partial^2 \varphi}{\partial y^2} = \frac{1}{c_0^2} \cdot \frac{\partial^2 \varphi}{\partial t^2} \tag{2.17}$$

Considering the geometry of the water area a rectangular finite element was chosen for this model. The mesh can be quickly generated by application of this simple element. The element has four nodes (Figure 2.9). Each node has three degrees of freedom: the velocity potential $\varphi$ and the first x- and y-coordinate derivatives ($\frac{\partial \varphi}{\partial x}$;), which represent

velocities in x and y directions. The presence of both the velocities and the potential in each node makes the application of the boundary conditions easier. An incomplete polynomial is chosen as the approximation function for this element:

$$\varphi(x,y) = \alpha_1 + \alpha_2 x + \alpha_3 y + \alpha_4 x^2 + \alpha_5 xy + \alpha_6 y^2 + \alpha_7 x^3 + \\ + \alpha_8 x^2 y + \alpha_9 xy^2 + \alpha_{10} y^3 + \alpha_{11} x^3 y + \alpha_{12} xy^3 \tag{2.18}$$

This approximation function provides continuity between elements for $\varphi$, but fails to provide normal derivative continuity along an element edge, meaning that this element is nonconforming. Nevertheless, this element provides good convergence [28].

The following shape functions are derived [28]:

$$\begin{aligned}
N_1(\xi,\eta) &= 1-3\xi^2-\xi\eta-3\eta^2+2\xi^3+3\xi\eta^2+2\eta^3-2\xi^3\eta-2\xi\eta^3+3\xi^2\eta \\
N_2(\xi,\eta) &= l_2\cdot(\eta-\xi\eta-2\eta^2+2\xi\eta^2+\eta^3-\xi\eta^3) \\
N_3(\xi,\eta) &= l_1\cdot(\xi-\xi\eta-2\xi^2+2\xi^2\eta+\xi^3-\xi^3\eta) \\
N_4(\xi,\eta) &= 3\xi^2+\xi\eta-2\xi^3-3\xi\eta^2+2\xi^3\eta+2\xi\eta^3-3\xi^2\eta \\
N_5(\xi,\eta) &= l_2\cdot(\xi\eta-2\xi\eta^2+\xi\eta^3) \\
N_6(\xi,\eta) &= l_1\cdot(-\xi^2+\xi^3+\xi^2\eta-\xi^3\eta) \\
N_7(\xi,\eta) &= -\xi\eta+3\xi^2\eta+3\xi\eta^2-2\xi^3\eta-2\xi\eta^3 \\
N_8(\xi,\eta) &= l_2\cdot(-\xi\eta^2+\xi\eta^3) \\
N_9(\xi,\eta) &= l_1\cdot(-\xi^2\eta+\xi^3\eta) \\
N_{10}(\xi,\eta) &= 3\eta^2+\xi\eta-2\eta^3-3\xi\eta^2-3\xi^2\eta+2\xi\eta^3+2\xi^3\eta \\
N_{11}(\xi,\eta) &= l_2\cdot(-\eta^2+\eta^3+\xi\eta^2-\xi\eta^3) \\
N_{12}(\xi,\eta) &= l_1\cdot(\xi\eta-2\xi^2\eta+\xi^3\eta)
\end{aligned} \tag{2.19}$$

Here $\xi = x/l_1$ and $\eta = y/l_2$

The vector of unknown degrees of freedom is defined:

$$\overline{q} = \left[\varphi_1, \frac{\partial\varphi_1}{\partial y}, \frac{\partial\varphi_1}{\partial x}, \varphi_2, \frac{\partial\varphi_2}{\partial y}, \frac{\partial\varphi_2}{\partial x}, \varphi_3, \frac{\partial\varphi_3}{\partial y}, \frac{\partial\varphi_3}{\partial x}, \varphi_4, \frac{\partial\varphi_4}{\partial y}, \frac{\partial\varphi_4}{\partial x}\right] \tag{2.20}$$

The potential $\varphi$ can be represented as:

$$\varphi = \sum_{j=1}^{12} q_j(t)\cdot N_j \tag{2.21}$$

Then this approximation is substituted into the equation (2.17):

$$-\sum_{j=1}^{12} q_j(t)\cdot\left(\frac{\partial^2 N_j}{\partial x^2}+\frac{\partial^2 N_j}{\partial y^2}\right)+\frac{1}{c_0^2}\cdot\sum_{j=1}^{12}\ddot{q}_j(t)\cdot N_j=0 \tag{2.22}$$

Bubnov-Galerkin's procedure is applied [28]:

$$\int_0^{l_1}\int_0^{l_2}\left[-\sum_{j=1}^{12} q_j(t)\cdot\left(\frac{\partial^2 N_j}{\partial x^2}+\frac{\partial^2 N_j}{\partial y^2}\right)+\frac{1}{c_0^2}\cdot\sum_{j=1}^{12}\ddot{q}_j(t)\cdot N_j\right]\cdot N_i\ dxdy=0 \tag{2.23}$$

Equation (2.23) can be rewritten as:

$$\sum_{j=1}^{12}\left(\ddot{q}_j\cdot m_{i,j}+q_j\cdot k_{i,j}\right)=0 \tag{2.24}$$

Here $m_{i,j}$ and $k_{i,j}$ are coefficients of the mass and the stiffness matrices of the finite element:

$$m_{i,j}=\frac{1}{c_0^2}\int_0^{l_1}\int_0^{l_2} N_i\cdot N_j\ dxdy \tag{2.25}$$

$$k_{i,j}=-\int_0^{l_1}\int_0^{l_2}\left(\frac{\partial^2 N_j}{\partial x^2}+\frac{\partial^2 N_j}{\partial y^2}\right)\cdot N_i\ dxdy \tag{2.26}$$

The global finite element equation is (here $\{B_w\}$ is the global load vector incorporating known values of potential and velocity on the boundary):

$$[M_w]\{\ddot{Q}_w\}+[K_w]\{Q_w\}=\{B_w\} \tag{2.27}$$

The time integration of equation (2.27) is performed by application of the Newmark method.

At time moment $t=0$:

$$\varphi=0$$

$$\frac{\partial\varphi}{\partial t}=0 \tag{2.28}$$

The boundary conditions are the following:

$$\frac{\partial\varphi}{\partial y}=V_{rb} \text{ under the rigid body}$$

$$\frac{\partial\varphi}{\partial n}=0 \text{ at the bottom and at the sides of the water tank} \tag{2.29}$$

$$\varphi=0 \text{ on the free surface}$$

The 1D code described earlier was extended to a 2D situation. If the width "b" of the rigid body corresponds to the width of the water tank "B" the problem has exactly the same solution as the 1D problem discussed before.

A number of models were developed in order to find the model sensitivity with respect to the number of finite elements, time increment, minimum number of elements under the rigid body etc. The results of the simulation were compared with an analytical solution, which is available for this problem. It was found that a model with a larger number of elements (especially larger number under the rigid body) gives better fitting of the analytical curve. If the time increment satisfies the Courant criterion mentioned before the analysis is stable. The analytical solution, which was used, predicts the hydrodynamic force on the rigid body as a function of time (it is assumed that the depth of the area is infinite, and the rigid body penetrates into the water with constant velocity) [39].

$$F = 2b\rho_0 c_0 V_{rb}\left(1-\frac{c_0 t}{2b}\right) \tag{2.30}$$

$F$ is hydrodynamic force per unit length since a 2D problem is under consideration.

Results of calculations are shown in Figure 2.10. A good agreement is found. The initial oscillations in Figure 2.10 occurring in the beginning of the impact in the numerical solution are caused by the time integration procedure.

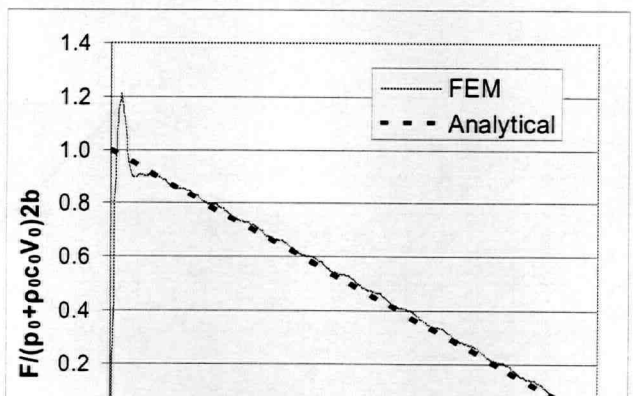


Figure 2.10. Hydrodynamic force on the rigid body as a function of time

### 2.3.2 Finite element method for incompressible fluid

The compressible fluid model discussed above is based on the wave equation. This means that the application of finite element analysis gives the solution in the time domain. However the incompressible potential flow is based on the Laplace equation, which requires a different treatment. Solution of the Laplace equation for a particular time moment with a particular set of boundary conditions gives a distribution of the velocity potential in the fluid region. This is a so called "linear solution". At the same time the slamming problem assumes that the structure penetrates into water. The boundary conditions change. The free water surface elevates. The Laplace equation has to be solved again. An incremental solution takes place. In other words the solution of the problem consists of step-wise linear solutions. The pressure in the water is found as a change of potential between the time increments. It is done in the same way as for the compressible flow (equation 2.13).

The author started the development of an incompressible potential flow model with consideration of linear solution. A simple 2D model for incompressible fluid is discussed in this section. The geometry of this model is similar to the model described in the previous section for compressible flow except the type of finite element (Figure 2.11). Here the water domain is subdivided into triangular elements. These elements are quite simple at the same time allowing easy mesh generation.

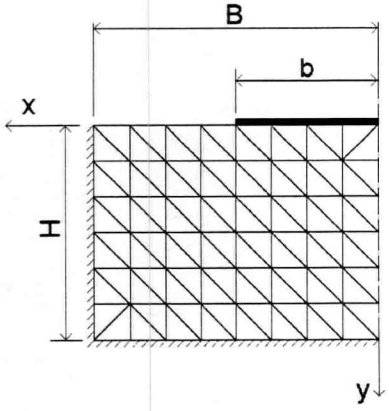


Figure 2.11. 2D model

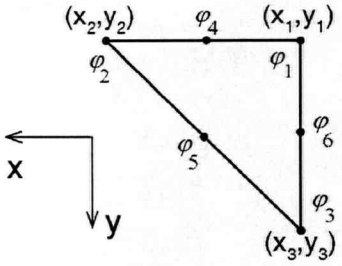


Figure 2.12. 2D triangular finite element

The governing equation for incompressible water is the Laplace equation:

$$\frac{\partial^2 \varphi}{\partial x^2} + \frac{\partial^2 \varphi}{\partial y^2} = 0 \qquad (2.31)$$

In order to obtain accurate results a quadratic approximation function is applied [33]. This function requires that the triangular element should have six nodes (Figure 2.12). Each node has one degree of freedom: the velocity potential $\varphi$. The quadratic approximation function is:

$$\varphi(x) = \alpha_1 + \alpha_2\xi_1 + \alpha_3\xi_2 + \alpha_4\xi_1^2 + \alpha_5\xi_1\xi_2 + \alpha_6\xi_2^2 \tag{2.32}$$

Here $\xi_1$ and $\xi_2$ are special coordinates of a triangle coordinate system. Coordinates in x-y coordinate system can be represented as:

$$\begin{aligned} x &= x_1\xi_1 + x_2\xi_2 + x_3\xi_3 \\ y &= y_1\xi_1 + y_2\xi_2 + y_3\xi_3 \end{aligned} \tag{2.33}$$

The following shape functions are derived:

$$\begin{aligned} N_1 &= \xi_1(2\xi_1 - 1) \\ N_2 &= \xi_2(2\xi_2 - 1) \\ N_3 &= \xi_3(2\xi_3 - 1) \\ N_4 &= 4\xi_1\xi_2 \\ N_5 &= 4\xi_2\xi_3 \\ N_6 &= 4\xi_3\xi_1 \end{aligned} \tag{2.34}$$

The vector of unknown degrees of freedom is defined:

$$\overline{q} = \left[\xi_1(2\xi_1 - 1), \xi_2(\xi_2 - 1), \xi_3(2\xi_3 - 1), 4\xi_1\xi_2, 4\xi_2\xi_3, 4\xi_3\xi_1\right] \tag{2.35}$$

The potential $\varphi$ can be represented as:

$$\varphi = \sum_{j=1}^{6} q_j(t) \cdot N_j \tag{2.36}$$

After substitution of this approximation in equation (2.31), taking into account the change of coordinate system and application of Bubnov-Galerkin's procedure, the stiffness matrix is found. The global finite element equation is:

$$[K_w]\{Q_w\} = \{B_w\} \tag{2.37}$$

The global load vector $\{B_w\}$ incorporates the following known values of potential and velocity on the boundary:

$$\begin{aligned} &\frac{\partial \varphi}{\partial n} = -V_{rb} \text{ under the rigid body} \\ &\frac{\partial \varphi}{\partial n} = 0 \text{ at the bottom and at the sides of the water tank} \\ &\varphi = 0 \text{ on the free surface} \end{aligned} \tag{2.38}$$

Solution of equation (2.37) gives a distribution of the velocity potential in the water domain. This is a linear solution, which corresponds to particular set of boundary conditions. A new code was developed to treat this incompressible water model. In order to verify the code a linear solution for a cylinder penetrating into the water was considered (Figure 2.13). Half of the area is modeled because of symmetry. An analytical solution is available. This solution predicts the velocity potential under the cylinder as a function of position along the contour [53]:

$$\varphi = V_0 R \sin\theta \tag{2.39}$$

The analytical solution assumes that the remote boundary is infinitely far away in the x- and y-directions. However in the numerical analysis the remote boundary was modeled as a rigid wall. A number of simulations were carried out in order to find the model sensitivity with respect to the number of finite elements, and the location of the remote boundary. Figure 2.14 shows that there is no significant influence of the rigid wall if the ratio $r/R \geq 8$. The ratio $r/R = 4$ gives 12% increase of potential. Here R is the radius of cylinder, and r is the distance from the center of coordinate system to the remote boundary.

Contrary to the linear solution considered above a time dependent problem of water penetration is non-linear and requires an incremental solution. Equation (2.37) has to be solved for each time increment, taking into account the dynamically changing boundary conditions including the free water surface elevation and the changes of the contact area between the structure and the water. This approach consisting of step-wise linear solutions will be discussed in Section 2.3.5.

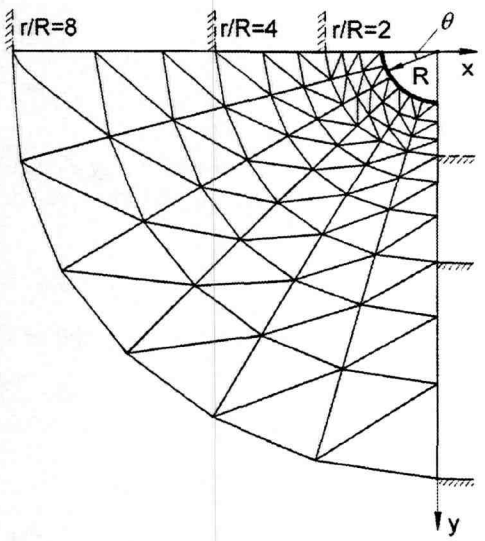


Figure 2.13. 2D model for cylinder

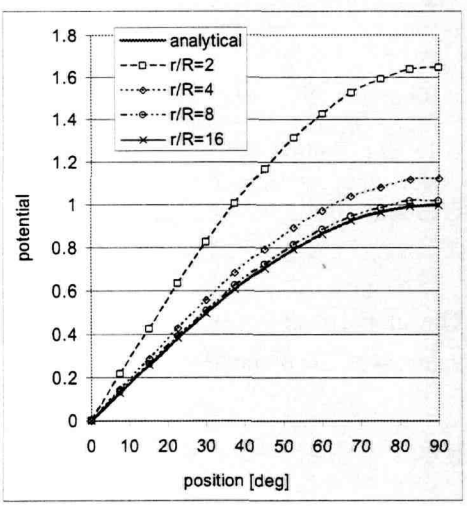


Figure 2.14. Velocity potential

### 2.3.3 Boundary element method for incompressible fluid

In order to study the boundary element method a simple model was considered (Figure 2.15). This model is exactly the same as the model of the previous section except that the boundary element method is applied instead of the finite element analysis. A linear solution of the Laplace equation is considered. The boundary conditions are the same as in the previous section (equation 2.38).

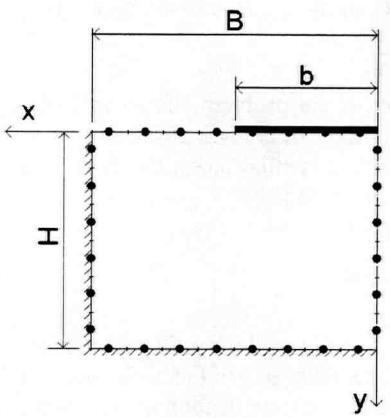


Figure 2.15. The model.

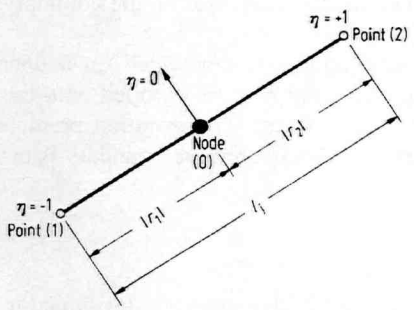


Figure 2.16. Constant boundary element.

The governing equation is the Laplace equation (equation 2.31). A constant boundary element with one node in the middle is applied for this model (Figure 2.16). The value of the velocity potential $\varphi$ and the velocity $\frac{\partial \varphi}{\partial n}$ are taken to be constant on each element and equal to their values at the midnode of the element. In each element the value of one of the two variables ($\varphi$ or $\frac{\partial \varphi}{\partial n}$) is known. Application of boundary element method gives the following equation [27]:

$$\frac{1}{2}\varphi_i + \int \varphi \frac{\partial \varphi^*}{\partial n} d\Gamma = \int \frac{\partial \varphi}{\partial n} \varphi^* d\Gamma \tag{2.40}$$

The integrals in (2.40) are taken over the water region boundary $\Gamma$.
Equation (2.40) can be rewritten as:

$$\frac{1}{2}\varphi_i + \sum_{j=1}^{N} \hat{H}_{ij}\varphi_j = \sum_{j=1}^{N} G_{ij}\left(\frac{\partial \varphi}{\partial n}\right)_j \tag{2.41}$$

Here $i$ is the node number and $j$ is the element number.
The following fundamental solution is available for the Laplace equation for the 2D case ($r$ is the distance from the source point to the field point):

$$\varphi^* = \frac{1}{2\pi}\ln\left(\frac{1}{r}\right) \tag{2.42}$$

The global boundary element equation is:

$$[H]\{U\} = [G]\{Q\} \tag{2.43}$$

The vector $\{U\}$ specifies the velocity potential on the boundary. The vector $\{Q\}$ includes the velocities. Solution of the equation (2.43) defines unknown values of velocity potential and velocities on the boundary.

A new code was developed for a linear solution of the problem shown in Figure 2.15, where a rigid body is dropped onto the water surface. An analytical solution is available for this problem. This solution predicts the velocity potential along the rigid body (it is assumed that the remote boundary is infinitely far away) [53]:

$$\varphi = V_{rb} b \sqrt{1 - \frac{x^2}{b^2}} \tag{2.44}$$

A number of models were developed in order to find the model sensitivity with respect to the number of boundary elements, number of elements under the rigid body, relation between the width and the depth of the water domain etc. Application of a greater number of boundary elements gives more accurate solution. Results of one of the models with a fine mesh are shown in Figure 2.17-Figure 2.18. The potential distribution in the water domain is shown in Figure 2.17. Comparison of the numerical results with the analytical solution is shown in Figure 2.18. Here the distribution of the potential along the rigid body is plotted. The numerical solution gives a 5% increase of the velocity potential in comparison with the analytical solution because the application of the rigid wall boundary condition. Here the relation between the width of the rigid body and the width of the water domain is 1:4. The depth of the water domain equals the double width of the rigid body. Modelling of the water region with larger depth and width reduces the difference between the numerical results and the analytical solution.

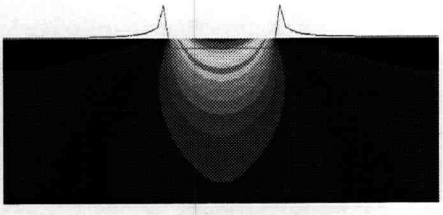

Figure 2.17. Velocity potential

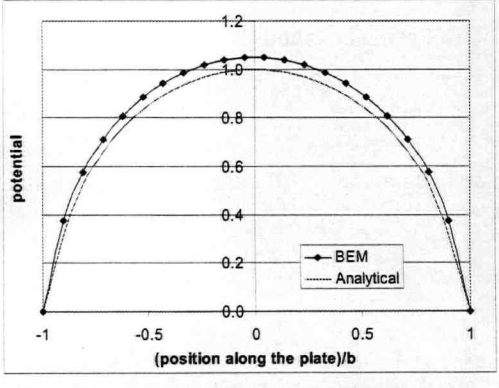


Figure 2.18. Potential under the rigid body

### 2.3.4 Structural analysis

Finite element analysis is applied for simulation of the structural response. A 2D case is modeled considering a cross-section of the ship's hull. For a case when this cross-section is assumed to be rigid and only the bottom of this cross-section is flexible the following model can be used. A 2D structure consisting of two beams connected at the center line (CL) is supported at its ends (the points where the side shells are originally located). The structure experiences hydrodynamic pressures p(t) (Figure 2.19). W(t) is the vertical displacement at CL.

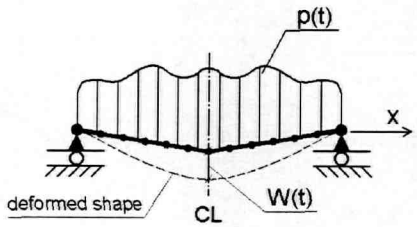


Figure 2.19. The model

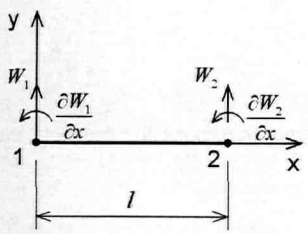


Figure 2.20. Beam finite element

A simple beam finite element is chosen for this model. The element has two nodes (Figure 2.20). Each node has two degrees of freedom, which include displacement and rotation. No axial force is considered in order to simplify the model.

The differential equation for this beam element is (the nodal forces already include the distributed loads):

$$EIW^{IV}(x) = 0 \tag{2.45}$$

The following cubic approximation function for beam displacement is used for this finite element [98]:

$$W(x) = \alpha_1 + \alpha_2 x + \alpha_3 x^2 + \alpha_4 x^3 \tag{2.46}$$

This approximation function is the same as for the 1D finite element for compressible fluid (equation 2.3). Consequently the shape functions are also the same (equation 2.4). These shape functions satisfy the following vector of unknown values:

$$\overline{q} = \left[ W_1, \frac{\partial W_1}{\partial x}, W_2, \frac{\partial W_2}{\partial x} \right] \tag{2.47}$$

Applying the shape functions (2.4) the displacement W can be represented as:

$$W = \sum_{j=1}^{4} q_j(t) \cdot N_j \tag{2.48}$$

In order to determine the element stiffness matrix the potential energy of element is considered:

$$E_{potential} = \frac{1}{2} EI \int_0^l [W''(x)]^2 dx \tag{2.49}$$

Then the approximation (2.48) is substituted into this equation:

$$E_{potential} = \frac{1}{2} \sum_{i=1}^{4} \sum_{k=1}^{4} k_{ik} q_i q_k \tag{2.50}$$

Here $k_{i,j}$ is the stiffness matrix of finite element:

$$k_{i,k} = EI \int_0^l \frac{\partial^2 N_i}{\partial x^2} \cdot \frac{\partial^2 N_k}{\partial x^2} dx \tag{2.51}$$

The mass matrix of the element can be found from consideration of kinetic energy:

$$E_{kinetic} = \frac{1}{2} \overline{m} \int_0^l \dot{W}^2(x,t) dx \tag{2.52}$$

Here $\overline{m}$ is mass per unit length of element.
The approximation (2.48) is substituted into this equation:

$$E_{kinetic} = \frac{1}{2} \{\dot{q}(t)\}^T [m] \{\dot{q}(t)\} \tag{2.53}$$

Here $m$ is the mass matrix of finite element:

$$m_{i,k} = \overline{m} \int_0^l N_i(x) \cdot N_k(x) dx \tag{2.54}$$

The global finite element equation is (here $\{P_s\}$ is the global load vector):

$$[M_s]\{\ddot{Q}_s\} + [K_s]\{Q_s\} = \{P_s\} \tag{2.55}$$

The time integration is performed in the same way as for the compressible water domain with application of the Newmark time integration method.

### 2.3.5 Fluid-structural coupling

In the previous sections the water and the structural models are described separately. Now the fluid-structural coupling will be introduced. The fluid-structural model with boundary conditions is shown in Figure 2.21. For both the water domain and the structural analysis an Eulerian mesh is applied [17]. For small structural deformations the application of the Eulerian mesh for the structural analysis will be quite accurate. Contrary to the structural analysis, a Lagrange mesh would be desirable for the fluid analysis. On the one hand, the penetration of the structure into the water as well as the free water surface elevation would

require remeshing of the fluid domain. On the other hand, implementation of a Lagrange mesh, requiring the usage of a remeshing algorithm, is rather complicated. In view of the above, the author decided to use an Eulerian mesh for the fluid analysis instead of a Lagrange mesh. This decision is taken in order to simplify the model and it is based on the assumption that the geometry of the model boundaries does not change much during the analysis. Obviously this assumption reduces the accuracy. Nevertheless, the expected error will not be critical since quite small deadrise angles are considered (in the range of 0-10 degrees). The water impact takes quite short time. The penetration of the structure into the water and the free water surface elevation are not large. Application of an Eulerian mesh also means that no water spray is considered, which also introduces inaccuracy in the model. In order to check the validity of these assumptions this approach will be compared with other solutions in Section 2.5.

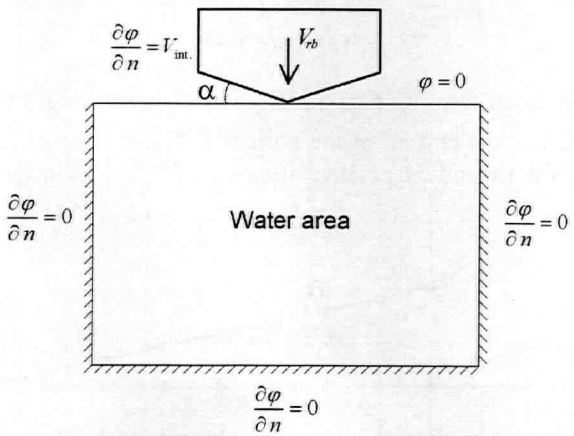


Figure 2.21. The fluid-structural model

To introduce the interface between the structure and the water a simplified contact problem is solved. In the first place the contact area has to be defined. The number of structural nodes is chosen so that this number corresponds to the number of water nodes in the interface area (Figure 2.22). The application of an Eulerian mesh does not support re-meshing of the water region in order to follow the free surface elevation. However, the free surface elevation is approximately defined through the vertical velocities of nodes lying on the free water surface. Defined in such a way, a new shape of the free surface is used to determine the contact boundary. This contact algorithm can be easily explained from consideration of Figure 2.22. Initially only one structural node is in contact with a water node. This node lies at the symmetry axis. During the impact the structure penetrates into the water and the structural nodes $n_i^s$ move downwards. At the same time the water nodes $n_i^w$ on the free surface move up due to elevation of the free water surface. Only vertical motion of nodes is considered. As soon as a new structural node comes into contact with a new water node the contact area increases. Both the structural and the water mesh remain the same. The contact algorithm allows redefining the boundary conditions only.

Clearly the consideration of the vertical velocities only is a quite severe assumption. Nevertheless, Section 2.5 will show that this assumption is not so critical. Moreover this approach gives a significant simplification of the contact algorithm of the program.
There are two types of boundary conditions in the interface area. Flow velocity is specified within the contact area for the fluid analysis. Hydrodynamic pressures are defined for the structural analysis. Figure 2.23 shows boundary conditions for the water domain within and outside of the contact area. The potential is zero on the free water surface outside of the contact area. The water boundary involved in the contact has the following boundary condition:

$$\frac{\partial \varphi}{\partial n} = -V_{\text{int.}} \tag{2.56}$$

The interface velocity boundary condition can be found as:

$$V_{\text{int.}} = V_{rb}(t)\cos(\alpha) - V_{str}(t) \tag{2.57}$$

Here $V_{rb}(t)$ is velocity of the ship penetration into water as a rigid body and $V_{str}(t)$ is velocity of deflection of the bottom in the normal to the bottom direction. The positive direction of $V_{rb}(t)$ is down and the positive direction of $V_{str}(t)$ is inside of the hull.

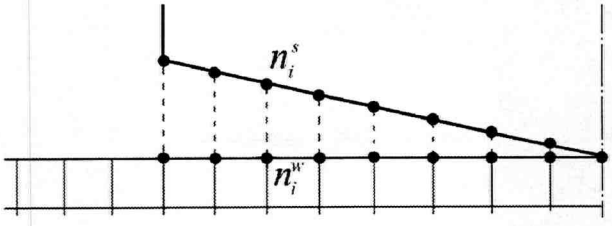


Figure 2.22. Contact area definition

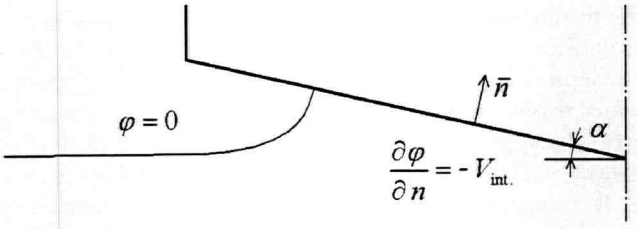


Figure 2.23. Contact boundary conditions

### 2.3.6 Final code

For the structural response and coupling algorithm the author considered only one approach (Section 2.3.4 and 2.3.5). However, for the fluid analysis there were more options. Both compressible and incompressible potential flows were considered with application of finite element analysis. The incompressible potential flow was also

modeled using a boundary element method. The good accuracy of all these approaches was confirmed comparing these approaches with analytical solutions. The goal, however, was to develop a code, which is quite simple but at the same time capable of modeling the hydroelastic problem. One of the intentions of the author was to evaluate the effect of water compressibility as well. For this reason it was decided to keep both the compressible and incompressible fluid models. For the incompressible flow the author had two possibilities of modeling: the finite element analysis (Section 2.3.2) and the boundary element method (Section 2.3.3). Both these approaches showed good accuracy. Nevertheless the author decided to use the finite element analysis only. It was much easier for programming since all other blocks of the final code would use the finite element analysis.

The final code incorporates the 2D model for compressible potential flow (Section 2.3.1), the 2D model for incompressible potential flow (Section 2.3.2), the 2D structural model (Section 2.3.4), and the interface algorithm described in Section 2.3.5. The structure of the code is shown in Figure 2.24. The code consists of two main blocks. The first block performs the water simulation. The incompressible or compressible potential flow models can be chosen. The second block performs the structural analysis. The author chose the weak formulation for fluid-structural coupling as it was explained in Section 1.5.2. The application of the weak formulation means that the fluid-structural coupling is performed not simultaneously at each time increment but with one time increment delay. At time moment zero, $t = 0$, the speed of the structure as a rigid body is known. The contact area between the water and the structure is found. The speed of the structure is the boundary condition for the water within the contact area. The fluid simulation is performed for the first time increment. The hydrodynamic pressures under the structure are found. These pressures are applied and the structural simulation is performed for this time increment. A new time increment $t = t + \Delta t$ starts. Again a new contact area is defined. This time not only the global structural motion as a rigid body is considered but also the structural response from the previous time step (meaning one step delay) is taken into account. New pressures are obtained. This allows performing a new increment for the structural simulation. The cycle repeats.

The code is written in FORTRAN. It has 79 subroutines with in total about 4500 statements. An additional code has been developed for post-processing of results. It shows animations of the pressure wave propagation in the water. It is also possible to make the most important plots.

With respect to the choice between the compressible and incompressible fluid models the following was found. Due to the fact that the code is based on the weak coupling formulation the incompressible fluid model appeared to be very unstable when the hydroelastic problem has to be solved. At the first time increment the structure is assumed rigid. Quite high hydrodynamic pressures are obtained. These pressures cause excessive structural response. This response leads to extreme reduction of pressures or even negative pressures at the second time step. The following increments bring an increase of oscillations. The analysis fails. Even the application of a very small time increment can not improve the stability of the analysis. Contrary to the incompressible flow the

compressible flow is treated as a transient dynamic process. The initial oscillations are damped out. The analysis runs steadily. This is the reason why almost all models based on the self-developed code and considered in this thesis use the compressible flow model. However the effect of water compressibility is studied in Section 3.6 where the compressible flow model is compared with incompressible flow model for a case of rigid body water penetration.

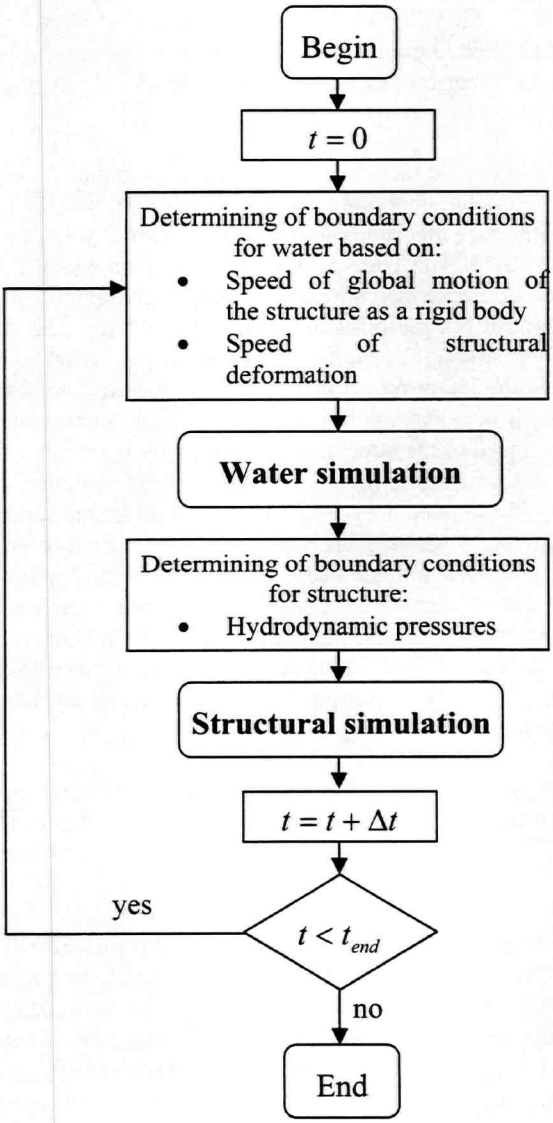


Figure 2.24. Structure of the code

## 2.4 Commercial codes

Development of new software is quite a heavy task. On the one hand such software is developed especially for the problem which has to be solved. Besides, the development of such code leads to better understanding by the author, of the problem, its physics and mechanism of interaction. On the other hand the capabilities of this software are limited. The code is not flexible. Moreover, investigation of 3D problems is impossible with the present code. These obvious reasons brought the author to the point of considering existing commercial packages.

### 2.4.1 Combination of self-developed code with MSC.Marc

As the first step the author decided to replace the structural analysis with an existing commercial code keeping the hydrodynamic part of the self-developed code [14]. This replacement would allow using a commercial code, which is very flexible for the structural analysis. At the same the fluid code developed by the author would give freedom in experimenting with fluid simulation. Numerical results discussed in this section will show the possibilities of the combination of the self-developed code with commercial software and will give conclusion if this approach can be useful for investigation of hydroelastic slamming problem.

MSC.Marc package was chosen for the structural analysis. The MSC.Marc is a commercial general purpose program for nonlinear finite element analysis [90]. Many different material models and types of finite elements are implemented in the code covering a large range of problems. This code also treats dynamic problems. Besides, this commercial software has a very advanced interface by means of user subroutines. Many different parameters can be read and modified during the simulation.

In Figure 2.24 MSC.Marc replaces the block "structural simulation". The compressible potential flow model is taken for the water simulation. The interface between the water domain and the structure is provided through application of two user subroutines available in MSC.Marc: FORCDT and IMPD. The FORCDT subroutine specifies the loads on the structure. The IMPD subroutine delivers the velocity of structural vibration thus defining boundary conditions for the fluid domain. The Newmark time integration scheme is chosen in MSC.Marc for this transient analysis. The time step is chosen from the point of stability of the integration and is the same for both domains.

First, it was decided to check if both the self-developed code and the coupled code give similar results. A simple 2D model was considered. The model is shown in Figure 2.1. The model consists of a body with flexible bottom structure (as described in Section 2.3.4) penetrating into the water with a constant velocity of 2.5 m/s. The water tank has a width of 5.6 m and a depth of 2.3 m. The width of the body is 2.5 m. These water tank and structural dimensions correspond to the TNO experimental setup (Section 2.2). The deadrise angle is zero. The flexible bottom is modeled as a beam supported at the ends and has properties which are quite close to the properties of the 14 mm steel panel in the

TNO experiment. The principal moment of inertia of the beam cross-section about the relevant centroidal axis (later in this thesis it will be called "moment of inertia") is 1.27e-5 $m^4$. The mass per unit length is 134.8 kg/m. Both the air entrapment and the gravity force are neglected.

Two simulations were performed. In the first case the problem was solved with application of the self-developed code. In the second case the coupled code was deployed. A Newmark time integration procedure was used in the both models for water simulation and for the structural analysis. A time plot of deflection of the bottom in the center relatively to undeformed shape (later in this thesis it will be called "displacement") is shown in Figure 2.25. A perfect agreement is found for both models. This gives confidence that the both structural parts of the codes work in a consistent way.

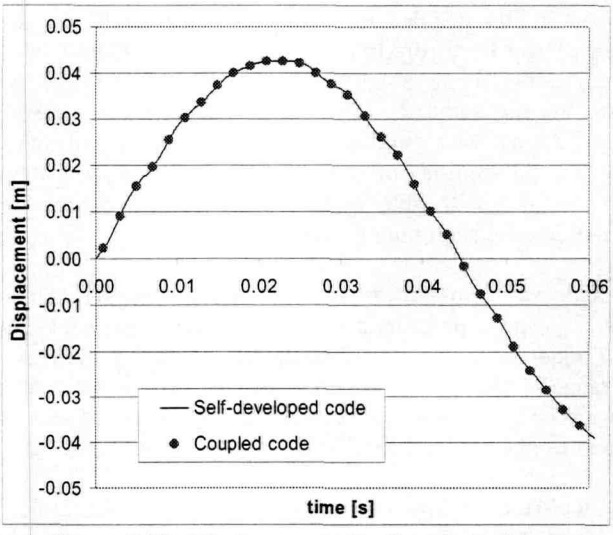


Figure 2.25. Displacement as a function of time

A new case was considered. Again the slamming test performed by TNO (described in Section 2.2) was studied. 2D and 3D structural models were created with application of MSC.MARC code. The 2D model is similar to the model described above, but the boundary conditions for the structure in the new model are described more accurately. The beam shown in Figure 2.26 represents a 2D model consisting of beam elements (MSC.Marc beam element N 52). The beam is supported close to its ends and at the points where the stiffeners of the TNO panel are located (Figure 2.3). Loads obtained from the water simulation are applied to the nodes of the structural model in the z direction. The moment of inertia and the area of cross-section of the beam are defined so that the beam reproduces approximately the same deflection under a uniform distributed load as the 14 mm steel panel from the test and possesses the same first vibration frequency.

The 3D structural model is shown in Figure 2.27 and consists of shell elements (MSC.Marc shell element N 75). The panel is supported at the sides and the node loads are applied in the z direction.

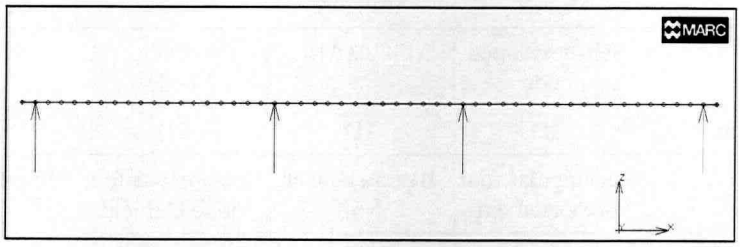


Figure 2.26. 2D mesh of the structure (element N 52)

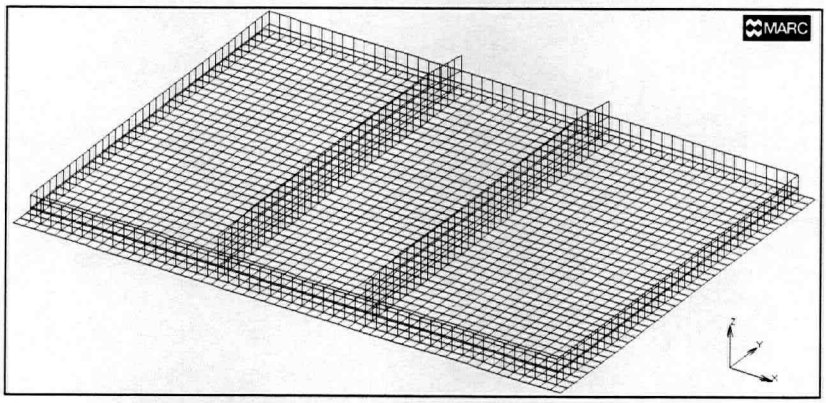


Figure 2.27. 3D mesh of the structure (element N 75)

In both cases the 2D and the 3D structural modes were coupled with a 2D fluid model since only a 2D situation is implemented in the fluid part of the self-developed code. These models are described in Table 2.1. The model N1 is purely two-dimensional. Application of a 2D beam model in MSC.Marc corresponds to a 2D-water model. In the model N2 a 2D-water model is coupled with a 3D model of the panel in MSC.Marc.

Since the self-developed code can only model the 2D situation, a special approximate technique was applied for the model N2. Hydrodynamic pressures obtained from the water simulation were applied directly to the corresponding nodes of the MSC.Marc model along the center line (along the x- axis of symmetry in Figure 2.27) $p(y=0) = p_{mid}$, in addition the same loads were applied to the rest of the structure along the y- axis in Figure 2.27 with parabolic reduction at the sides $p(y) = p_{mid}(1-(y/b)^2)$. Here $b$ is the distance from the center to the side of the panel in y- direction. Figure 2.28 shows the model combined of the two parts.

Table 2.1. Description of the models

| | Model N1 | | Model N2 | |
|---|---|---|---|---|
| | Water | Structure | Water | Structure |
| Software | Self-developed code | MSC.MARC | Self-developed code | MSC.MARC |
| Dimensions | 2D | 2D | 2D | 3D |
| Type of FE | Rectangular four node element | Beam element N52 | Rectangular four node element | Shell element N75 |
| Time integration | Newmark | Newmark | Newmark | Newmark |

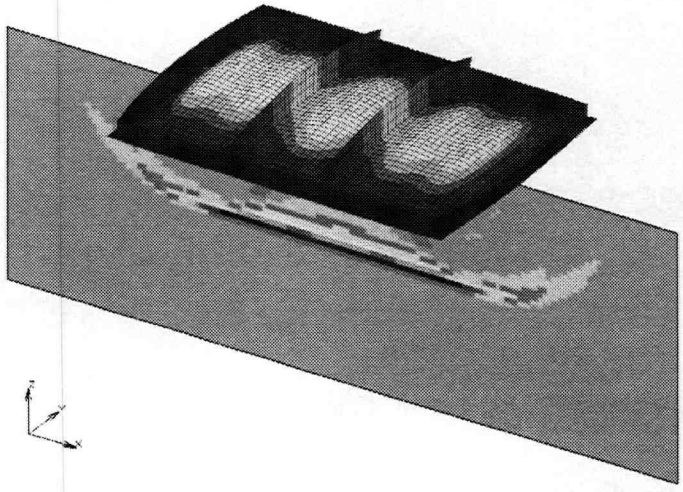

Figure 2.28. Combined model

It is important to mention that the stability of calculations plays a key role in the achievement of a successful simulation of the present hydroelastic problem. The behavior of the water and the structure are modeled in the time domain through application of direct time integration procedures. If only one part of the model experiences lack of stability, it brings a disturbance to the other part – thereby causing the whole simulation to become unstable. Due to this, a large number of simulations was carried out for the combined model as well as separately for each of the parts. The purpose of the simulations was to find the best parameters for time integration procedures. It was found that the Newmark method with coefficients set to give some damping provides the best results for both the water simulation and the structural analysis.

The maximum displacements of the structure have been studied as well as the acoustic wave propagation in the water domain. Results for the model N1 are shown in Figure

2.29-Figure 2.32. The magnified deformed shape of the beam from the 2D MSC.Marc model for time $t = 0.001\,\mathrm{s}$ is shown in Figure 2.29. Figure 2.30 illustrates the pressure distribution in the water corresponding to the same time moment. Figure 2.31 shows the displacement of the beam in two points. The location of the points is indicated in Figure 2.32.

The 3D panel from the model N2 is shown in Figure 2.33. The results of model N2 are given in Figure 2.34-Figure 2.36. Figure 2.34 illustrates the pressure distribution. Figure 2.35 shows the displacement of the panel in three points. The location of the points is indicated in Figure 2.36.

Comparison of the total hydrodynamic force on the structure as a function of time for the model N1 and the model N2 is shown in Figure 2.37. The first peak on the graph is caused by the maximum pressures, which appeared in the beginning of the impact. The secondary peaks following each other indicate the return of the acoustic waves reflected from the water tank bottom. The locations of the maximum displacements in both simulations are found in the point between the side and the stiffener (point N1 in Figure 2.32 and Figure 2.36). Comparison of displacements in the point N1 for both simulations is shown in Figure 2.38. In spite of the application of quite a simplified approach for definition of the beam properties in the model N1, the results of both simulations are in a good agreement. The only real discrepancies are that the hydrodynamic force in the model N1 in the beginning of the impact is slightly higher in comparison with the model N2 and that the 2D beam needs less time to reach the maximum displacement in the point N1. This difference exists because the 2D-beam model has an extra support in the point where in the 3D structural model the stiffener is located (Figure 2.26). As a result this point of the 2D model cannot move in the z direction while in the 3D case the stiffener has some freedom. This makes the 2D beam model stiffer, which results in a higher natural frequency of vibration. The same effect results in slightly different pressure distributions (Figure 2.30 and Figure 2.34).

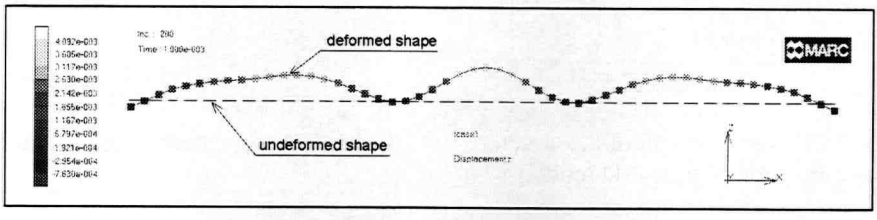


Figure 2.29. 2D MSC.Marc model ( $t = 0.001\,\mathrm{sec}$ )

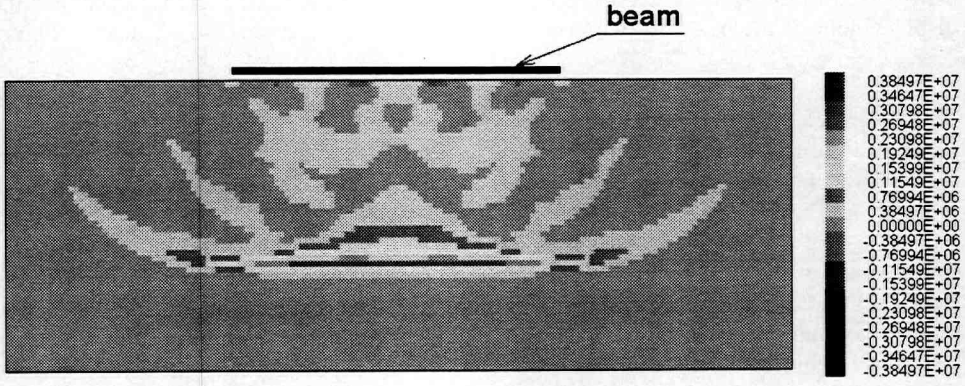


Figure 2.30. Pressure distribution in the water ( $t = 0.001$ sec )

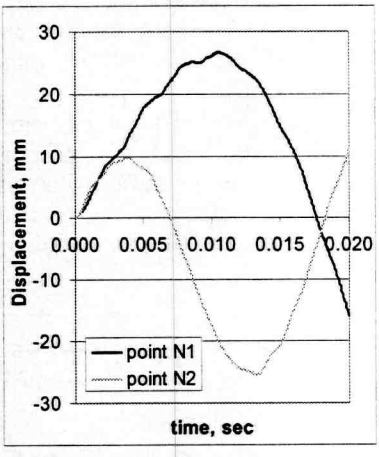


Figure 2.31. Displacement of the structure as a function of time (2D model)

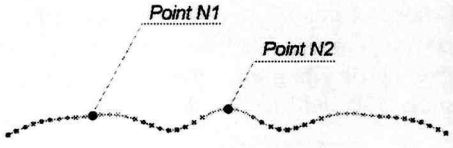


Figure 2.32. Location of the points

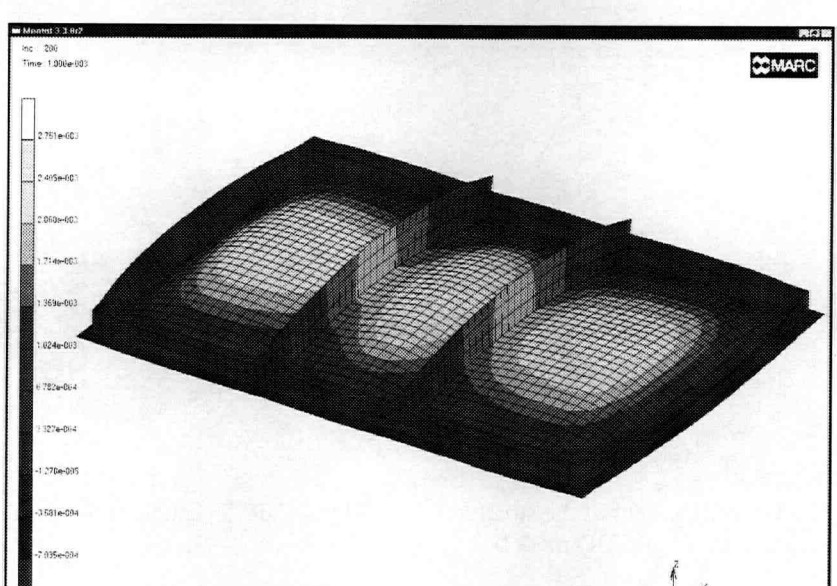


Figure 2.33. 3D MSC.Marc model ( $t = 0.001\,\text{sec}$ )

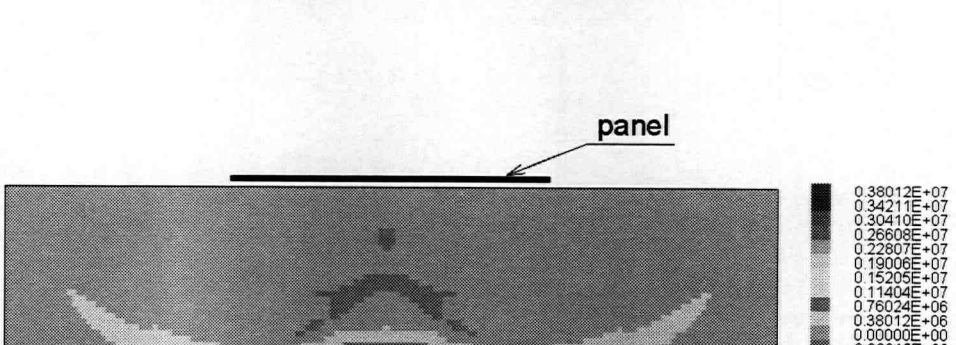


Figure 2.34. Pressure distribution in the water ( $t = 0.001\,\text{sec}$ )

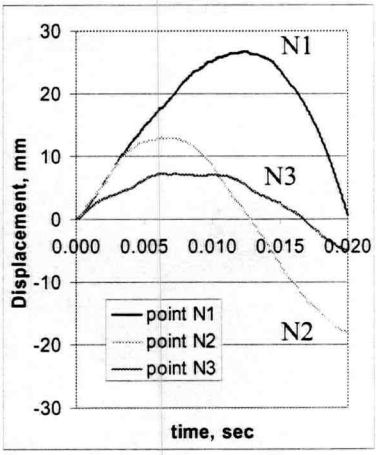


Figure 2.35. Displacement of the structure as a function of time (3D model)

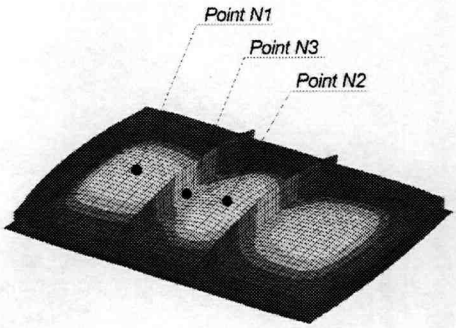


Figure 2.36. Location of the points

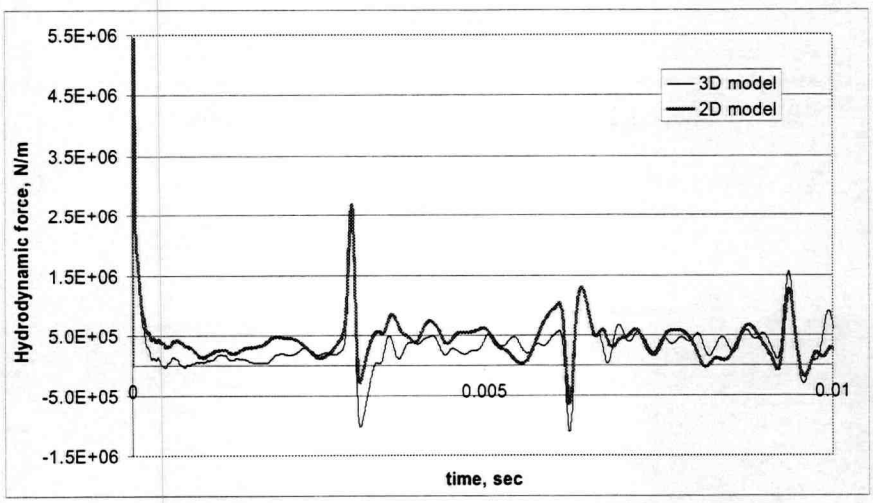


Figure 2.37. Hydrodynamic force on the structure as a function of time

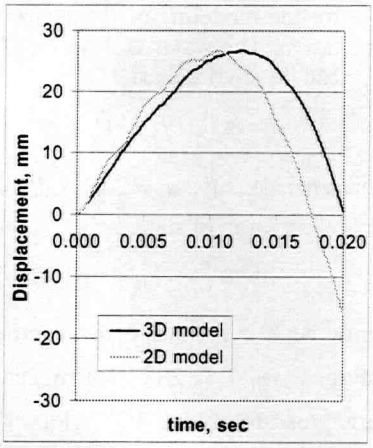


Figure 2.38. Displacement of the structure as a function of time (point N1)

Summarizing the results it can be stated that the combination of MSC.Marc and the self-developed code is a powerful and flexible tool for studying the hydroelastic problem. Changes of geometry and other parameters of the water domain as well as changes of the structural model in MSC.Marc can be performed separately from each other giving a considerable degree of freedom for investigation of the bottom-slamming phenomenon. This is the advantage of the weak formulation for the fluid-structural coupling as it is explained in Section 1.5.2.

However, application of the 2D-water model coupled with 3D MSC.Marc structural analysis can not provide a completely accurate prediction of the interaction since the real nature of this phenomenon is three-dimensional. Only further development of the self-developed code to 3D could give more precise results. At this point the author decided to switch from further development of his own code to the application of MSC.Dytran.

### 2.4.2 MSC.Dytran

MSC.Dytran is commercial software, and is a 3D-analysis code based on an explicit integration procedure, which can be used for dynamic fluid-structure interaction problems [89]. For the structural analysis a finite element formulation is used with application of a Lagrange mesh, which allows accurate modeling in the case of large structural deformations. The fluid analysis is performed using the finite volume formulation and application of an Eulerian mesh. In MSC.Dytran the Eulerian mesh is fixed in space but material can flow through the mesh. Several different materials can be defined within the Eulerian mesh. This is a major step forwards since in MSC.Dytran modeling of air entrapment becomes possible. A coupling procedure introduced within the code provides the fluid-structure interaction at each time increment. The loads obtained from the fluid analysis are applied to the structure and the structural response is the boundary condition for the fluid analysis. This allows modelling of hydroelastic interaction.

There are several possibilities for the modeling of fluids and gases. The following model was chosen for the water simulation. The water is described by a polynomial equation of state, which for the linear case can be rewritten as:

$$p = a_1(\rho/\rho_0 - 1) \tag{2.58}$$

Here $\rho_0 = 1000$ kg/m$^3$ is reference density; $a_1 = 2.25$ GPa is the bulk modulus.
Air is described by a gamma law equation of state:

$$p^{air} = (\gamma - 1)\rho^{air} e \tag{2.59}$$

Here $\gamma = 1.4$ is ratio of specific heat; $e$ is the specific internal energy per unit mass. The initial density of air is assumed $\rho_0^{air} = 1.2887$ kg/m$^3$ and $e = 196000$ J/kg, which corresponds to the atmospheric pressure $p_0 = 0.101$ MPa.

The water and air regions have to be subdivided into Eulerian solid elements. But the strict boundary between the water and air elements exists in the beginning of the analysis only. Later on, some elements become devoid of water because they are covered by the structure. Also a water-air mixture is formed near the free surface and the impact area. This means that some elements can be partly filled with air and water at the same time. If the model includes both water and air, atmospheric pressure is initially applied to both domains. If no air is modeled (the top part of the mesh consists of so called "void" elements) the cavitation pressure in water is assumed $p_{cav} = -0.101$ MPa. A flexible structure can be modeled with shell elements. If the intention is to run the analysis neglecting the effect of hydroelasticity the analysis is performed in two steps. First a problem of water penetration of a rigid body is simulated. The hydrodynamic pressures on the body are stored. Then the second analysis starts when only a dry structure is considered under the pressure loads from the previous simulation. The MSC.Dytran user-subroutine EXPLD is employed to apply these loads.

### 2.4.3 LS-Dyna

The LS-Dyna code is quite similar to MSC.Dytran. The LS-Dyna also allows modelling the fluid-structure interaction problem, where air can also be present. Equations of state for water and air can be taken the same as for the MSC.Dytran model described above. Information about LS-Dyna is very limited in this thesis since this software was not available for this research project. However, a very simple problem was solved with application LS-Dyna at TNO in order to compare LS-Dyna and MSC.Dytran. The results of this comparison are described in the next section.

## 2.5 Comparison of approaches

In order to compare the different software described above a simple 2D model is considered. The model is shown in Figure 2.1. The model consists of a wedge-shaped flexible body penetrating into the water with a constant speed of 2.5 m/s. The water tank has a width of 5.6 m and a depth of 2.3 m. The width of the body is 2.5 m. These water tank and structural dimensions correspond to the TNO experimental set-up (Section 2.2). The deadrise angle $\alpha$ varies between 0 and 10 degrees. Only the bottom of the body is modeled as a flexible structure. The properties of the structure are similar to the 14 mm steel panel investigated in the TNO tests.

Three methods described in the previous sections were applied to solve the problem. Additionally Wagner's solution [116] is used to determine the hydrodynamic force under the structure. A brief summary for all these methods is given in Table 2.2.

Table 2.2. Methods

| | Hydroelasticity | Entrapped air | Small deadrise angles (0-5 deg) | Larger deadrise angles (>5 deg) |
|---|---|---|---|---|
| Wagner's solution | no | no | poor | good |
| Self-developed code | yes | no | good | poor |
| MSC.Dytran | yes | yes | good | good |
| LS-Dyna | yes | yes | good | good |

Wagner's solution is one of the first solutions for a wedge-shaped body penetrating into water. The body is rigid. Entrapped air and gravity force are neglected in Wagner's solution. If the speed of penetration $V_{rb}$ is constant the hydrodynamic force is defined by the following equation:

$$F = \pi\left(\frac{\pi}{2\ \alpha} - 1\right)^2 \rho_0 V_{rb}{}^2 h \tag{2.60}$$

Here $h$ is the depth of penetration into the water.
Wagner's formula can not be used for zero-deadrise angle since it predicts an infinite force. This simple formula will be used for verification of the numerical models for a non-zero angle.

A number of simulations have been performed with application of the approaches discussed in the previous sections in order to compare the results and check the consistency of these approaches.

First, the penetration of a rigid wedge with 5-degree deadrise angle was studied. Numerical results were compared with Wagner's solution. Figure 2.39 shows the hydrodynamic force acting on the body as a function of time for Wagner's solution, the

self-developed code, and MSC.Dytran code. All three approaches give similar results in spite of the fact that the Wagner's solution considers incompressible potential flow while the self-developed code and the MSC.Dytran operate with compressible fluids.

Further results with hydroelastic interaction obtained by application of the self-developed code, MSC-Dytran and LS-Dyna codes are compared. The deadrise angle is zero. In order to perform a proper comparison between all these models air entrapment is not considered since the self-developed code does not treat air entrapment. The bottom structure is modeled as a beam. The moment of inertia of the beam cross-section is 1.27e-5 $m^4$. The mass per unit length is 134.8 kg/m. The displacement of the bottom in the center is shown in Figure 2.40. Obviously the results are in quite good agreement. For both the maximum displacement and the period of vibration the difference amounts to 10-15%.

In addition to the water impact of the bottom structure with zero-degree deadrise angle discussed above, more calculations were performed with $\alpha = 2°$, $5°$, and $10°$, in order to compare the maximum displacement of the bottom at the center using the self-developed code and the MSC.Dytran code. Here the bottom structure is modeled by means of two beams rigidly connected at the center line (axis of symmetry) as it is shown in Figure 2.19. The moment of inertia of beam cross-section and the beam mass per unit length are the same as for zero-degree deadrise angle. The maximum displacement of the bottom at the center as a function of deadrise angle is shown in Figure 2.41. A good agreement is found.

Summarizing the results the following can be stated. In spite of application of different approaches, the results are in good agreement. This proves the consistencies of these approaches thus giving confidence that these numerical tools can be used for further research.

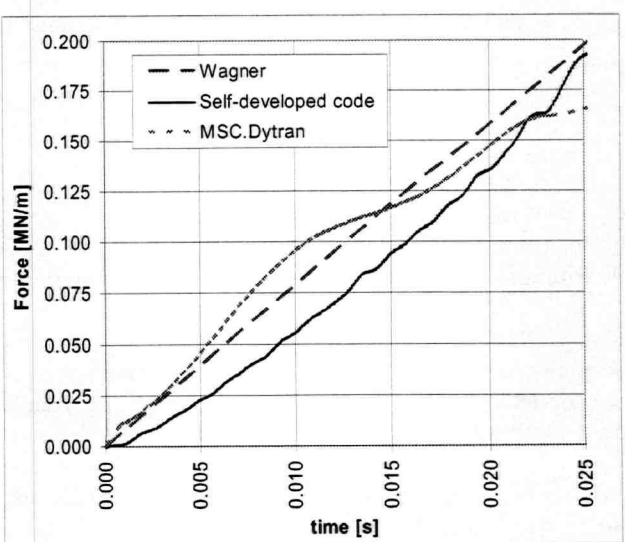


Figure 2.39. Force on the body as a function of time ( $\alpha = 5^o$, penetration of a rigid body)

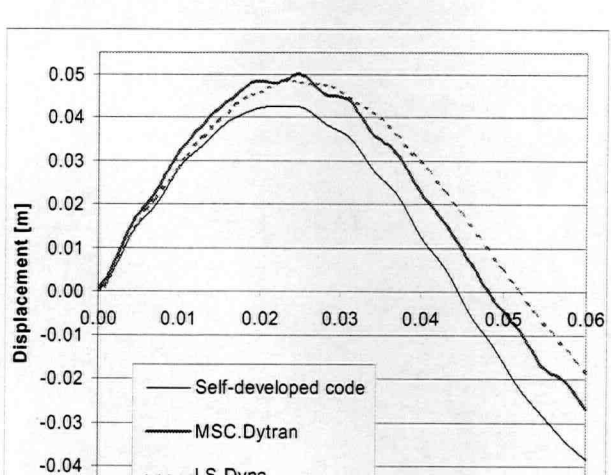


Figure 2.40. Displacement as a function of time ($\alpha = 0^o$, hydroelastic interaction)

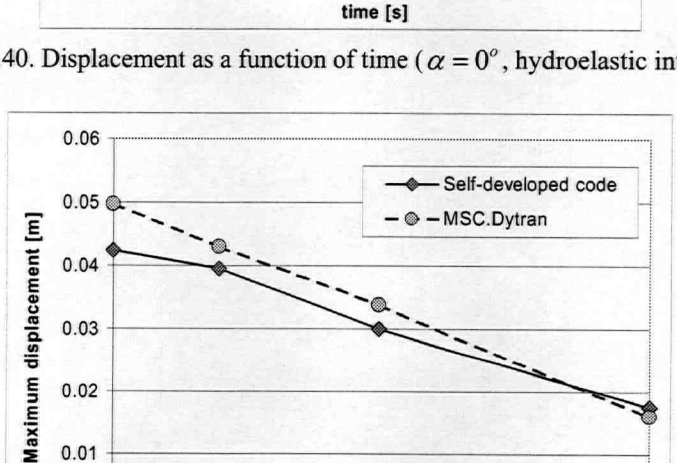


Figure 2.41. Maximum displacement as a function of deadrise angle (hydroelastic interaction)

# Chapter 3

## 2D PROBLEM

Slamming with hydroelasticity involved is a rather complicated and non-linear phenomenon. A significant number of different factors, such as deadrise angle, structural stiffness, water compressibility, air entrapment, etc, influencing slamming make the investigation of the slamming phenomenon extremely complicated. Consideration of these factors together prevents finding the most important of them. In spite of the fact that the author had quite powerful software capable to model many of these factors the author began investigation of the slamming phenomenon with simple problems. This gave an opportunity to study some of these factors separately. Subsequently a gradual introduction of many of these factors in rather complicated models at the later stage of the research resulted in a quite accurate numerical modeling confirmed with experimental data.

Investigation of the influence of hydroelasticity in the slamming problem starts with a 2D problem in this chapter. Section 3.1 discusses results of a numerical study of a structure subjected to impulsive loading. Slamming on the bottom structure of a sterntrawler is studied in Section 3.2. The effect of speed of impact (Section 3.3), influence of cargo (Section 3.4), influence of deadrise angle (Section 3.5), and water compressibility (Section 3.6) are also discussed in this chapter. Sections 3.1-3.5 present results of the first stage of the research and air entrapment is not considered here. Models discussed in these sections are created with application of the self-developed code, which is rather suitable for such models when air entrapment is not included. At the second stage of the research the air entrapment is introduced, first for water penetration of a rigid body (Section 3.7), and then for a hydroelastic problem (Section 3.8). Here the MSC.Dytran code is applied, which is capable to handle air entrapment. The model of Section 3.8 is the most accurate incorporating most of the factors involved in the slamming problem. A detailed analysis of results obtained in Section 3.8 is presented in Section 3.9. Section 3.10 shows comparison between numerical results obtained by the author and numerical results and experimental data by Arai [5]. Section 3.11 gives conclusive remarks based on an overview of all results discussed in this chapter.

## 3.1 Impulse loading

Slamming occurs when the ship hull hits the water surface, or a wave hits the hull. In both cases the velocity of impact is a critical parameter, which is involved in determining the energy of the impact. However the velocity of impact is usually not constant. This gives problems in determining the duration and the force of slamming impact. At the same time the duration and the force of impact are very important factors for the structural response. In order to analyze these factors, the following 2D model was developed [19]. A ship frame (a cross-section of the ship's hull) with a flat bottom is initially in contact with the

water surface. The model is shown in Figure 3.1. Here, due to symmetry, only half of the model is considered. Having zero initial velocity the ship frame experiences an impulse loading. This is not quite realistic, because slamming does not occur when the relative velocity between the hull and the water surface is zero. However this approach gives us a powerful control on the impact loads, which allows us to focus more on the structural response. In result the sensitivity of the fluid-structure system to the duration and the force of the impulsive load can be analyzed.

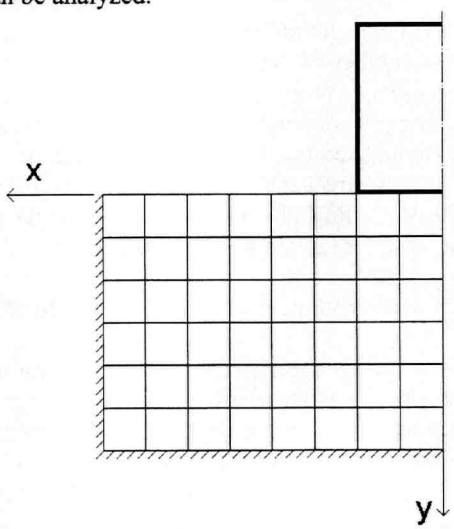


Figure 3.1. The model (impulse loading)

The self-developed code is applied in order to model this problem. The frame is modeled by means of beam finite elements as described in Section 2.3.4. The compressible fluid model of Section 2.3.1 is applied for the water simulation. The width and the depth of the water tank are 16 m and 6 m respectively. Dimensions, moment of inertia, and mass per unit length of frame beams are given in Table 3.1.

Table 3.1. The frame properties

| frame member | length [m] | moment of inertia [$m^4$] | Mass per unit length [kg/m] |
|---|---|---|---|
| bottom beam | 4.0 | 0.002 | 140 |
| side beam | 4.0 | 0.000045 | 60 |
| deck beam | 4.0 | 0.00005 | 65 |

The frame is subjected to the impulse load $I_{imp}$ (Figure 3.2):

$$I_{imp} = F_{imp}(t)\Delta t_{imp} \tag{3.1}$$

Here $F_{imp}(t)$ is force of the impulse, and $\Delta t_{imp}$ is duration of the impulse. The force of the impulse is applied vertically along the frame sides (Figure 3.3). Thus, the external loads on the horizontal members of the ship frame consist of the inertial loads on the beams and hydrodynamic forces on the ship bottom.

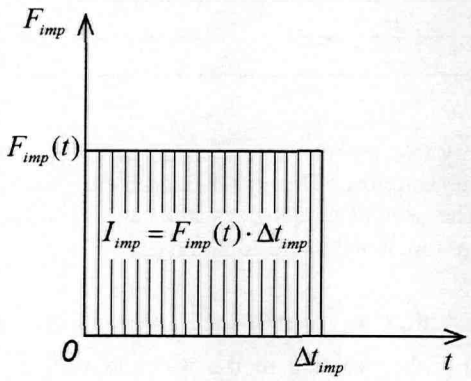


Figure 3.2. Impulse

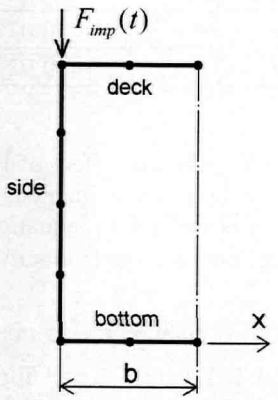


Figure 3.3. Application of impulse

The differential equation of the ship frame vertical motion as a rigid body is:

$$M\ \dot{V}_{rb}(t) = F_{imp}(t) - F(t) + \int_0^b \overline{m}\ddot{W}(t,x)dx \qquad (3.2)$$

Here $M$ is mass of the ship frame including cargo, which is fixed to the ship; $F(t)$ is hydrodynamic force on the ship bottom; $\int_0^b \overline{m}\ddot{W}(t,x)dx$ is inertial component due to bending vibrations of the horizontal beams; $W(t,x)$ is displacement of beams relatively to undeformed shape; $\overline{m}$ is mass per unit length of beam.

A number of simulations have been performed. The duration $\Delta t_{imp}$ and the force applied during the impulse $F_{imp}(t)$ are varied (Table 3.2). The force of impulse is taken per unit length since a 2D model for a ship's cross-section is considered. But the value of the impulse $I_{imp}$ remains the same for all simulations. The value of impulse $I_{imp}$ is chosen in such a way that the ship frame accelerates to the speed of 2.5 m/s under action of this impulse. The durations of the impulses $\Delta t_{imp}$ are taken up to the first period of natural vibration of the dry frame (this period is 0.02 s as calculated from the finite element analysis). It is expected that the structural response is the most sensitive to these durations and the results of simulations will give a good insight into the physics of the fluid-structural interaction. Moreover the impact durations in vicinity of the first period of the structural vibration are quite probable for slamming loads.

Table 3.2. Duration and force of impulse

| N | Impulse duration $\Delta t_{imp}$ [s] | Force of impulse $F_{imp}(t)$ [MN/m] |
|---|---|---|
| 1 | 0.0001 | 1000 |
| 2 | 0.005 | 20 |
| 3 | 0.01 | 10 |
| 4 | 0.02 | 5 |

In order to study the effect of hydroelasticity two models were considered for each load case. The first model includes hydroelastic coupling. The interface velocity boundary condition is defined by equation (2.57). The second model does not have hydroelastic coupling. The structural velocity $V_{str}(t)$ is not included in the equation (2.57).

Results of simulation for an impulse with duration $\Delta t_{imp} = 0.01\,\text{s}$ are given in Figure 3.4-Figure 3.7. Figure 3.4 and Figure 3.5 show the pressure in the water as well as the deformed shape of the frame (the deformations are magnified) at the moment $t = 0.028\,\text{s}$. A history plot of the hydrodynamic force acting on the bottom is presented in Figure 3.6. The oscillations of the hydrodynamic force for the hydroelastic solution in Figure 3.6 are caused by the time integration procedure. These oscillations take place twice: in the beginning of the simulation when the impulse is applied and at the moment when the force of impulse becomes zero. Figure 3.7 shows the displacement of the center of the bottom beam as a function of time. Plots in Figure 3.8 and Figure 3.9 incorporate all results showing the maximum hydrodynamic force acting on the bottom and the maximum displacement of the bottom beam in the centre respectively.

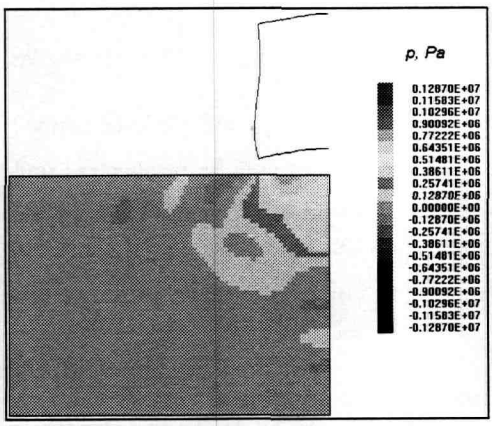


Figure 3.4. Pressure in water (hydroelastic coupling)

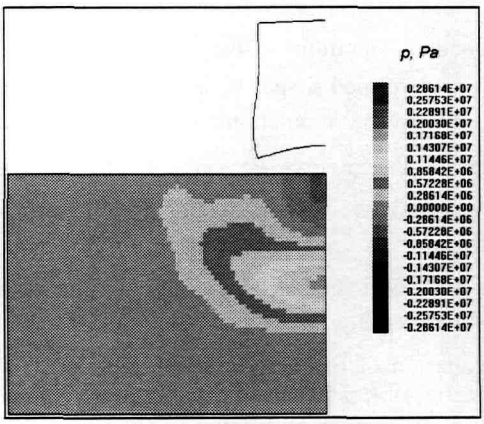


Figure 3.5. Pressure in water (no hydroelastic coupling)

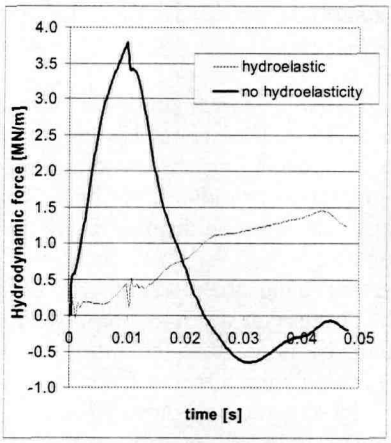


Figure 3.6. Hydrodynamic force on the bottom as a function of time

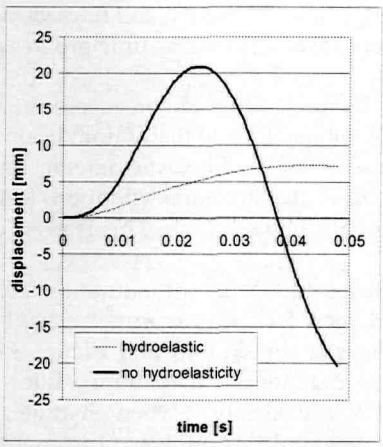


Figure 3.7. Displacement of the bottom beam in the centre as a function of time

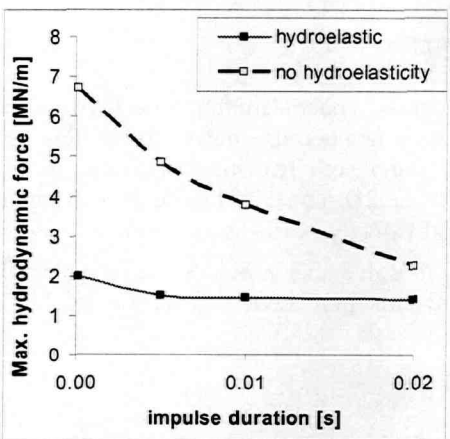


Figure 3.8. Maximum hydrodynamic force on the bottom as a function of impulse duration.

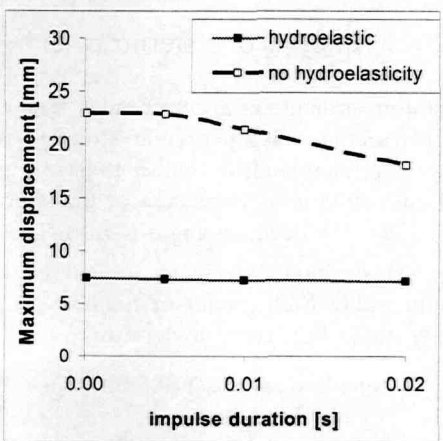


Figure 3.9. Maximum displacement of the bottom beam in the centre as a function of impulse duration.

The figures and the diagrams clearly demonstrate the behavior of the water domain and the structure. The pressure waves in the water area for the case of hydroelastic coupling and the case of no hydroelasticity are quite different. If no hydroelasticity is considered the energy of the impact is directly transferred into the water and under the bottom of the ship frame there is the field of pressure having the maximum in the center. In the case of hydroelastic coupling, at the start of the impact some energy is transferred to the structure and the distribution of pressure has a completely different nature. The maximum pressure appears close to the vertical supports of the side shell being the most rigid point. At the same time the pressure in the center is not as high since the bottom beam has maximum displacement in this point relative to the side beam. The structure absorbs some energy at

the start of the interaction and releases it forming a secondary pressure wave. This process repeats with attenuation as time progresses.

When hydroelasticity is considered the time period between the beginning of the impact and the moment when the bottom beam reaches maximum displacement is longer than in the case of no hydroelastic interaction. The water surrounding the structure becomes involved in the structural vibration. Moreover hydroelasticity reduces the hydrodynamic force on the bottom beam. This leads to a reduction of stresses and displacements.

With respect to the impulse duration the following was found: the effect of hydroelasticity is the largest for a shorter impulse and becomes less important when the impulse duration is increased (Figure 3.8 and Figure 3.9). It should be noted that the influence of the impulse duration on maximum values of the hydrodynamic force and displacement is reduced considerably when hydroelasticity is taken into account. However, the investigation of this influence for impulses with longer durations was out of the scope of the present work.

## 3.2 Analysis of a sterntrawler bottom section

A bottom structure of a sterntrawler "Frank Bonefaas" under slamming load is considered in this section. This particular structure is chosen not because this vessel suffers very large slamming loads but rather to have a good example of a realistic design, with specific stiffness and mass parameters of the structure. The 2D model of Figure 2.21 is applied here [20]. The deadrise angle is zero. The initial velocity of the impact is $V_0 = 2.5$ m/s. The self-developed code is applied in order to solve this problem incorporating the compressible fluid model of Section 2.3.1 and structural model of Section 2.3.4. The dimensions of the sterntrawler are:

Length over all is 119.55m.
Breadth is 17.5m.
Depth upperdeck is 11.02m.
Draft is 7.16 m.

Only the bottom beam of the ship's frame is considered. When a 2D model is applied, there remains the question of how to define the bottom beam parameters so that they represent the behavior of the bottom section of the ship. The moment of inertia and mass of the representative beam have to be found. The application of parameters of a separate floor does not represent the real 3D situation accurately. In order to find representative bottom beam parameters a special approach was applied. The bottom section of the sterntrawler between sides and bulkheads was modeled using the MSC.Marc code. In the FEM analysis the simplified model of the bottom section is supported along the whole perimeter, the rotations are not restrained. The bottom beam has to bend under uniform distributed loading in the same way as the section. Equating the maximum displacement of the beam and the section, the moment of inertia of the beam can be found. Comparison of the first frequency of vibration of the representative beam and the section makes it possible to determine the mass of this beam.

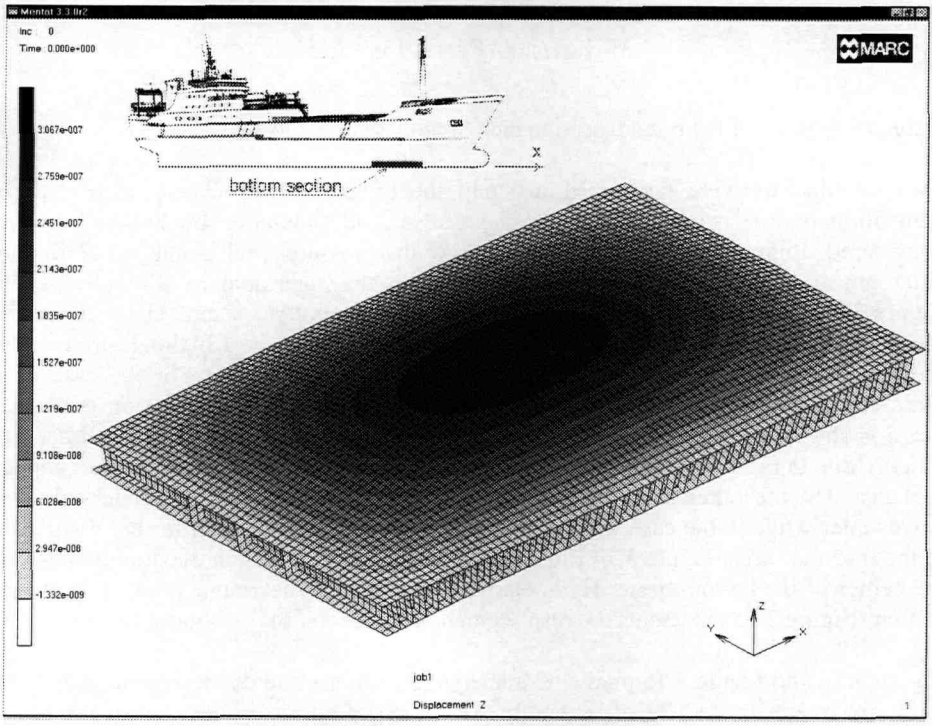


Figure 3.10. The bottom section

From elastic finite element analysis the maximum displacement $W_{\max}$ in the middle of the bottom section (Figure 3.10) due to a static uniform distributed pressure $p$ is found.

The moment of inertia of the beam of unit width with the length $l$ (the beam is supported at the ends, the rotations are not restrained) can be found as:

$$I = \frac{5ql^4}{384EW_{\max}} = 0.0193\,\mathrm{m}^4 \tag{3.3}$$

The first frequency of free vibration of the dry section from elastic modal FEM analysis is $\lambda = 113\,\mathrm{Hz}$.
The mass of the beam of unit width is:

$$m = \frac{EI\pi^4}{l^4\lambda^2} = 328\,\mathrm{kg/m} \tag{3.4}$$

The velocity of the vertical motion of the structure as a rigid body is not constant. This velocity depends on the hydrodynamic force and other parameters as it is seen from the following expression:

$$M\ \dot{V}_{rb}(t) = -F(t) + \int_0^b \overline{m}\ddot{W}(t,x)dx \tag{3.5}$$

Here $M$ is mass of the bottom section including mass of cargo.

Two simulations were performed to study the effect of hydroelasticity. In the first simulation hydroelasticity is included. For the second simulation no hydroelasticity is considered. Figure 3.11 and Figure 3.12 show the pressure field in the water for both situations at the same time step. Curved lines above the water domain in Figure 3.11 and Figure 3.12 show the magnified deformed shape of the bottom beam. The difference of the pressure fields for both situations is significant. In the case of hydroelastic coupling the zone with high pressure in front of the wave is very narrow. For the case of no hydroelasticity this zone is much larger. The hydrodynamic force acting on the bottom beam is shown in Figure 3.13. In the case of hydroelastic coupling the force drops very quickly due to rapid bending of the beam. In the case without hydroelasticity this happens less fast. On the other hand structural vibration introduces several secondary pressure waves later while in the case without hydroelasticity there is no much further distribution in the interface area. Figure 3.14 illustrates significant differences in maximum stresses in the center of the bottom beam. Hydroelasticity reduces the maximum stresses by a factor of four. Figure 3.15 represents the displacement in the center of the bottom beam.

Figure 3.14 and Figure 3.15 predict extremely high stresses and displacements. Obviously these are overestimated for of several reasons. First of all the whole area of the bottom comes into contact with the free water surface instantly. This is an extreme case. Secondly no air entrapment between the structure and the water surface is considered. Thirdly a 2D problem is solved. 3D models usually give lower hydrodynamic loads.

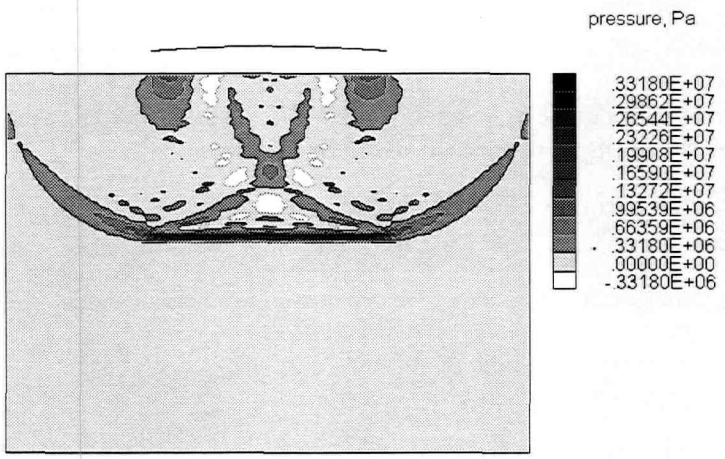


Figure 3.11. Pressure in water (hydroelastic coupling)

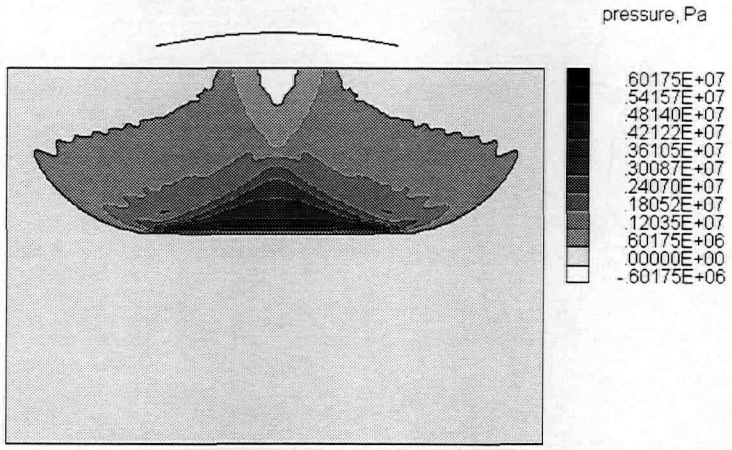


Figure 3.12. Pressure in water (no hydroelasticity)

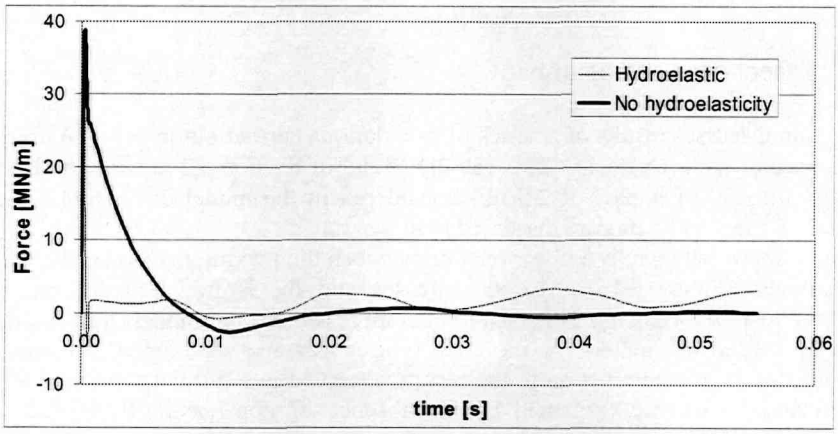


Figure 3.13. Hydrodynamic force on the bottom beam as a function of time

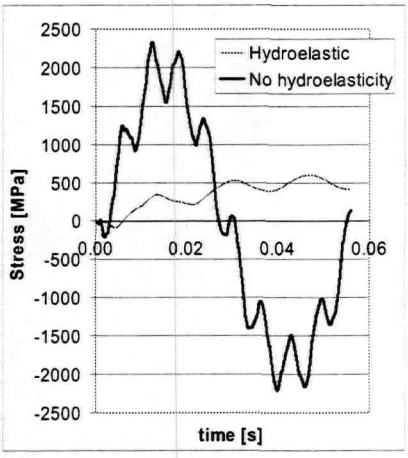


Figure 3.14. Maximum stress in the centre of the bottom beam as a function of time

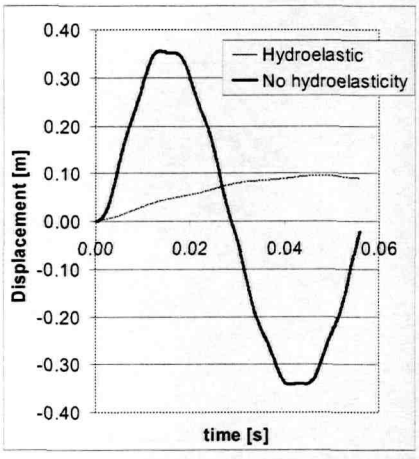


Figure 3.15. Displacement in the center of the bottom beam as a function of time

## 3.3 Effect of speed of impact

This section discusses results of a series of calculations carried out in order to investigate the influence of impact velocity [20]. The 2D model of Section 3.2 is used. Additional to the initial velocity of impact of 2.5 m/s considered in the model of Section 3.2, initial velocities of 1 m/s and 5 m/s are discussed here.

The results show that there is a linear relation between the maximum displacement and the initial velocity (Figure 3.16). Also the stresses and the hydrodynamic force depend linearly on the initial velocity. This feature of compressible water models has already been noticed by several researchers. At the same time it was also mentioned that such linear proportionality is in contradiction to the results observed in a normal slamming situation [62]. Probably it can be explained by the absence of non-linear effects such as air entrapment, the water spray generation, etc in the present model.

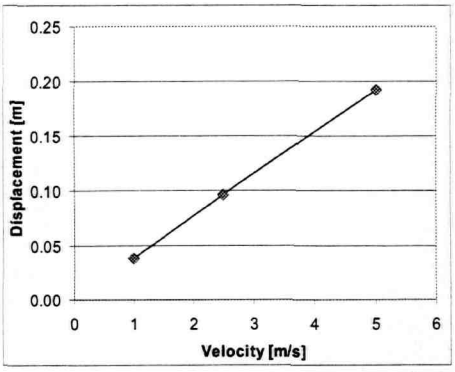


Figure 3.16. Maximum displacement of the centre of the bottom beam as a function of the initial velocity of the impact

## 3.4 Influence of cargo

The 2D model of Section 3.2 is considered again to check how cargo in the ship's hold can influence hydroelastic interaction [18]. The velocity of impact is constant and equals to 2.5 m/s. Five different situations are considered for this hydroelastic model with the amount of cargo starting from zero and up to 100% (Figure 3.17). The total mass of the ship's hull cross-section of unit length is calculated as the ship breadth multiplied by the ship draft and density of the water. The mass component of the ship's hull in the cargo area is only about 10% of the total mass. Thus, the maximum mass of the cargo is 90% of the total mass. To simplify the model the mass of the cargo is attached directly to the bottom beam. The cargo has no stiffness. Thus, the stiffness of the beam remains the same for all cargo load cases. Figure 3.18 shows the hydrodynamic force on the bottom beam at the beginning of the impact. It is clear that an increase in the amount of cargo results in a more gradual change in the force, which means that the bottom beam takes more time to bend. At the same time the maximum value of the force increases slightly with an increasing amount of cargo.

Contrary to what might be expected, cargo attached to the bottom beam does not change significantly the time which the bottom beam needs to reach the maximum displacement (Figure 3.19 and Figure 3.20, please note that the vertical axis in Figure 3.20 does not start from zero). If free vibration of a dry beam is considered, the frequency of the vibration is inversely proportional to the square root of the beam mass. However, application of the hydroelastic model shows a completely different behavior of the structure. The results of the calculations indicate a reduction of the maximum deflection of the bottom beam with an increasing amount of cargo (Figure 3.21, please note that the vertical axis in Figure 3.21 and Figure 3.22 does not start from zero), while the maximum hydrodynamic force increases (Figure 3.22). Figure 3.23 shows the maximum stress in the centre of the bottom beam. The dependence of the stresses on the amount of cargo is not large. The maximum value of the stress is observed for the empty ship hold. Summarizing it should be mentioned that an increase of the beam mass changes the hydrodynamic pressure under the beam, which affects the structural response.

Obviously attaching the cargo mass directly to the bottom beam is a considerable simplification. The cargo itself probably behaves in a more complicated way because it carries some load and it absorbs some energy introducing damping.

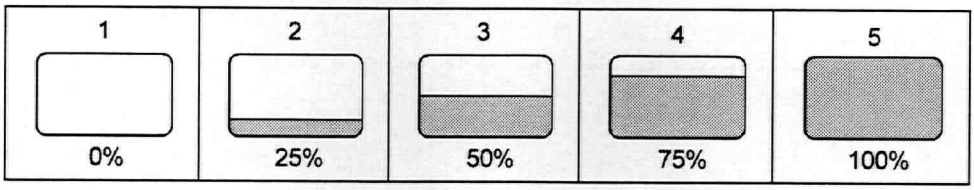


Figure 3.17. Loading of the hold

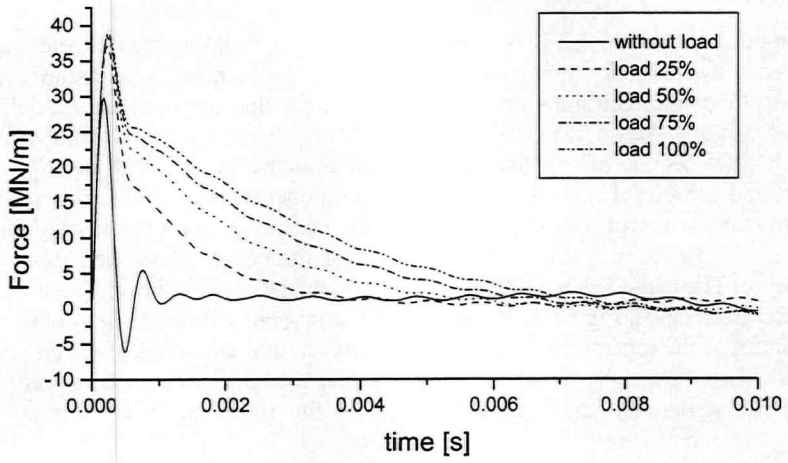


Figure 3.18. Hydrodynamic force on the bottom beam as a function of time

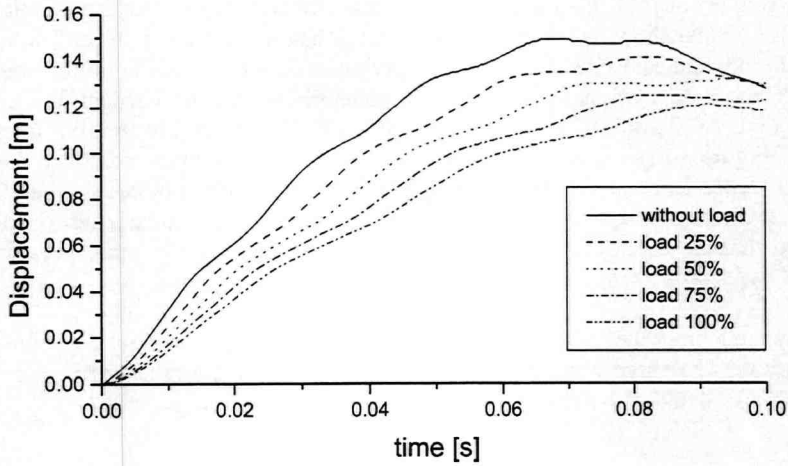


Figure 3.19. Displacement of the centre of the bottom beam as a function of time

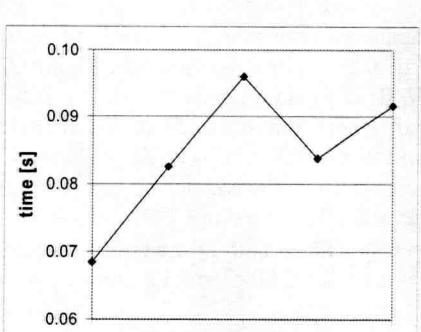


Figure 3.20. Time to reach maximum displacement of the centre of the bottom beam as a function of loading of the hold

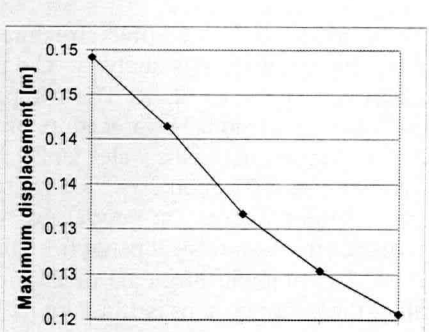


Figure 3.21. Maximum displacement of the centre of the bottom beam as a function of loading of the hold

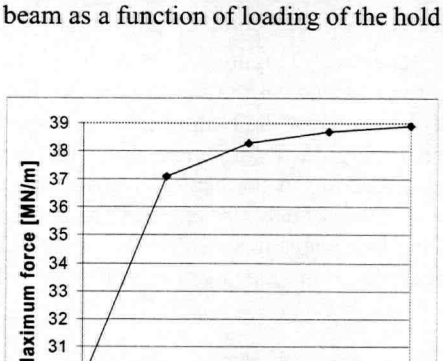


Figure 3.22. Maximum hydrodynamic force on the bottom beam as a function of loading of the hold

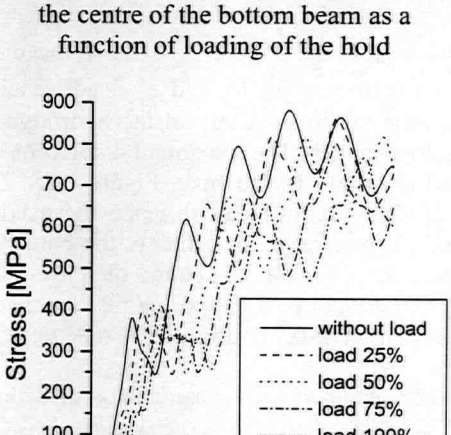


Figure 3.23. Maximum stress in the centre of the bottom beam as a function time

## 3.5 Influence of deadrise angle

The deadrise angle $\alpha$ (or the angle between the structure and the water surface in the more general case) plays an important role in slamming [17]. The slam duration is very short in the case of a zero or a small deadrise angle, while the total hydrodynamic force is high. A larger deadrise angle increases the impact duration and reduces the hydrodynamic force. In order to investigate this, the 2D model of Figure 2.21 was considered. The wedge-shaped body penetrates into water with constant velocity $V_{rb} = 2.5\,\text{m/s}$. Only the

bottom is modeled as a flexible structure by means of two beams. The self-developed code is used again for this analysis. The model of the structure is shown in Figure 2.19 and described in Section 2.3.4. The compressible fluid model of Section 2.3.1 is applied for the water simulation. The procedure of fluid-structural coupling is described in Section 2.3.5. The dimensions of the water tank correspond to the dimensions of the water tank of the TNO drop test (Section 2.2). The width and the depth of the water tank are 5.6 m and 2.3 m correspondingly. The properties of the bottom structure are quite close to the properties of the 14 mm steel panel from the drop test. The breadth of the bottom structure is 2.5 m. The moment of inertia of the bottom beams is 1.27E-5 $m^4$. The mass per unit length of the bottom beams is 134.8 kg/m.

A number of calculations have been carried out for the following deadrise angles: $0^\circ$, $2^\circ$, $5^\circ$, and $10^\circ$. For each angle two simulations were carried out: with hydroelastic coupling and without.

Figure 3.24 and Figure 3.26 show the displacement of the center of the bottom as a function of time for $0^\circ$ and $5^\circ$ deadrise angles respectively. Figure 3.25 and Figure 3.27 illustrate the time history of the hydrodynamic force acting on the bottom for the same deadrise angles. The maximum displacement of the center of the bottom as a function of deadrise angle is shown in Figure 3.28. Figure 3.29 gives information about the time which the bottom needs to reach the maximum deflection in the center. The maximum bending moment in the center of the bottom as a function of deadrise angle is presented in Figure 3.30. Figure 3.31 shows the elevation of the free water surface and the penetration of the structure for two particular time moments. For the hydroelastic case the deformation of the bottom can also be observed.

Results obtained with consideration of hydroelasticity differ considerably from the case of no hydroelasticity for zero and $2^\circ$ deadrise angles. But at $5^\circ$ angle and more this difference vanishes. At $10^\circ$ angle, both models give almost the same results. At zero-deadrise angle the difference for the maximum displacement and the maximum bending moment of the bottom is significant. The hydroelastic model gives lower vibration frequency of the bottom structure because this model fully considers the fluid-structure interaction. This means that the mass of water surrounding the structure is also involved in this vibration (the use of added mass approach in many practical applications gives similar effect). In the hydroelastic model the bottom reaches the maximum deflection 0.015-0.020 s later than in the model without hydroelasticity (Figure 3.29). This difference remains the same for all considered deadrise angles.

In Figure 3.27 oscillations of the hydrodynamic force can be observed. These oscillations take place because of the application of the Eulerian mesh. Each new water node coming into contact with the structure causes an increase in the hydrodynamic force. Application of a Lagrange mesh, which follows the free surface elevation and finds the exact position where structure touches the water surface, can prevent these oscillations. At the same time the present approach is expected to give quite accurate results for the structural analysis. The structure is very inertial. This means that these high frequency oscillations of the force do not affect significantly the structural response (displacements and stresses).

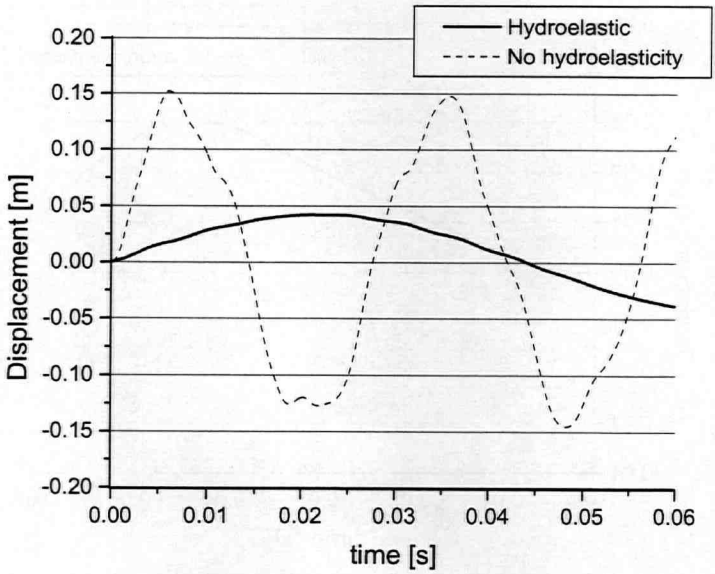


Figure 3.24. Displacement of the center of the bottom as a function of time (zero-deadrise angle)

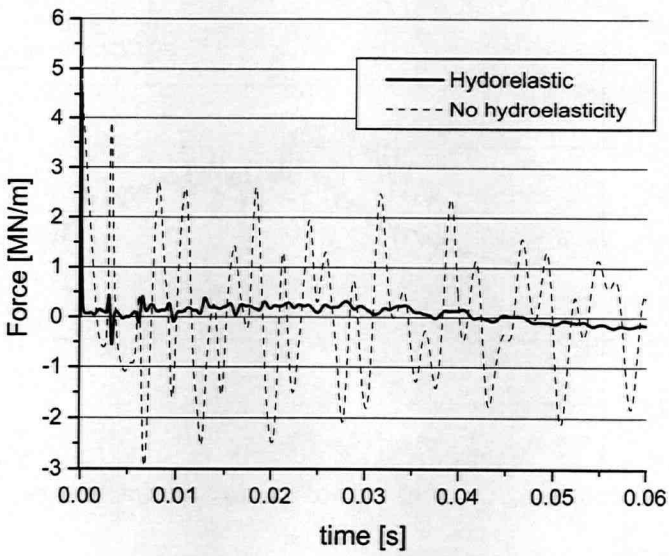


Figure 3.25. Hydrodynamic force on the bottom as a function of time (zero-deadrise angle)

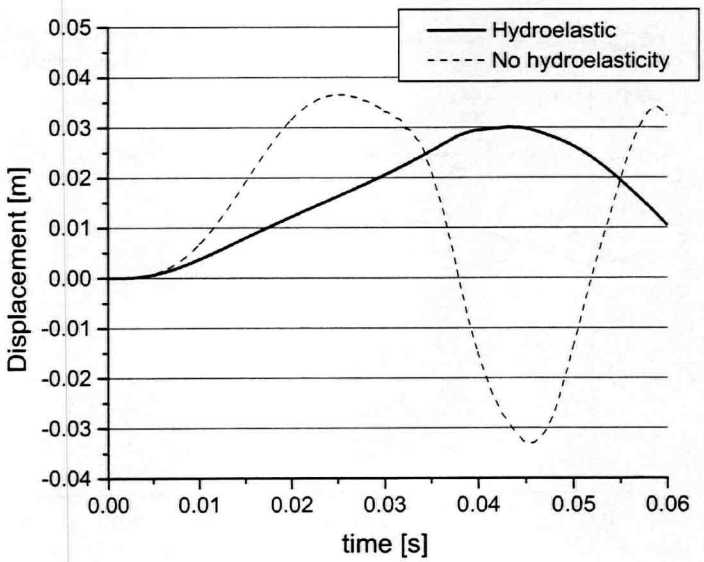


Figure 3.26. Displacement of the center of the bottom as a function of time ( 5° deadrise angle)

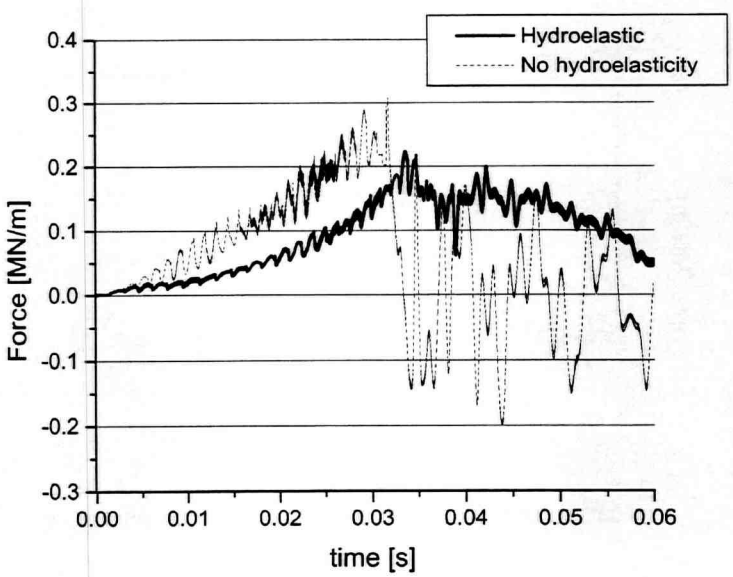


Figure 3.27. Hydrodynamic force on the bottom as a function of time ( 5° deadrise angle)

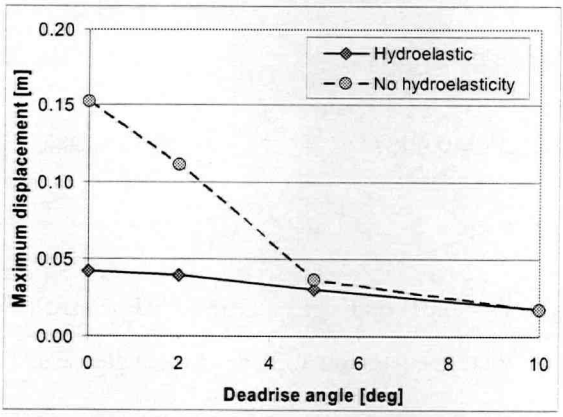


Figure 3.28. Maximum displacement of the center of the bottom as a function of the deadrise angle

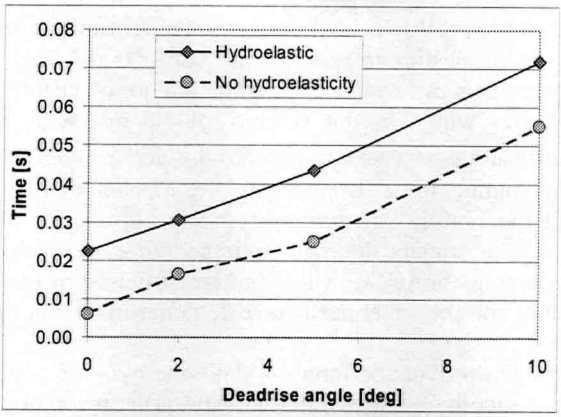


Figure 3.29. Time required for reaching of maximum deflection of the bottom

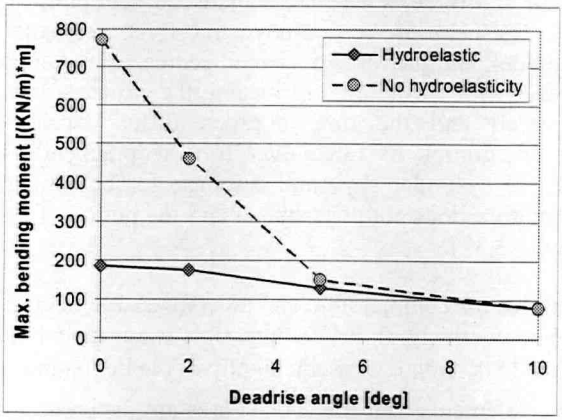


Figure 3.30. Maximum bending moment in the center of the bottom as a function of the deadrise angle

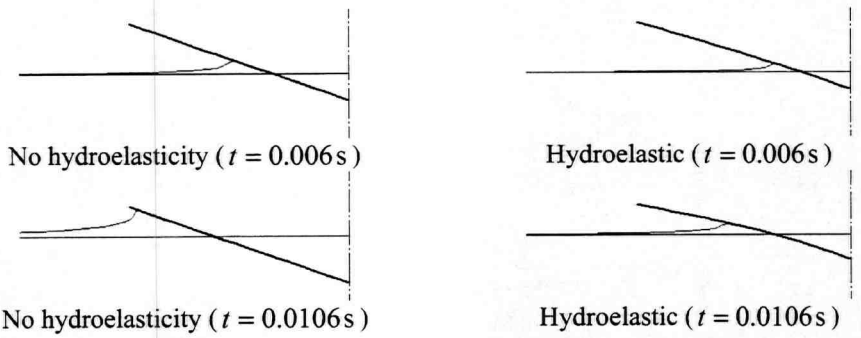


Figure 3.31. Water penetration at $2^\circ$ deadrise angle (scale factor 10)

## 3.6 Water compressibility

The effect of water compressibility is studied for the model explained in Section 3.5 [17]. The case without hydroelastic interaction is considered. The compressible and incompressible water models of Section 2.3.1 and 2.3.2 are compared here. The structure penetrates into the water with constant velocity of 2.5 m/s with a deadrise angle of $0.057^\circ$. This particular angle is chosen in order to provide a smooth contact with gradual growth of the hydrodynamic force. Considering the number of nodes of the structural mesh, the breadth of the bottom structure, and the speed of penetration, this particular angle allows bringing into contact one new node per time increment. In other words it takes 26 time increments to bring the whole bottom structure in contact with the water since both the structural and the water mesh have 26 nodes in the interface area.

Figure 3.32 shows the hydrodynamic force on the bottom as a function of time for both the compressible and incompressible water models. The incompressible water model gives a considerably higher peak in the hydrodynamic force in the beginning of the impact. At a later time the force is zero since there are negligibly small changes in the boundary conditions. The peak of the hydrodynamic force is smaller in the case of the compressible water model. But the force does not become zero after the whole area of the bottom is in the contact with the water, still loading the structure. Note that although the maximum force exerted and the time duration differ considerably, the impulse transmitted, i.e. the integration of force over time is practically the same for both situations. This leads to a similar structural response for both models. The maximum displacement of the bottom does not differ much and the period of structural vibration is almost the same (Figure 3.33).

The pressure in the water for compressible and incompressible models is shown in Figure 3.34 and Figure 3.35 respectively. In the compressible water model the acoustic wave has a limited speed ($V_{ac} = 1500$ m/s). Consequentially at the beginning of the impact only a small number of water elements near the contact area are disturbed. At the same time for the incompressible water model, the pressure field is obtained for the whole mesh instantly.

An interesting phenomenon was discovered for the compressible water model at a deadrise angle of $0.057°$. At this angle the area of contact increases with a velocity, which is higher than the speed of sound in water. In other words the contact area increases with a supersonic speed. Due to this phenomenon there is no free water surface elevation before a new water node comes into contact with the structure. In this case the compressible water model can be simplified and the free surface elevation can be neglected for the determination of the contact boundary conditions.

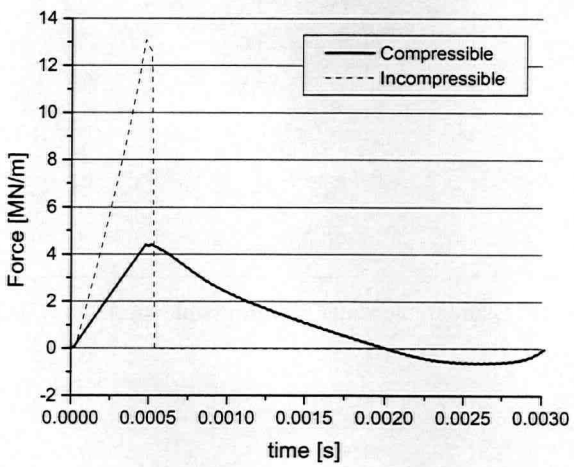


Figure 3.32. Hydrodynamic force on the bottom as a function of time at the beginning of the interaction ($0.057°$ deadrise angle)

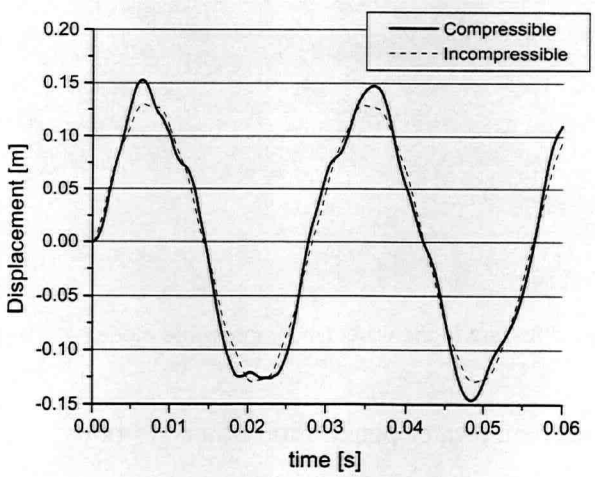


Figure 3.33. Displacement of the center of the bottom as a function of time ($0.057°$ deadrise angle)

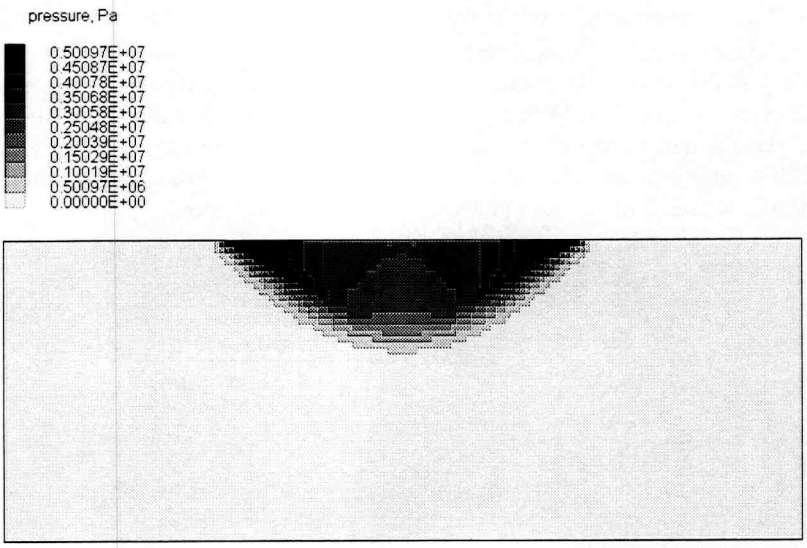


Figure 3.34. Pressure in the water (compressible model, $t = 0.00056\text{s}$)

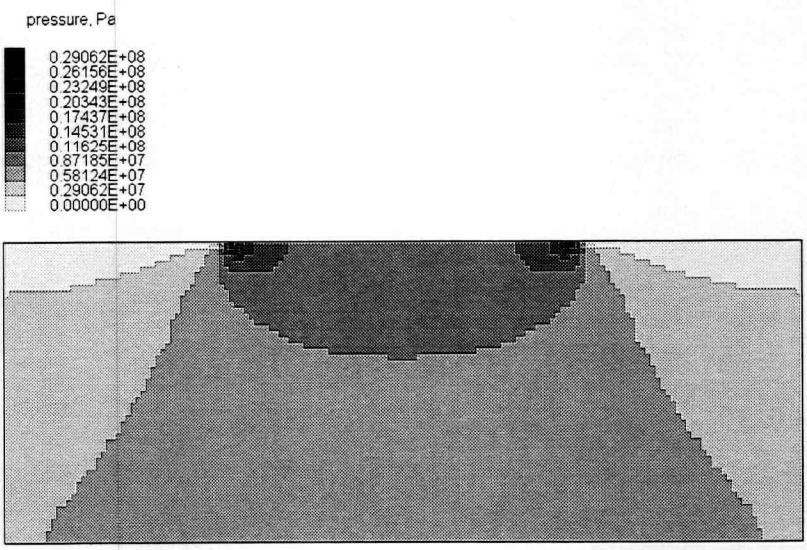


Figure 3.35. Pressure in the water (incompressible model, $t = 0.00056\text{s}$)

## 3.7 Air entrapment (water penetration of a rigid body)

Results discussed in the previous sections are based on simplified models assuming that there is no air entrapment. However it is expected that air entrapment plays quite an important role in the slamming problem. The first step in the investigation of the effect of

entrapped air is discussed in this section. Water penetration of a rigid body is considered. The influence of entrapped air on the hydrodynamic force acting on a rigid body as a function of the deadrise angle is studied.

The generalized model for the bottom slamming problem is shown in Figure 2.1. A wedge-shaped rigid body penetrates into the water at a constant velocity $V_{rb} = 2.5$ m/s. The water domain has a width of 5.6 m and a depth of 2.3 m, which corresponds to the TNO drop test set-up. The width of the body is 2.5 m. The MSC.Dytran code, capable of modeling not only the fluid-structural interaction but also air entrapment, is applied. The mesh of the MSC.Dytran model is shown in Figure 3.36 (because of symmetry only half is considered). The top part is initially filled with air and the rest with water. MSC.Dytran can handle only solid elements for an Eulerian mesh. In order to build a 2D model a thin slice of water and air is considered as having only one solid element in thickness. In other words, this is a 3D mesh with a number of solid elements in x- and y- directions, and only one solid element in the direction perpendicular to the x-y plane (Figure 3.36). A rigid wall boundary condition is applied at the sides of the air-water region. The analysis starts when the air gap between the body and the water surface is about 10 cm. It was found from an additional series of calculations that this is the optimal distance. A greater distance is more time consuming for the simulation, while there is no visible change of air pressure until the distance is reduced to about 10 cm.

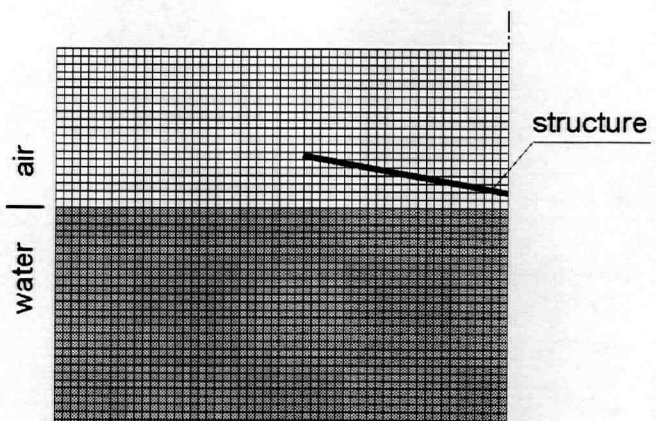


Figure 3.36. The mesh

Two series of calculations were carried out for water penetration at different angles: $\alpha = 0°$, $2°$, $5°$, and $10°$ (Figure 2.1). In the first series air is not considered and the top part of the mesh consists of so called "void elements". Water can enter the void part of the

mesh freely during the penetration forming a new free water surface. The vertical component of the hydrodynamic force acting on the body is shown in Figure 3.37 as a function of time. The second series of calculation is performed taking air into account. The vertical component of hydrodynamic force is shown in Figure 3.38 (note that there is a scale difference by factor 10 between Figure 3.37 and Figure 3.38).

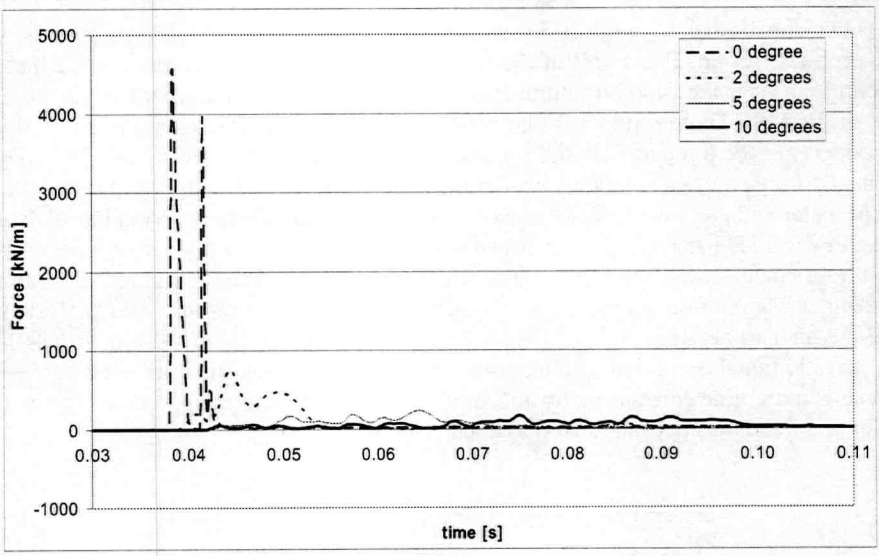


Figure 3.37. Hydrodynamic force on the rigid body (no air)

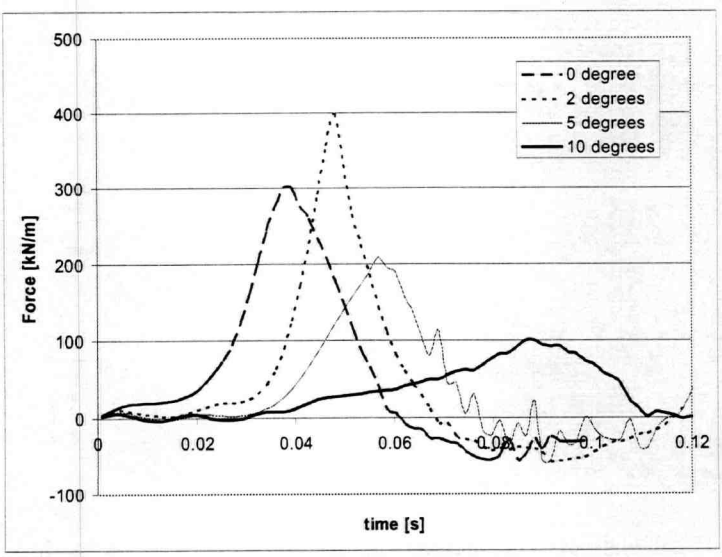


Figure 3.38. Hydrodynamic force on the rigid body (air is modeled)

Results for water penetration at zero and five-degree angles are compared in Figure 3.39 and Figure 3.40 respectively (note that there is a scale difference by factor 20 between Figure 3.39 and Figure 3.40). A summary of all results is given in Figure 3.41, where the maximum hydrodynamic force is shown as function of deadrise angle. In the case when air is not modeled the highest force is found for zero-angle. The force has a very high peak in the beginning of the impact since the whole area of the body comes into contact with water instantly. The second peak, which is somewhat smaller, is caused by a pressure wave reflected from the bottom of water tank (Figure 3.37). For the case when air is modeled, the highest force corresponds to the water penetration at a two-degree deadrise angle (Figure 3.38).

Summarizing the results the following should be mentioned with respect to the influence of entrapped air on the hydrodynamic force acting on the rigid body:

- A layer of air entrapped between the body and the water surface forms a very effective cushion making the impact force smaller. The most significant contribution of the entrapped air is found for zero- and 2-degree deadrise angles.
- Entrapped air is less important for water penetration at non-zero deadrise angles since the air can escape the impact area. Even at a two-degree deadrise angle some air escapes. This results in a higher peak of force for a two-degree angle than for zero-angle.

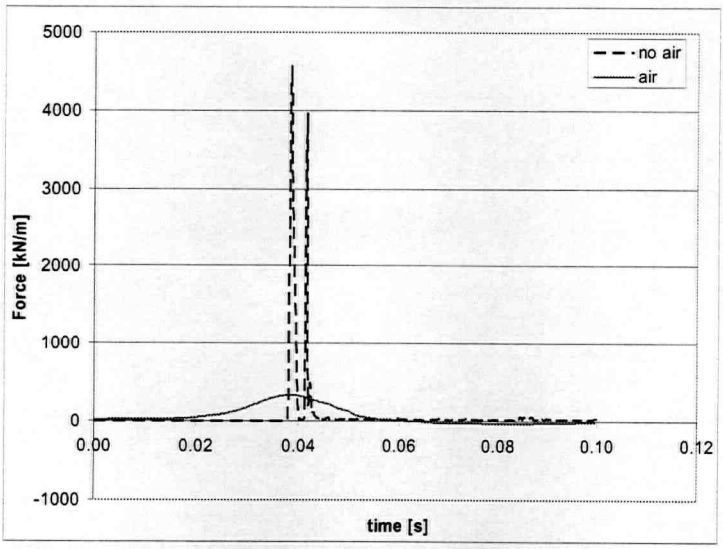


Figure 3.39. Hydrodynamic force on the rigid body (zero-angle)

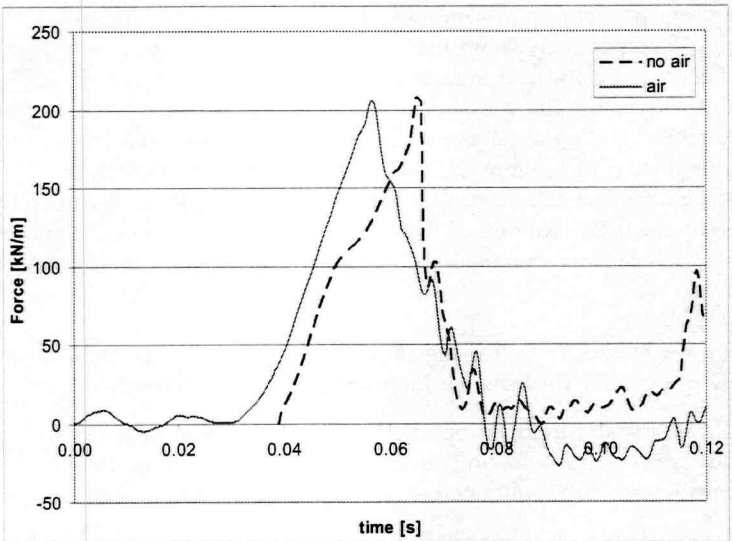


Figure 3.40. Hydrodynamic force on the rigid body (5° angle)

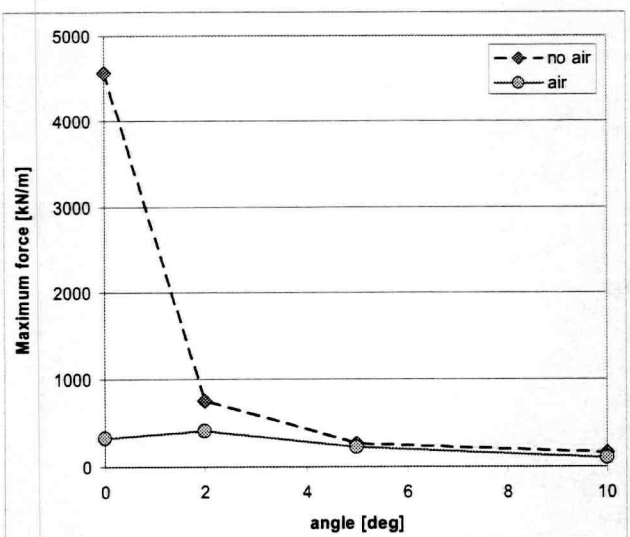


Figure 3.41. Maximum hydrodynamic force on the rigid body as a function of angle

## 3.8 Influence of deadrise angle, air entrapment, and structural stiffness

The previous section showed the importance of entrapped air when the deadrise angle is close to zero. However these results were obtained for water penetration of a rigid body. Now water penetration of a flexible body is considered [13, 16]. The model is exactly the same as the model of the Section 3.7 but the bottom part of the body is modeled by means of two flexible beams having the same properties and rigidly connected at the axis of symmetry (Figure 2.19). A constant velocity of water penetration of 2.5 m/s is considered, which allows performing proper comparison between different models.

The effect of hydroelasticity is studied as a function of three variables: deadrise angle, presence of entrapped air, and the structural stiffness (Figure 3.42). These are the most important factors involved in the slamming phenomenon.

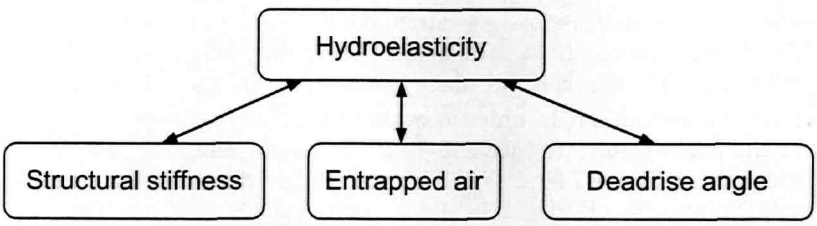


Figure 3.42. Hydroelasticity as a function of three variables

In order to study the influence of the structural stiffness on the hydroelasticity, four different sets of beam properties are considered (Table 3.3). The moment of inertia and the mass per unit length of each beam are chosen so that the first frequency of natural vibration of the dry bottom structure would vary linearly with respect to the mass per unit length (Table 3.3 and Figure 3.43). The moment of inertia of the beam as a function of the first frequency is shown in Figure 3.43. Parameters of the bottom structures assembled of beams N1 and the beams N3 approximately correspond to the stiffness and the mass parameters of the 6 mm and the 14 mm steel panels investigated in the TNO drop test. The displacement of the bottom in the center W(t) (Figure 2.19) is monitored during the analysis.

Table 3.3. Properties of beams forming the bottom structure

| Beam | First frequency of natural vibration [Hz] | Moment of inertia [$m^4$] | Mass per unit length [kg/m] | Modulus of elasticity [GPa] |
|---|---|---|---|---|
| N1 | 19.0 | 1.61e-6 | 59.3 | 210 |
| N2 | 27.2 | 5.42e-6 | 97.1 | 210 |
| N3 | 35.4 | 1.27e-5 | 134.8 | 210 |
| N4 | 43.6 | 2.47e-5 | 172.5 | 210 |

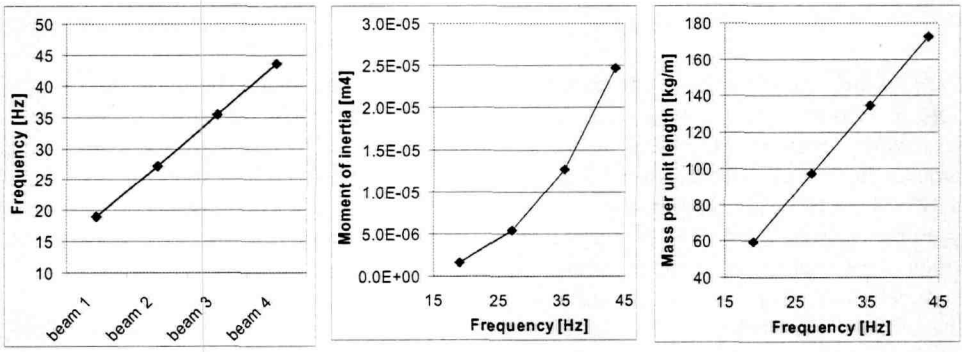


Figure 3.43. Beam properties

An advanced series of calculations was carried out for each of the four bottom structures assembled of the beams from Table 3.3 with the following deadrise angles: $\alpha = 0°, 2°, 5°, \text{and } 10°$. For each of these cases two variants are investigated; with entrapped air and without air. In order to evaluate the effect of hydroelasticity for each model, two simulations are performed and the maximum displacement in the center of the bottom is monitored. In the first case the hydroelastic problem is solved. In the second case no hydroelasticity is considered. In all together 64 models were generated.

A typical history plot of the displacement at the center of the bottom is shown in Figure 3.44 for the bottom structure assembled of the two beams N3 impacting the water surface at zero-deadrise angle. The maximum displacement corresponds to the case of "no hydroelasticity" without consideration of entrapped air. The smallest displacement is found for the hydroelastic case with air included. The importance of entrapped air in hydroelastic models is clearly visible comparing Figure 3.45 (no air) and Figure 3.46 (with air), where the displacement in the center of the bottom (beam N3) is shown for several deadrise angles. Figure 3.46 indicates that for the case when air is modeled, the maximum displacement of the bottom is found for a two-degree deadrise angle. At the same time for the model without air (Figure 3.45), the maximum displacement is found for a zero-deadrise angle. The same trend is found for the hydrodynamic force from the previous series of calculations for a rigid body, where the highest force was also found for a two-degree angle taking air into account and for a zero-angle without air (Section 3.7).

Figure 3.47-Figure 3.52 show results of all calculations. Here the maximum displacement is shown as a function of deadrise angle for all four bottom structures. The surface diagram (Figure 3.51) shows the maximum displacement as a function of two parameters: the deadrise angle and the first frequency of natural vibration of the bottom structures (or in other words the bottom stiffnesses). This figure represents results for the hydroelastic case with consideration of entrapped air. A summary of all results is also plotted in the surface diagram of Figure 3.52. The most accurate model (the hydroelastic case with consideration of entrapped air) predicts the smallest displacements.

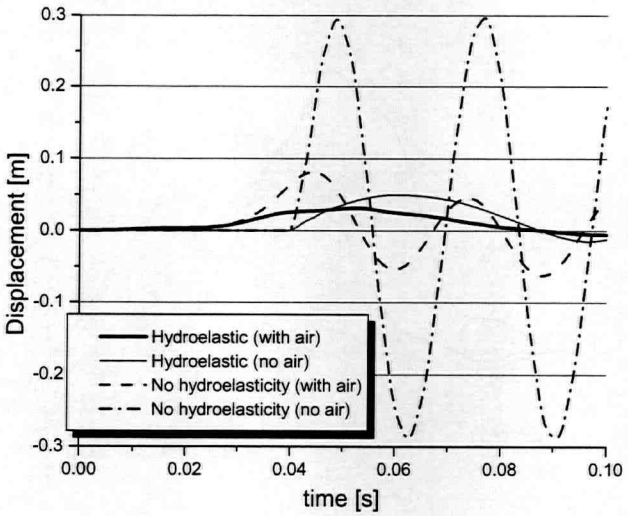


Figure 3.44. Displacement as a function of time (beam N3, $\alpha = 0°$)

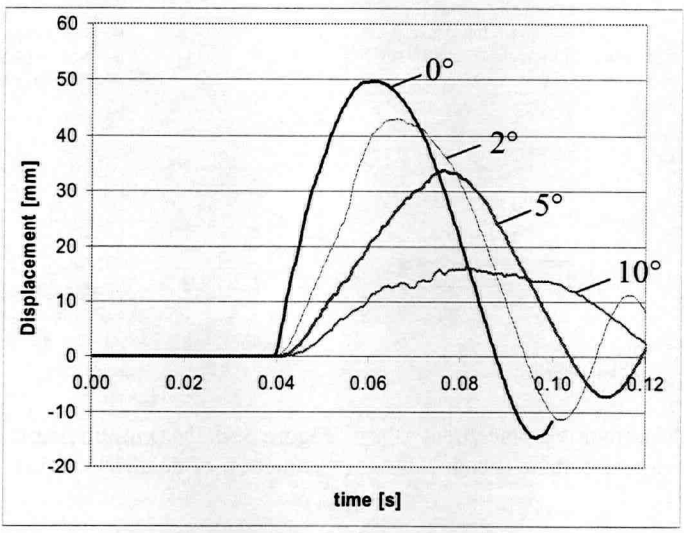


Figure 3.45. Displacement as a function of time (beam N3, no air)

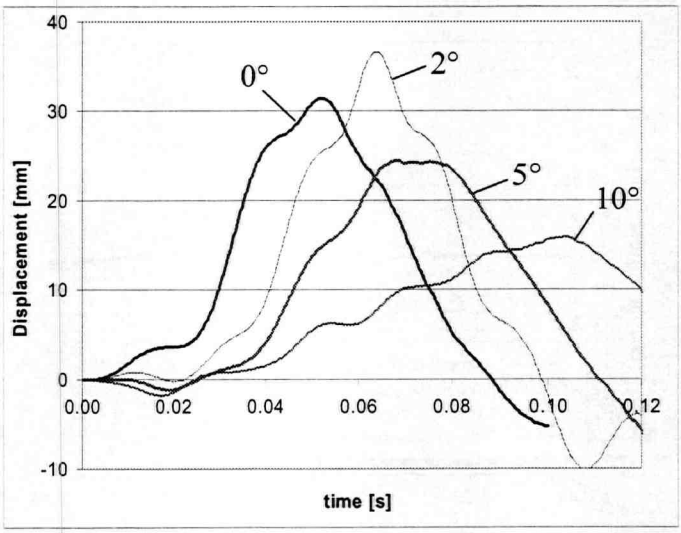


Figure 3.46. Displacement as a function of time (beam N3, air is modeled)

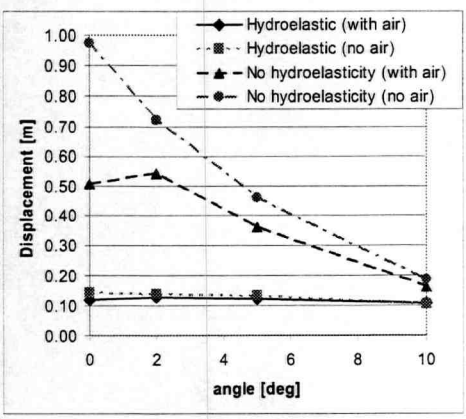


Figure 3.47. Maximum displacement as a function of deadrise angle (beam N1)

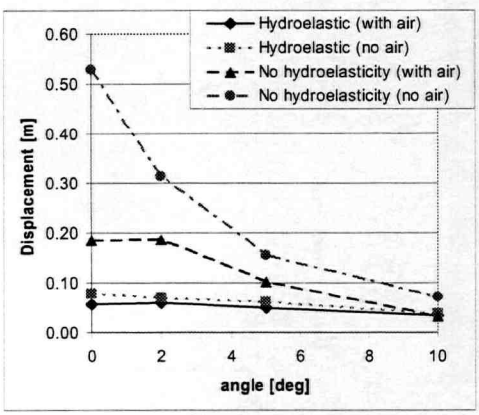


Figure 3.48. Maximum displacement as a function of deadrise angle (beam N2)

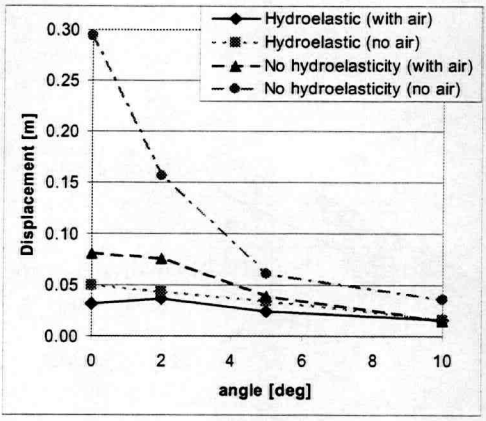


Figure 3.49. Maximum displacement as a function of deadrise angle (beam N3)

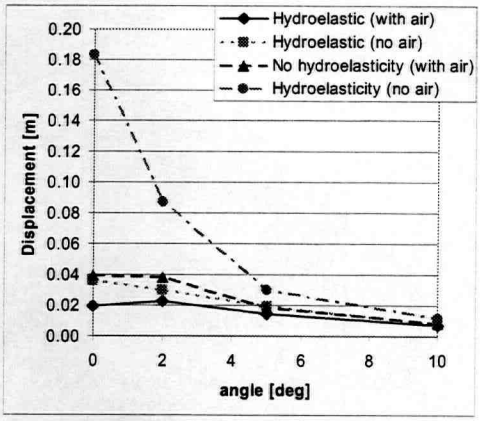


Figure 3.50. Maximum displacement as a function of deadrise angle (beam N4)

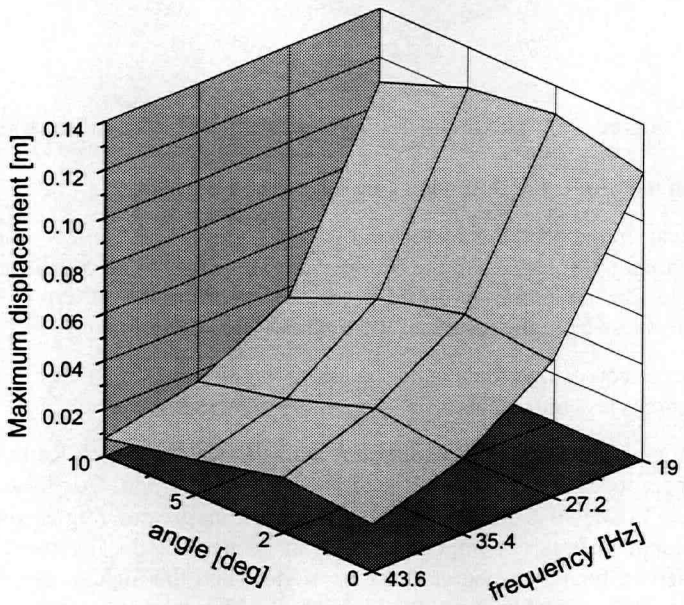


Figure 3.51. Maximum displacement of the bottom (hydroelastic case, with air)

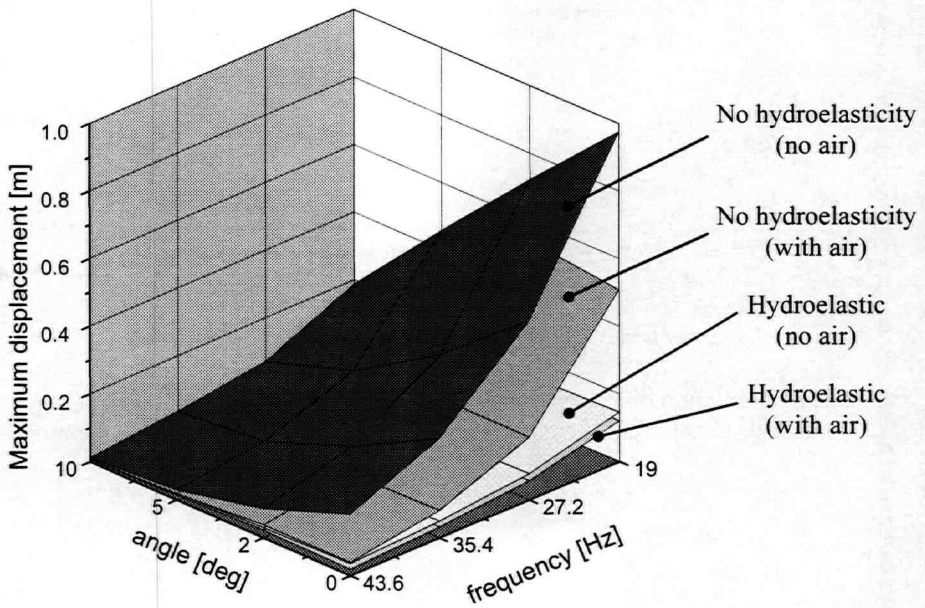


Figure 3.52. Maximum displacement of the bottom (all results)

Summarizing the results the following conclusions can be made:

- It was found that the effect of hydroelasticity is extremely important for the slamming problem when the deadrise angle is close to zero. With increases of the angle, the structural response predicted ignoring the effect of hydroelasticity differs less from the results of the hydroelastic solution.
- The effect of hydroelasticity is more significant for flexible structures and becomes less important as the structural stiffness increases.
- Entrapped air between the structure and the water surface leads to reduction of impact loads for very small deadrise angles ($0° - 5°$). For these angles the air plays a role of a quite effective cushion. For greater angles the effect of the entrapped air is not important and can be neglected. The most severe case is observed for a two-degree deadrise angle when the air can escape the interface area. This makes the impact loads higher, which leads to a more severe structural response. At the same time, for zero-angle the response is slightly less because more air is trapped.
  However it should be clear that the range of deadrise angles between $0° - 5°$ is a function of several factors such as the velocity of impact, dimensions of the structure, presence waves on the free water surface etc. Perhaps in some cases the air entrapment can be important for even larger deadrise angles or vice versa.

## 3.9 Criterion of importance of hydroelasticity

The previous section gives some indications about the effect of hydroelasticity considering several factors involved in this fluid-structure interaction problem. Specific slamming conditions, which make the effect of hydroelasticity important, have been discussed. However it is desirable to introduce a criterion for determining whether hydroelasticity should be taken into account or not [16]. After analysis of the results of Section 3.8 the following suggestion is made. The reduction of displacement of the bottom in the center as a result of the effect of hydroelasticity can be defined as follows:

$$reduction = \frac{\left(W_{no\,hyd.}^{\max} - W_{hyd.}^{\max}\right)}{W_{no\,hyd.}^{\max}} 100\% \tag{3.6}$$

Here $W_{hyd.}^{\max}$ is the maximum displacement obtained from the hydroelastic solution. $W_{no\,hyd.}^{\max}$ is the maximum displacement found for the case when the hydroelasticity is ignored.

This reduction is considered as a function of the ratio between the duration of impact and the first period of natural vibration of the dry bottom structure:

$$ratio = \frac{duration}{period} \tag{3.7}$$

The duration of the impact is found from Figure 3.38 as the impulse duration for the rigid body penetration (effect of air is included). The shape of each impulse is approximated by a triangle with the base of this triangle representing the duration of the impact. Durations of impacts for all deadrise angles are summarized in Table 3.4. Figure 3.53 shows the reduction of deformation as a function of the ratio defined in equation (3.7). This figure shows a clear trend of the reduction (equation 3.6) as a function of the ratio (equation 3.7). The effect of hydroelasticity gives a very strong reduction of the deflection (up to 76%) for impacts with short duration. But when the ratio becomes greater than 2.0 the effect of hydroelasticity does not play a significant role. It should be noted that this figure incorporates all results for bottom structures with different stiffnesses, and in spite of this fact the tendency remains. Probably it can be better to define the ratio in a different way taking the impulse duration from the hydroelastic simulation. It can give a better fitting line for all points (Figure 3.53). But the idea behind it is that the designer can use the results of the rigid body penetration model, which is much more simple to build, in order to decide if a hydroelastic simulation is necessary for more accurate results.

It is also important to mention that the choice of the displacement of the bottom as a factor responsible for the structural response does not seem to be obvious. There are at least two more parameters, which seem to be more suitable to analyse the structural response. They are stresses and accelerations. However the displacement is chosen for the following reasons. First of all, the bottom of the ship is modeled here by means of beams without strictly specified cross-sections. It would be difficult to define stresses in this case. Secondly, the application of accelerations as a factor responsible for the structural response would lead to another problem. The pressure beneath the structure changes very

rapidly. There is a considerable amount of numerical noise caused by the numerical scheme of the contact algorithm. It will be quite difficult to evaluate the structural response considering the accelerations, even after filtering. The displacement is considered to be the most reliable factor for this kind of analysis, as it is a very integral factor. The structure is so inertial that even strong pressure oscillations do not affect significantly the structural deformation. For this reason the analysis discussed here is based on the structural displacements.

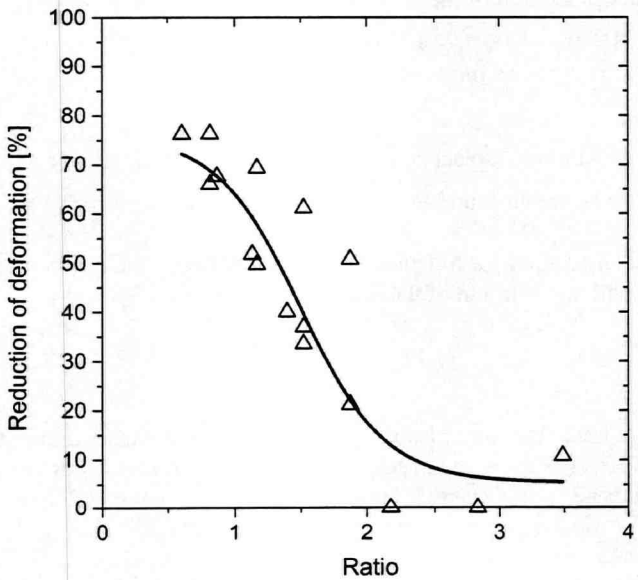


Figure 3.53. Reduction of deformation as function of ratio between the duration of impact and the first period of natural vibration of the dry bottom structure

Table 3.4. Duration of impact

| Deadrise angle [deg] | 0 | 2 | 5 | 10 |
|---|---|---|---|---|
| Duration [s] | 0.043 | 0.032 | 0.043 | 0.080 |

Based on the above findings, the author suggests the following procedure in order to determine if the effect of hydroelasticity should be taken into account or not, and if not what kind of error can be expected. First the hydrodynamic force is found from a rigid body water penetration model. The duration of the impact is defined. Secondly, the first period of natural vibration of the dry structure is calculated. The ratio as defined by equation (3.7) is found. If the ratio is more than 2.0 the effect of hydroelasticity can most likely be neglected (Figure 3.54). In case the hydroelastic problem can not be solved Figure 3.53 can give some ideas of how serious the expected error can be.

The author assumes that this criterion is quite universal. This however should be confirmed by carrying out more extensive investigation. At the same time in spite of the fact that the 2D model studied in this section is quite simple the physics of the hydroelastic interaction is understood quite well. This means that this approach would probably be helpful not only for a simple 2D model, where the bottom structure is assembled of two beams only, but also for more complicated structures covering a quite large range starting from local structures like the skin between stiffeners and ending with global structures such as the bottom section including a number of stiffeners, as far as it is limited by the range where impact pressures create direct response.

Figure 3.53 indicates that the effect of hydroelasticity is most important for impacts with a relatively short duration. Such an impact can occur if a large area of the structure comes instantly into the contact with the water surface. This can take place for structures with deadrise angle close to zero. Here the effect of entrapped air becomes very important. Figure 3.38 shows that even for the case of zero-deadrise angle the hydrodynamic impact force has quite a long duration. So there is always a limit. Due to the presence of entrapped air the duration of the impact is prevented from becoming extremely short.

Referring to publications by Faltinsen [43], and Kapsenberg and Brizzolara [72] it is noted that these authors found a similar effect concerning the deadrise angle. Faltinsen [43] found that the effect of hydroelasticity becomes more important with reduction of deadrise angle. Kapsenberg and Brizzolara [72] suggest that there is almost no influence of hydroelasticity for bow flare slamming. This conclusion is based on an evaluation of advanced series of model tests performed for a high-speed monohull with a large deadrise angle.

All numerical models discussed in this section are considered for water penetration with a constant velocity, which is the same for all calculations. Increase of this speed will lead to a reduction of the impact duration making the effect of hydroelasticity more important, and vice versa reduction of the velocity will reduce this effect. If the velocity is not constant it will change the duration of the impact. It is important to realize that the trend line shown in Figure 3.53 is expected to be valid for all situations. However this is only a preliminary conclusion based on a limited number of models. This means that more detailed investigation is recommended.

It is clear that the stiffness of the structure influences the reduction of deformation. Figure 3.55 illustrates the maximum reduction of deformation for all considered deadrise angles in the range 0-10 degrees as a function of the structural stiffness. At the same time it is important to mention that the reduction of deformation is not very sensitive to the structural stiffness. The bottom structure with frequency of 19.0 Hz is very flexible. The bottom structure with frequency 43.6 Hz is extremely stiff. The moment of inertia of beams of the stiff bottom structure is 15 times higher than the moment of inertia of beams of the flexible bottom structure. However the reduction of deformation drops from 76% for the flexible bottom structure to 51% for the stiff one only.

Summarizing the results of this discussion it can be stated that the ratio defined by equation (3.7) is the key criterion for defining when hydroelasticity should be taken into

account or can be neglected, while the structural stiffness has a secondary effect in taking this decision.

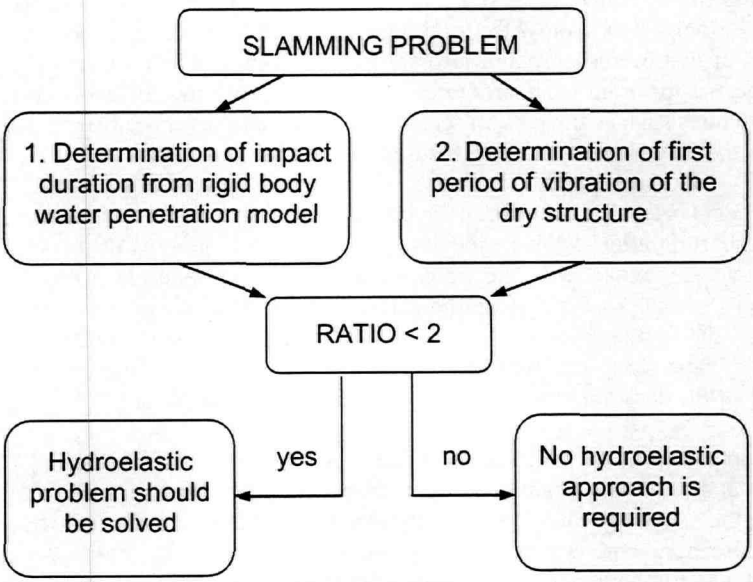


Figure 3.54. Criterion of importance of hydroelasticity

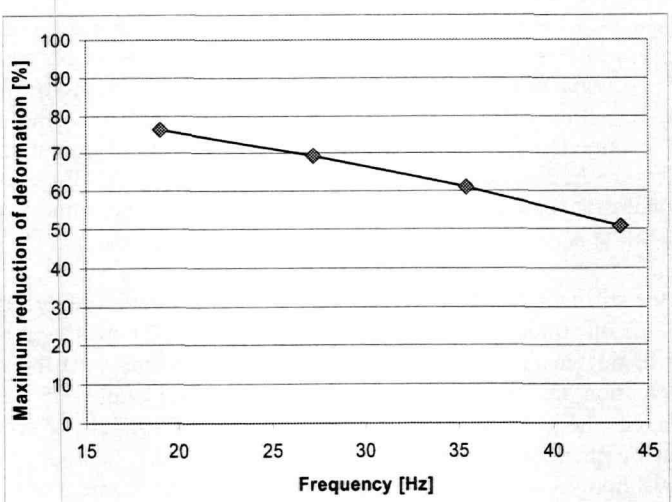


Figure 3.55. Maximum reduction of deformation as a function of the first frequency of natural vibration of the dry bottom structure

## 3.10 Water penetration of a flexible cylinder

The previous sections discussed results of numerical studies. All statements and conclusions made above are based on numerical result only. However, a purely numerical study is not reliable without an experimental verification. Arai carried out an advanced series of drop tests for water penetration of cylinder including hydroelastic interaction [5]. His research also included an advanced numerical study. This presented a good opportunity to check the numerical tools, which the author of this thesis used in his research. A 2D MSC.Dytran model was developed in order make comparison with numerical and experimental investigations performed by Arai. The model is shown in Figure 3.56 (because of symmetry only half of model is considered). Two drop heights of 1 m and 0.75 m are considered. The material of cylinder is aluminium having a modulus of elasticity of 75 GPa and density of 2760 kg/m$^3$. Poisson's ratio is 0.34. The cylinder has an external diameter of 306 mm and a plate thickness of 3 mm.

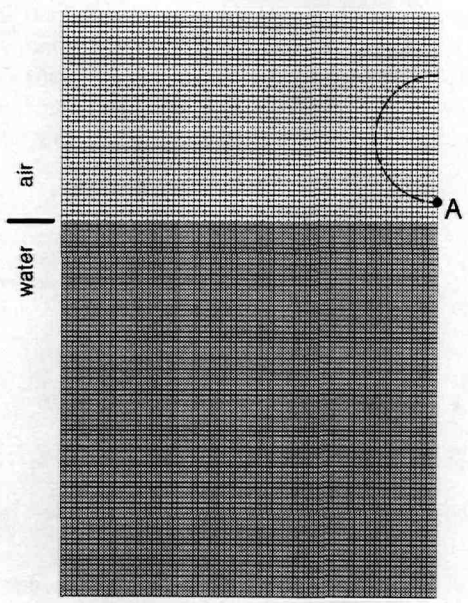


Figure 3.56. MSC.Dytran model

The MSC.Dytran model is similar to the 2D model discussed in Section 3.8. This model consists of water domain, air domain, and a cylindrical shell modeled with application of shell elements. The global motion of the cylinder in MSC.Dytran model is calculated based on the cylinder mass, gravity force, and the hydrodynamic force. A brief comparison of this model with the model of Arai is given in Table 3.5. Arai considered an incompressible fluid for modeling the water, while MSC.Dytran operates with a compressible fluid. However as it was shown in Section 3.6 both these models are expected to give similar results. Inclusion of air in the MSC.Dytran model provides a more smooth contact between the cylinder and the air/water regions during the interaction.

At the same time there is no considerable difference between the MSC.Dytran model and the model by Arai since a minor air entrapment is expected for the water penetration of a body having a cylindrical shape. In other words both models should give quite similar results in spite of the fact that these models are generated based on the application of different formulations.

Table 3.5. Comparison of approaches

| | Hydroelasticity | Entrapped air | Water compressibility |
|---|---|---|---|
| Arai | yes | no | no |
| MSC.Dytran | yes | yes | yes |

Several simulations were performed. First the global motion of the center of gravity (COG) of the cylinder was compared. Figure 3.57 shows the vertical position of center of gravity of the cylinder as a function of time (the drop height is 0.75 m). A good agreement is found. A strain history plot is given in Figure 3.58. Maximum strain in the point "A" is shown here (location of this point is indicated in Figure 3.56). The MSC.Dytran model gives better agreement with the experimental data than the numerical model of Arai. However, MSC.Dytran underestimates the strain, while the numerical model of Arai overestimates it.

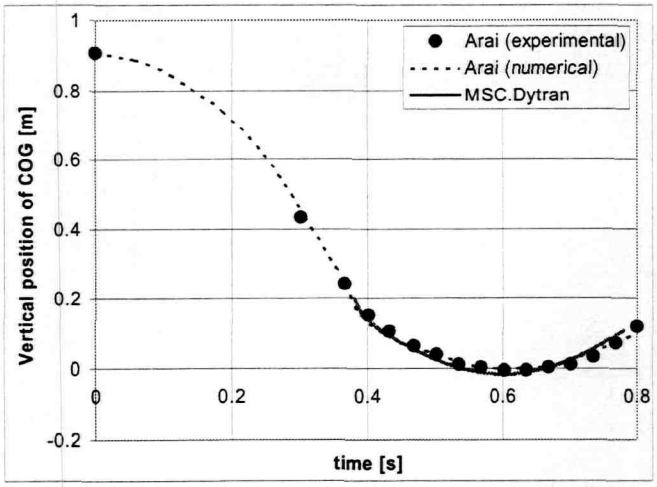


Figure 3.57. Vertical position of center of gravity of the cylinder (drop height is 0.75 m)

The displacement of the point "A" relative to undeformed shape is presented in Figure 3.59. The agreement of the amplitude of displacement is quite good, while the period of vibration is different. This difference can probably be explained by the fact that the model of Arai does not consider cavitation, which is modeled in the MSC.Dytran model. In the model of Arai the water surrounding the cylinder is constantly attached to the cylinder

lowering the frequency of vibration. In the MSC.Dytran model both cavitation and ventilation appear beneath the cylinder during the impact. This means that during some time the shell vibrates in the air having a higher frequency of vibration.

Obviously the agreement between the MSC.Dytran model and the results of Arai is reasonable. This is not surprising in the light of the considerable differences in chosen approaches and numerical tools. However the author accepts this as a satisfactory result considering the complexity of the problem.

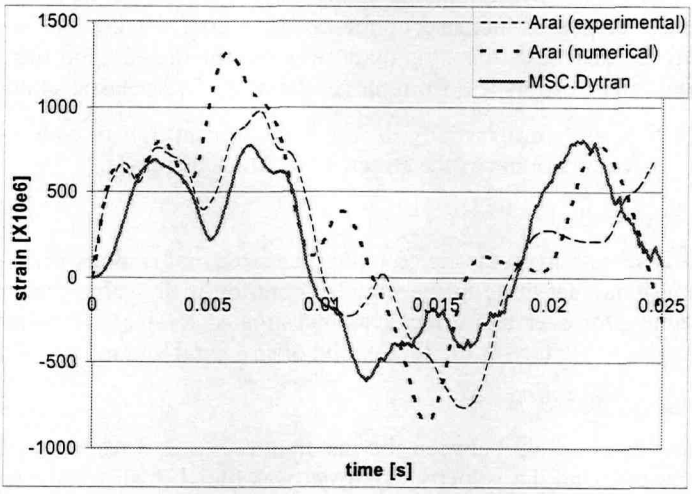


Figure 3.58. Strain history (point "A" in Figure 3.56, drop height is 1 m, the record starts from the moment when the cylinder touches the water surface)

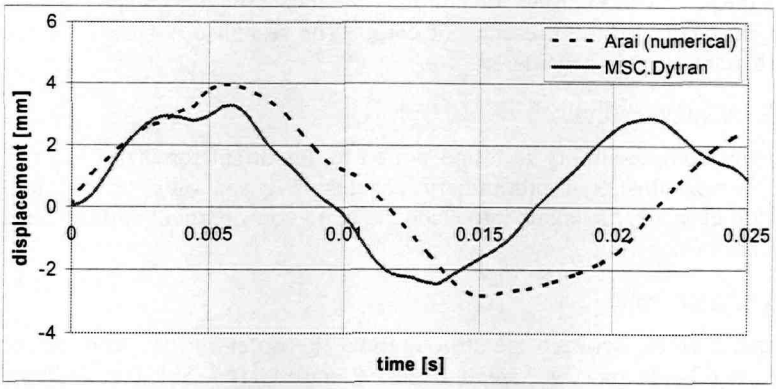


Figure 3.59. Displacement history (point "A" in Figure 3.56, drop height is 0.75 m, the record starts from the moment when the cylinder touches the water surface)

## 3.11 Conclusive remarks

The most important findings of this chapter are summarized:

- Hydroelasticity

  It was found that effect of hydroelasticity is extremely important for the slamming problem when the deadrise angle is close to zero, which means that the duration of the impact is quite short. Hydroelasticity generally leads to a reduction of the hydrodynamic loads and consequently to a reduction of the structural response. Increase of the deadrise angle makes the impact duration longer. In this case the structural response predicted ignoring the effect of hydroelasticity differs less from the results of the hydroelastic solution.

  The effect of hydroelasticity is more significant for flexible structures and becomes less important as the structural stiffness increases.

- Impulse loading

  In the case with hydroelastic coupling, the structural response caused by impulse loading is not sensitive to the impulse duration if the value of impulse remains the same. However this effect was investigated for the case when the impulse duration is in vicinity of the first period of structural vibration.

- Velocity of impact

  A linear relationship between the maximum structural response (displacements, stresses etc.) and the velocity of impact was found (hydroelastic solution, no air entrapment is considered).

- Influence of cargo

  In the case with hydroelastic coupling the local structural response is not affected significantly by the presence of cargo. The response is similar to the situation when no cargo is considered.

- Water compressibility

  Water compressibility is found not to be important for the structural response. However, this is a preliminary conclusion based on a model in which no hydroelasticity is taken into account. Only one particular deadrise angle was considered.

- Air entrapment

  Entrapped air between the structure and the water surface leads to reduction of impact loads for very small deadrise angles ($0° - 5°$) the air being a quite effective cushion. For greater angles the effect of the entrapped air is not important and can be neglected. The most dangerous case is observed for a two-degree deadrise angle when the air can escape the interface area. This makes the impact loads higher, which leads to a more severe structural response. At the

same time, for zero-angle the response is slightly less because more air is trapped.

However it should be clear that the range of deadrise angles between $0° - 5°$ is a function of several factors such as the velocity of impact, dimensions of the structure, presence waves on the free water surface etc. Perhaps in some cases the air entrapment can be important for even larger deadrise angles or vice versa.

- Criterion of importance of hydroelasticity

  It was found that the importance of the effect of hydroelasticity can be predicted by a special ratio. This is the ratio between the duration of the slamming impact and the first period of natural vibration of the dry structure. From an advanced numerical study it was found that hydroelastic effects are only important if the ratio is less than 2. This ratio is proposed to be used as a key criterion in deciding whether a hydroelastic analysis is required or that the effect of hydroelasticity can be neglected.

- Water penetration of a flexible cylinder

  A quite satisfactory agreement between numerical results obtained by the author and experimental data and numerical results of Arai [5] was found for water penetration of a flexible cylinder. This gave a certain confidence in reliability of the finding of this chapter based on purely numerical results.

- 2D problem

  This chapter discusses results of 2D modeling. However, it is expected that 2D modeling can overestimate the hydrodynamic loads and hence the structural response. An investigation of the effect of three-dimensionality is required. This will be discussed in Chapter 4.

# Chapter 4

# 3D PROBLEM

Results of a series of advanced 2D numerical simulations discussed in Chapter 3 give good insight into the mechanism of slamming. However the effect of three-dimensionality is still an issue. Moreover an accurate verification of numerical tools used in Chapter 3 is required by the available experimental data.

First, a numerical analysis of the TNO drop tests is discussed in this chapter showing a good agreement between the numerical results and the experimental data (Section 4.1). Then, the effect of three-dimensionality is studied for water penetration of a rigid body in Section 4.2.

## 4.1 Numerical analysis of the TNO drop tests

The TNO drop test is studied numerically in this section with application of the MSC.Dytran code [15]. The numerical results are compared with the experimental data. The experimental set-up is described in Section 2.2 [34, 35, and 115].

A case of a flat impact is modeled, which means that the angle between the panel surface and the water surface is zero. The analysis starts when the air gap between the body and the water surface is about 10 cm. At this moment the panel has a specific velocity. This velocity is determined from consideration of the initial drop height. The global motion of the panel is not restricted in the numerical analysis. This motion is calculated based on the panel mass, gravity force, and the hydrodynamic force.

Several bottom panels, including steel panels with plate thicknesses of 6 mm and 14 mm, were tested in the TNO experiment with drop heights of 0.75 m and 1.5 m. Four simulations were performed for these two steel panels for both drop heights.

A 3D MSC.Dytran model is shown in Figure 4.1. This model consists of the water domain, the air domain, and the flexible bottom panel. Some air elements are not shown in the figure in order to make the panel visible. Due to symmetry only a quarter of the model is considered. The panel is subdivided into shell elements. An ideal elastic-plastic model is applied to describe the material of structure. Modulus of elasticity is $E = 210\,\text{GPa}$. Yield stress is $\sigma_y = 250\,\text{MPa}$. Density is $\rho = 7850\,\text{kg/m}^3$.

Figure 4.2 shows the velocity of the center of gravity of the box for one of the simulations (plate thickness is 6 mm, drop height is 0.75 m). Numerical results are in quite good agreement with the experimental data. This agreement in prediction and measurements of

the global motion is a very important issue. Because this means that the global motion is simulated in a correct way and further analysis can take place.

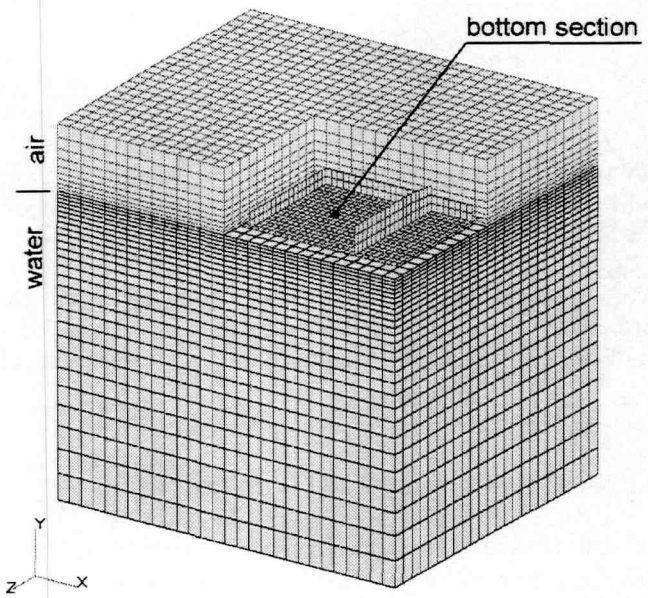


Figure 4.1. 3D model for the TNO drop test

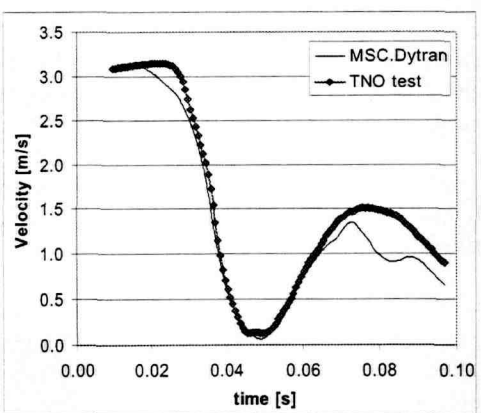


Figure 4.2. Vertical velocity of the center of gravity of the box (plate thickness is 6 mm, drop height is 0.75 m)

The deformation of the water surface is shown in Figure 4.3. The pressure field in the water is shown in Figure 4.4 for the time moment when the pressures are at the maximum

value. This moment occurs at the beginning of the water impact when the air gap between the structure and water is almost closed. The displacement of the panel in y- direction is shown in Figure 4.5. The panel has its maximum displacement at the point which is located between the side of the panel and the stiffener. This is point N1 in Figure 4.5. The displacement of this point is monitored during the analysis. Comparison with the experimental data is given in Figure 4.6-Figure 4.9 for two drop heights and two plate thicknesses. The first peak is the most important one because that is the moment when the panel has maximum displacement. The agreement with the experimental data is quite good. The difference in prediction of the first peak does not exceed 5% except for the simulation for the panel with the plate thickness of 14 mm and drop height of 0.75 m (Figure 4.8). Here the difference increases to 20%. For all models the numerical results are in good agreement with the experimental data at the beginning of the impact up to the time moment of 0.06 s. Later this agreement deteriorates especially for the drop height of 1.5 m (Figure 4.7 and Figure 4.9). This can be explained by some complications in the interpretation of the experimental data. The reason of this is the following. In the experiment the data was taken from accelerometers. In order to find the structural displacements a double integration was required. For short term analysis the displacements were calculated with sufficient accuracy. However, for a longer period of time the data is less reliable. In spite of this, the comparison of the first peak of displacement seems to be sufficient for determining the most severe structural response, because this response takes place at the beginning of the impact.

Summarizing the results it is clear that the numerical simulations reproduce the experimental data quite well. Or in other words the present model proves the capability of the numerical tools to predict the slamming loads and structural response with quite high accuracy giving strong confidence in the reliability of numerical results obtained earlier.

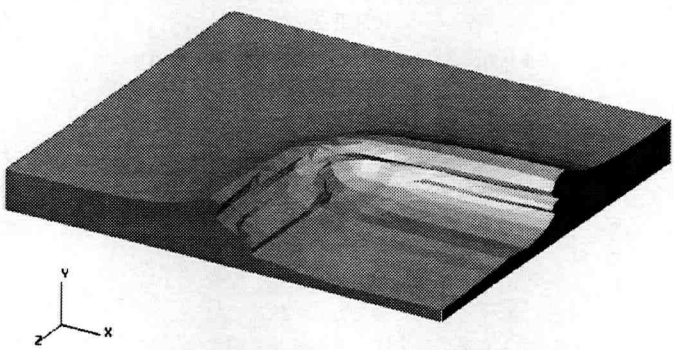


Figure 4.3. Deformation of free water surface
(plate thickness is 14 mm, drop height is 0.75 m)

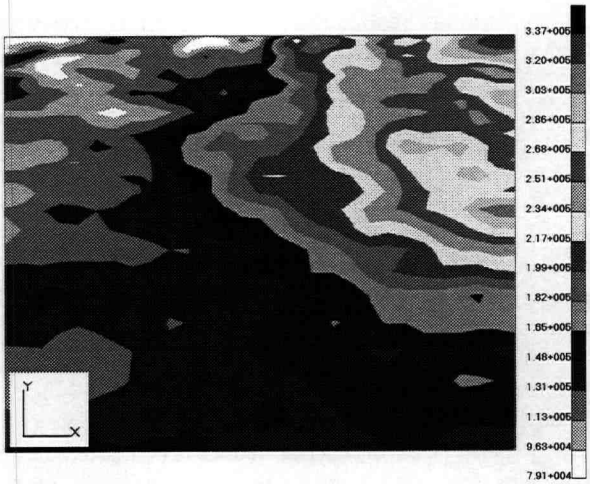


Figure 4.4. Pressure in water in the symmetry plane X0Y [Pa] (plate thickness is 14 mm, drop height is 0.75 m)

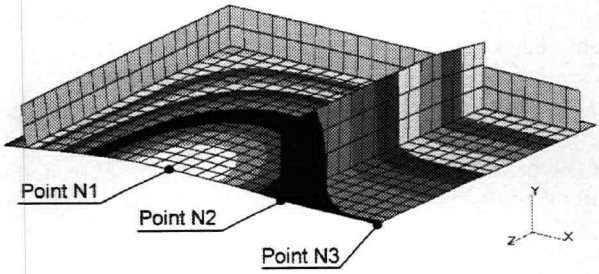


Figure 4.5. Bottom panel deflection

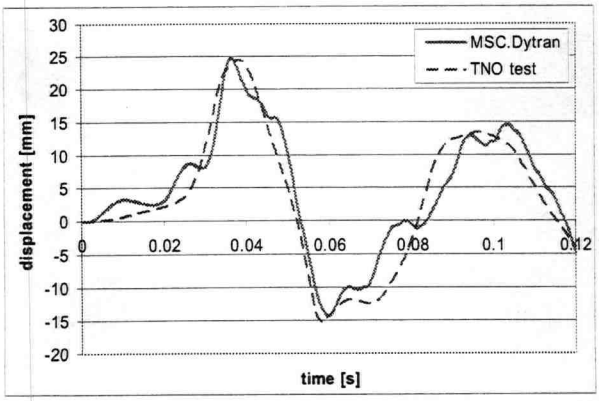


Figure 4.6. Displacement in the middle of the panel between the stiffener and the side as a function of time (plate thickness is 6 mm, drop height is 0.75 m)

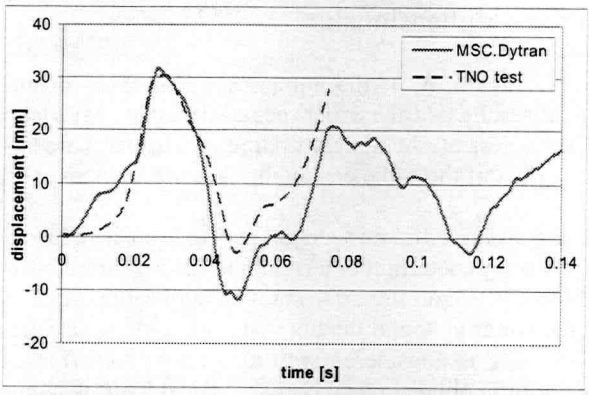


Figure 4.7. Displacement in the middle of the panel between the stiffener and the side as a function of time (plate thickness is 6 mm, drop height is 1.5 m)

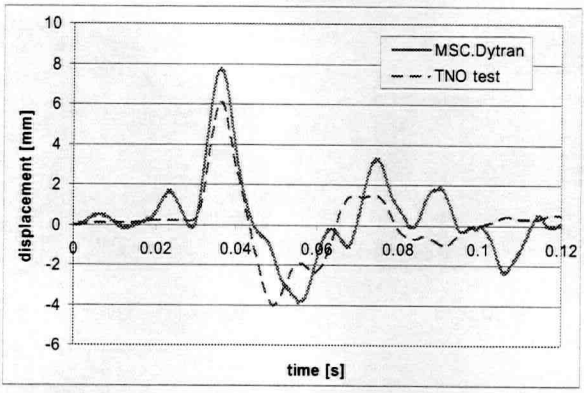


Figure 4.8. Displacement in the middle of the panel between the stiffener and the side as a function of time (plate thickness is 14 mm, drop height is 0.75 m)

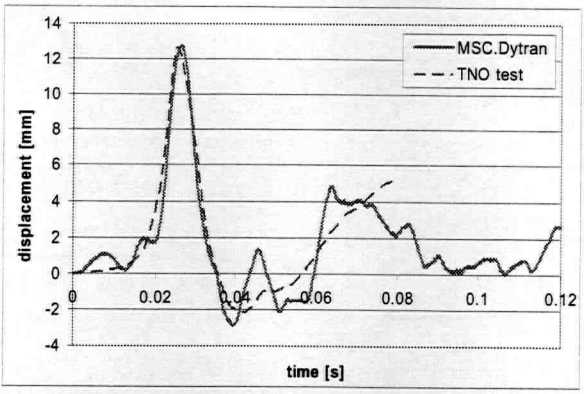


Figure 4.9. Displacement in the middle of the panel between the stiffener and the side as a function of time (plate thickness is 14 mm, drop height is 1.5 m)

## 4.2 Effect of three-dimensionality

Section 4.1 proves the reliability of the numerical tools based on the good agreement between the numerical results and the experimental data. The calculations are carried out for a 3D model. Nevertheless all theoretical finding of Chapter 3 are based on 2D models. At the same time the effect of three-dimensionality has not been investigated yet.

Two simple models are discussed in this section giving some insight in the effect of three-dimensionality [15]. Water penetration of a rigid body at zero-deadrise angle is studied for 2D and 3D cases (Figure 4.10 and Figure 4.11) with application of the MSC.Dytran code. The dimensions of the water tank and the body are the same as in Section 4.1. The mean pressure on the rigid body is considered with air and without (Figure 4.12 and Figure 4.13). The mean pressure is obtained as the total vertical hydrodynamic force divided by the bottom area of body. This is done to make quantitative comparison of the hydrodynamic loads acting on the body.

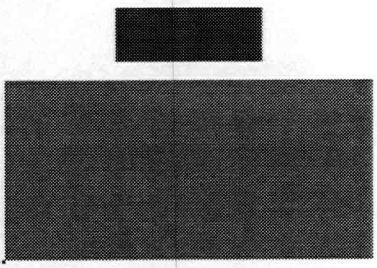

Figure 4.10. 2D model

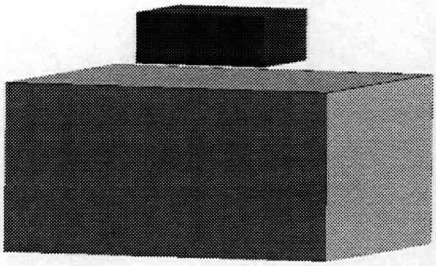

Figure 4.11. 3D model (the bottom of the rigid body is square)

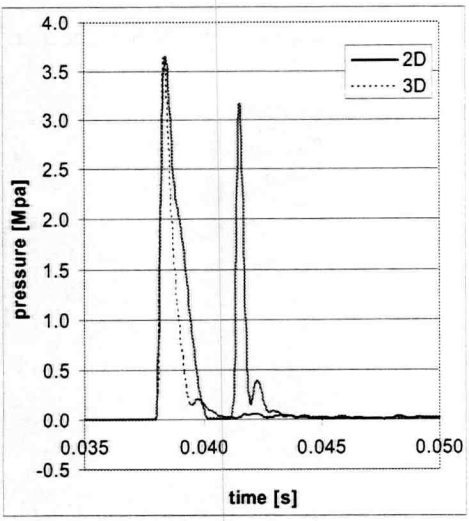


Figure 4.12. Mean pressure (no air)

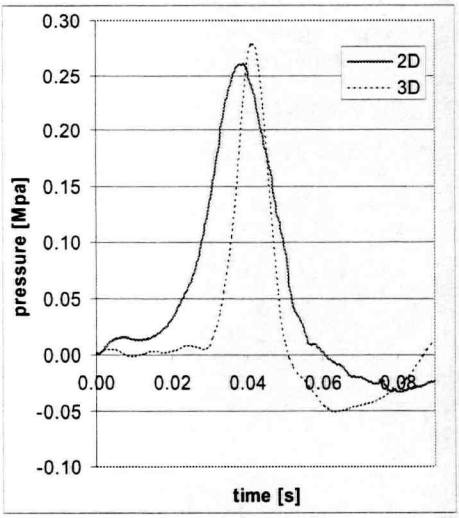


Figure 4.13. Mean pressure (with air)

A significant difference is seen for the case when air is not considered. In the 2D problem the pressure curve has two peaks and the 3D model gives only one peak. This difference is caused by a completely different nature of the pressure wave propagation. In the 2D case most of the pressure wave goes down and then reflects from the bottom hitting the body again. In the 3D model the pressure wave spreads not only down but also in two horizontal directions causing very fast energy diffusion across the whole water volume. As a result there are no visible reflected pressure waves and the pressure peak is shorter. At the same time the force amplitude at the first peak is quite similar in both cases, which is quite typical for the flat impact.

For the case when air is modeled both models give only one pressure peak with approximately the same amplitude. The duration of the impact is, however, shorter for the 3D case. In the 3D model there is more freedom for air and water to spread into different directions. Probably that is why the pressure peak for the 3D model is a slightly higher: air escapes the interface area quicker making the water impact harder (the pressure is higher and the duration of impact is shorter).

The effect of three-dimensionality is shown to be significant. However, the conclusions of Chapter 3, which are based on 2D models, remain valid because these are qualitative conclusions. In Chapter 3 two 2D models are typically compared with each other, whether it is comparison of a hydroelastic model with a model where hydroelasticity is not considered, or this is investigation of effect of entrapped air. These are both 2D models, which means that they both can overestimate the hydrodynamic forces and, hence, the structural response in comparison with 3D modeling. But the qualitative estimation of each particular effect within a 2D formulation remains valid. In other words 2D modeling is a very effective tool in the investigation of the different factors involved in the slamming problem. However if more detailed study is required a 3D modeling should be carried out.

# Chapter 5

## PRACTICAL IMPLICATIONS OF HYDROELSTICITY IN SHIP DESIGN

The review of research on the hydroelasticity shows that understanding of the subject has been increased but discussions of practical implications of hydroelasticity to ship design are rare. The author aimed to change this and investigated how allowance for the hydroelasticity affects assessment of ship performance. In order to illustrate this, a structure of a typical modern cruise liner is analyzed in this chapter [21]. Aftship slamming has been chosen as a case study, because several modern cruise liners are prone to it (Figure 5.1). Slamming impact can initiate ship vibrations with quite high accelerations along the whole ship. These accelerations affect passengers' comfort. The whipping part of the vibrations produces an additional global vertical bending moment, which has to be accounted for in the strength assessment of the hull girder. In the slamming zone the local structure can experience very high stresses.

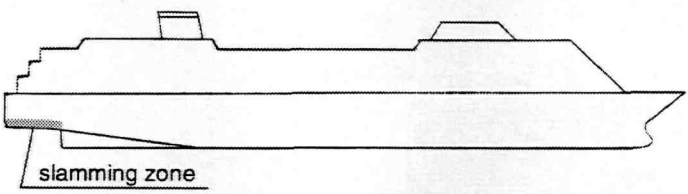


Figure 5.1. A typical modern cruise liner

Traditionally hydroelasticity is not taken into account in a practical design process. The contribution of slamming to the global bending moment is typically determined without consideration of the effect of hydroelasticity [84, 91, 102, and 119]. At the same time if hydroelasticity is considered it is done for quite simple cases with a number of limitations. In this section the hydroelastic aspects are discussed for a simplified MSC.Dytran model of the whole ship including both the local and the global structural members.

The following typical cruise liner is modeled here:

Length overall – 290 m.
Breadth – 32 m.
Design draft – 8 m.
Displacement – 42 000 t.

The model is shown in Figure 5.2. Because of the symmetry only the port side is modeled. The model consists of the hull girder, the ship transverse frame in the slamming zone, and air domain and water. The frame is attached to the girder at the point where bottom and the side meet by means of coupling motion of degrees of freedom. In other words, the model consists of a 2D-hydroelastic model for the cross-section of the ship involved in the

impact and the hull girder. The width of the water/air domain is 72 m (half of this domain is modeled because of symmetry). The water region has a depth of 30 m. The height of the air area is 15 m. The dimensions of the frame are the following: the height is 23.8 m, and the width is 16 m (half because of symmetry). The frame is shown in Figure 5.3. MSC.Dytran can handle only solid elements for the Eulerian mesh. In order to build a 2D model a slice of water and air is considered having only one solid element in longitudinal direction (x-axis in Figure 5.2). The length of this element is 14 m. This is the length of the area involved in the aftbody slamming. A rigid wall boundary condition is applied at the sides of the air-water region. The analysis starts when the air gap between the body and the water surface is about 2 m. It was found from an additional series of calculations that this is the optimal distance for this particular model. A greater distance is more time consuming for the simulation, while there is no visible increase of air pressure until the distance is reduced to about 2 m. The frame is modeled using shell elements. The hull girder is modeled as a beam.

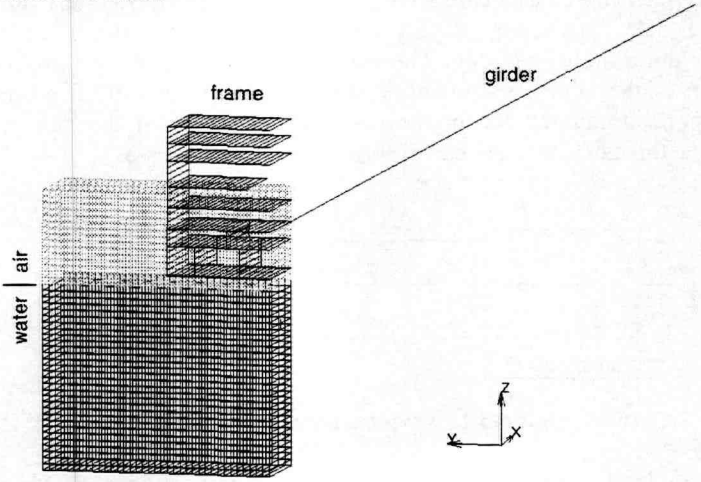


Figure 5.2. The hydroelastic model

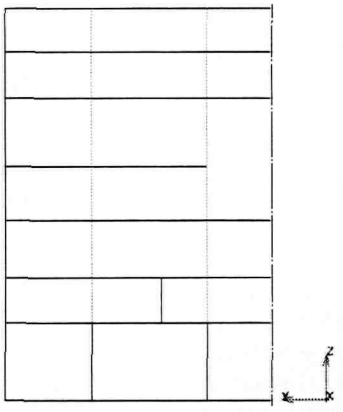


Figure 5.3. Aftship transverse frame at slamming area

The first natural frequency of the dry frame and girder are 7.3 Hz and 0.91 Hz, respectively. At the beginning of the simulation the hull girder with the attached frame falls down freely with initial velocity of 1.5 m/s. Gravity is instantly applied to all members of the numerical model as the analysis starts. Due to the gravity force the hydrostatic pressure in the water is a linear function of the water depth. In order to specify this pressure gradient, a slightly different water density is applied depending on the distance from the free surface. To compensate the gravity force on the structure, a uniformly distributed force is applied to all members of the structure depending on their mass and in a direction opposite to the vector of the gravity force.

As the water penetration begins the frame experiences hydrodynamic loads. The velocity of the frame penetration decreases. This motion change excites the hull girder. Both the frame and the girder start vibrating. The hydrodynamic force acting on the frame and then transmitted to the girder is the only force, which changes the global motion of the girder. All other forces influencing the global motion of the girder, like varying buoyancy caused by interaction of the ship with waves, are disregarded in order to simplify the model. This assumption is expected to be valid for estimation of the whipping of the girder, since the force of the slam has the greatest contribution. Moreover, the simulation covers the time period of 2 seconds only. This period is enough to determine the local structural response as well as the response of the girder, while the global ship motion is not affected much.

The frame and the hull girder are flexible. Thus, these contribute to the hydroelasticity. In order to investigate their contribution, together and separately, several models have been considered (Table 5.1):

Table 5.1. Description of models

| Model | Approach | Structural members in water simulation | Structural members in structural analysis |
|---|---|---|---|
| 1 | full hydroelastic coupling | flexible girder<br>flexible frame | |
| 2 | traditional global approach | rigid girder<br>rigid frame | flexible girder<br>rigid frame |
| 3 | traditional local approach | rigid girder<br>rigid frame | rigid girder<br>flexible frame |
| 4 | local hydroelastic coupling | rigid girder<br>flexible frame | |
| 5 | global hydroelastic coupling | flexible girder<br>rigid frame | |

Model 1. A full hydroelastic coupling is performed. Both the hull girder and the frame are flexible.

Model 2. A traditional 2-step global approach is applied. First, the water simulation is performed assuming that the hull girder and the frame are rigid. Then, the hydrodynamic force from the first step is used to find the response of the girder. This is a typical case when the slamming loads are determined numerically or from experiments and the girder response is found based upon application of these loads.

Model 3. The third model is the same as the second model but the frame is flexible in the structural analysis, while the girder is assumed to be rigid. Again it would be a typical case when the slamming loads are determined numerically or from experiments and the local structural response is found based upon application of this loads.

Model 4. This model considers a hydroelastic interaction assuming that the girder is rigid and the frame is flexible. This model will help to evaluate the contribution of the flexibility of the girder to this hydroelastic interaction.

Model 5. This model is similar to the fourth model, but the contribution of the local structure is studied.

First the results obtained for the fully hydroelastic model (model 1) and the traditional global model (model 2) are compared. Figure 5.4 shows that the allowance for the hydroelastic coupling results in 33% lower maximum midship vertical bending moment. The maximum total vertical hydrodynamic force acting on bottom is reduced by 34% (Figure 5.5). At the same time the maximum absolute vertical acceleration at midship remains the same. The acceleration time trace contains, however, a dominant 7.3 Hz component that corresponds to the first natural frequency of aftship frame (Figure 5.6). Note that in model 2, the 7.3 Hz component cannot be present, as the frame is rigid.

After that the results obtained for the fully hydroelastic model (model 1) and the traditional local model (model 3) are compared. Figure 5.7 and Figure 5.8 show that the allowance for hydroelastic coupling reduces the maximum bottom displacement and stress at the center line (CL) by 30%.

Subsequently, the contributions of hull girder and frame flexibility are determined by comparing the local and global hydroelastic models (models 4 and 5) with the fully hydroelastic model (model 1). First, the case of the rigid girder (model 4) is compared with the fully hydroelastic solution (model 1) in Figure 5.9 and Figure 5.10. It can be seen that the girder flexibility reduces the maximum bottom displacement and stress at CL by about 25%. Then, the model 5 with global hydroelastic coupling (flexible girder but rigid frame) is compared with the fully hydroelastic model (model 1). Figure 5.11 shows that the frame flexibility reduces the maximum midship vertical bending moment by 10%.

Therefore, it can be concluded that the girder flexibility contributes more than the frame flexibility to the reduction of the maximum midship bending moment and bottom stress. However, the frame flexibility contributes significantly to the overall reduction.

Implications of the effect of hydroelasticity in ship design are considered by evaluation of the following ship design criteria: the longitudinal strength of the hull girder, the local plating thickness, and the passenger's discomfort.

It should be emphasized that the aftship slamming analyzed here quantitatively represents an extreme slamming event. The resulting maximum total vertical hydrodynamic force equals (model 1) about 22 MN. On the one hand this value, representing more than 5% of the ship displacement, equals about 75% of the design wave shear force. On the other hand the maximum average slamming pressure equals only 50 kPa. In general, slamming design pressures for the present ship would be one order higher. However, the analyzed slamming is extreme, because the whole aftship area (32m x 14m) hits the water surface simultaneously and not because the impact velocity is high (1.5 m/s).

Further, it can be the case that the present 2D hydroelastic model produces higher pressures than the real 3D case would do as it was discussed in Section 4.2. However it can be expected that qualitative conclusions made in this section remain valid whereas their quantitative content will change.

Design criteria for longitudinal strength, which are specified by IACS (International Association of Classification Societies), do not explicitly account for additional bending moments produced by hydrodynamic impacts. In general, the hull load carrying capacity has to be compared with the maximum bending moment that is defined by a joint probability distribution of wave bending moment, still water bending moment and hydrodynamic moments. Such an approach is outside of the scope of the present research project and the author restricted himself to comparing the maximum whipping moment with the design wave bending moment, which equals 3.75 GNm for the present ship. Figure 5.4 shows that the maximum bending moment equals about 1.3 GNm and 0.88 GNm without and with hydroelastic coupling, respectively. In both cases the whipping bending moment is very significant and consumes respectively 35% and 23% of the design wave bending moment. On the one hand it has to be concluded that a large flat aftship has to be avoided in ship design. On the other hand introduction of podded propellers desires such an aftship. This contradiction has to be balanced in the design process. The present investigation gives an indication that hydroelasticity is an important tool in reaching that balance. As stated before the traditional approach (without using hydroelastic coupling) overestimates whipping bending moments by 33% (Figure 5.4).

Design criteria for local plating subjected to lateral pressure, which are specified in different classification society rules, are based on limiting the maximum permanent plate deflection. They relate the plate thickness to the square root of the slamming pressure. Figure 5.5 shows that reduction in maximum average pressure over the bottom plate equals about 34%. This means that the allowance for hydroelasticity would result in about 19% thinner bottom plating based on slamming considerations (19 mm instead of 23 mm

in the present case) in comparison with the case when the plate thickness is determined in accordance with the traditional local approach (model 3).

Passengers' discomfort is a crucial consideration in the design of cruise ships. However, there are no rules available which explicitly provide acceptance criteria for the evaluation of passengers' discomfort when a ship is responding to hydrodynamic impacts. Elements of ISO (1997) norm [63] are used in order to assess the discomfort to whole hull vibration. The time traces of midship accelerations, which are shown in Figure 5.6, have been analyzed. As can be seen, they include several components: 0.91 Hz (whipping), 7.3Hz (transverse frame natural frequency) and higher components above 30 Hz. Only the first two components are in the frequency range that affects human comfort. The MTVV (Maximum Transient Vibration Value) of weighed accelerations equals 2.5 $m/s^2$ irrespective of hydroelastic coupling. Such acceleration levels are extremely uncomfortable on board of a cruise ship and a designer would need to reduce them by a factor of five as the acceptable accelerations are lower than 0.5 $m/s^2$. For now however a more important conclusion is that the evaluation of a discomfort criterion is not affected by hydroelasticity. The validity of this conclusion has to be further investigated although the result has a clear physical (and not numerical) background. One of the factors to be investigated is the effect of structural damping, which has been disregarded in the present analysis.

It has been found that applying the hydroelastic approach, instead of the traditional 2-step approach, leads to significant reduction of the hydrodynamic loads due to aftship slamming. The hull girder flexibility contributes twice as much to that reduction as the frame flexibility. This is due to the fact that the first period of natural vibration of the local structure is shorter that the duration of the slam pressure pulse (the ratio is about 1:7), whereas for the hull girder this ratio is 1:1.

The following conclusions have been made with respect to the longitudinal strength, the local strength and the passengers' discomfort:

- The traditional approach (without using hydroelastic coupling) overestimates the whipping bending moment by 33%. This overestimation is significant since the whipping bending moment can correspond to 23% (in case of hydroelastic model) and 35% (in case of model without hydroelastic coupling) of the design wave bending moment.
- The local structural response (the response of the bottom of the aftship transverse frame is considered) is also less severe in case of hydroelastic coupling. The reduction of displacements and stresses reaches 30%.
- With respect to the passengers' discomfort it has been concluded that the evaluation of discomfort criterion in not affected by hydroelasticity. Both the hydroelastic modeling and modeling without hydroelasticity give similar acceleration levels.

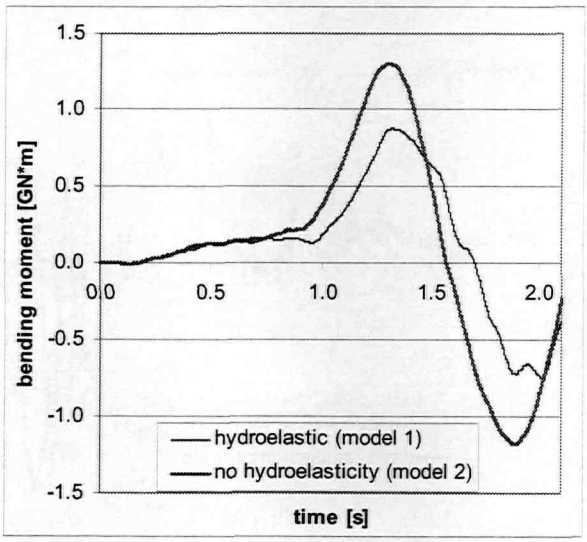


Figure 5.4. Midship vertical bending moment (comparison of models 1 and 2)

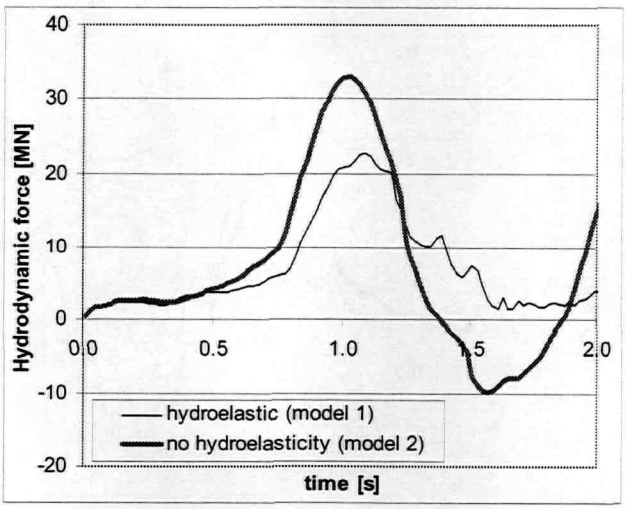


Figure 5.5. Total vertical hydrodynamic force acting on bottom (comparison of models 1 and 2)

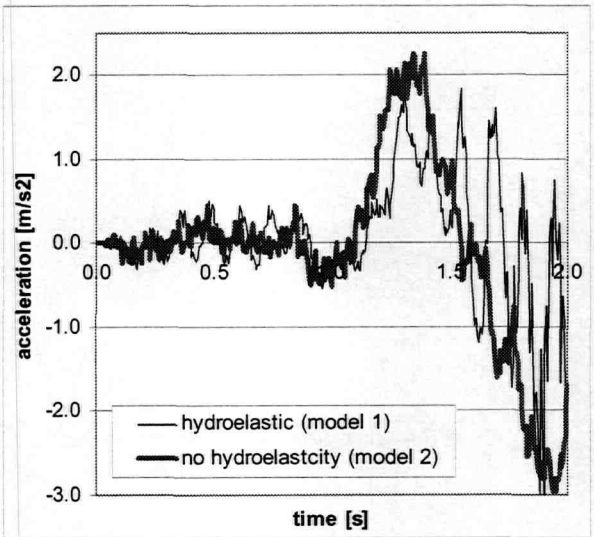


Figure 5.6. Midship vertical acceleration (comparison of models 1 and 2)

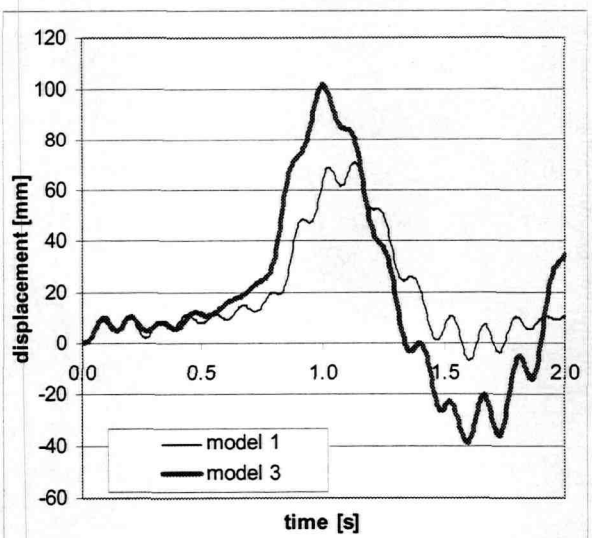


Figure 5.7. Bottom displacement at CL (comparison of models 1 and 3)

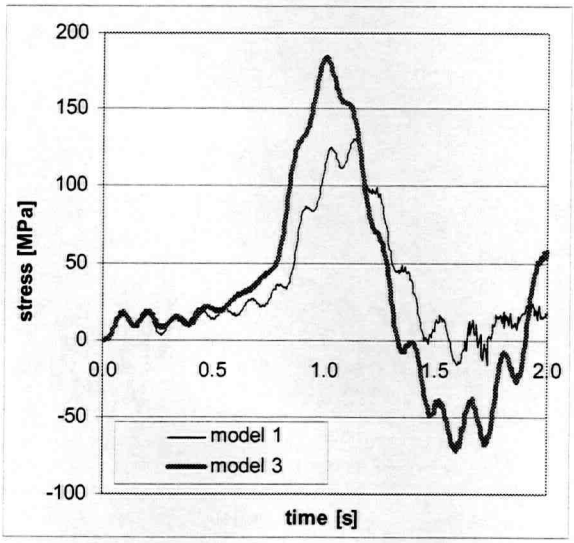


Figure 5.8. Bottom stress at CL (comparison of models 1 and 3)

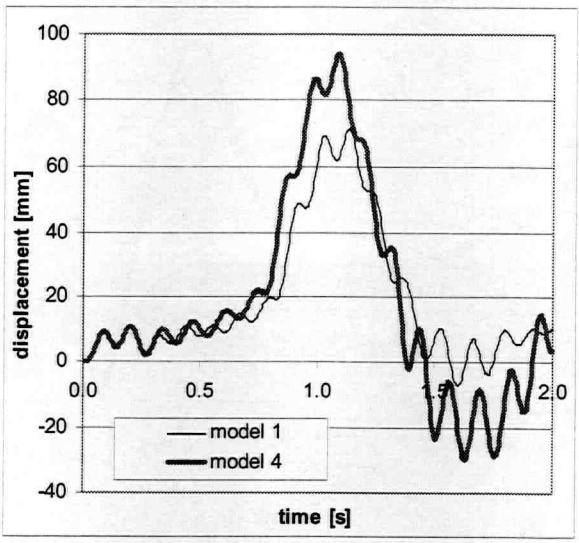


Figure 5.9. Bottom displacement at CL (comparison of models 1 and 4)

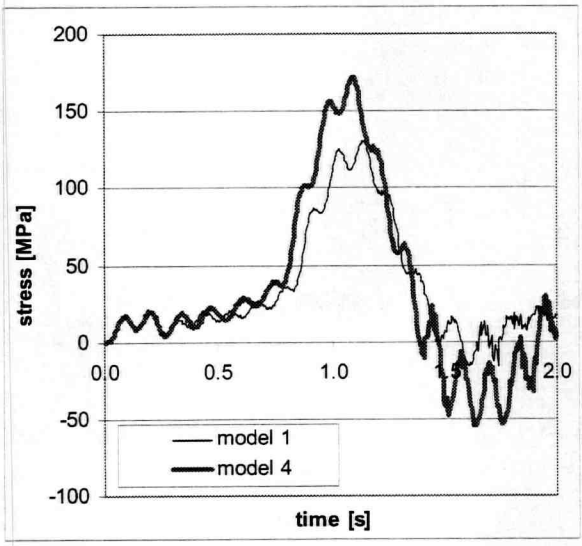


Figure 5.10. Bottom stress at CL (comparison of models 1 and 4)

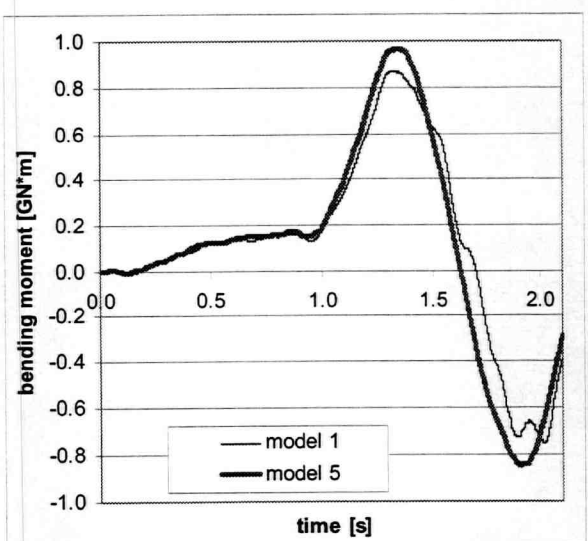


Figure 5.11. Midship vertical bending moment (comparison of models 1 and 5)

# Chapter 6

# DISCUSSION AND CONCLUSIONS

## Summary of discussion

This thesis gives a broad overview of many aspects of the effect of hydroelasticity in ship's slamming and identifies the most important ones. These aspects are considered not only separately but also in combination with each other. This thesis is not only a theoretical discussion but considers real structures. An advanced numerical study based on different approaches implemented in the author's own code and commercial codes gives a new and more objective insight in the physical aspects of the slamming phenomenon. This numerical study is verified with some experimental data, which was available from the TNO and open publications. The author is convinced that the findings of this thesis will lead to better knowledge and understanding of the slamming phenomenon resulting in more accurate prediction of hydrodynamic impact loads, and hence the structural response. This can generally improve the ship design making the sea transportation more safe, more attractive economically and environmentally friendly.

Slamming is recognized as a local phenomenon causing damage to the ship structure locally. This is the reason that the majority of models studied in this thesis describe local structures, most of the time considering 2D problems. However the global effects such as whipping of the hull girder caused by slamming are also discussed.

The author has considered neither the ship motion analysis nor the stochastic analysis but has concentrated on hydroelastic aspects of the slamming phenomenon. It was found that hydroelasticity contributes to a significant reduction of the structural responses in comparison with the traditional 2-step approach, where the loads are determined separately from the structural response. Obviously performing a hydroelastic analysis is not a simple task. Not many ship design offices can afford this, especially if it is not clear of how large the effect of hydroelasticity is for each particular case. In order to resolve this situation the author has introduced a criterion. This criterion is based on the value of a ratio between the duration of the slamming impact and the first period of natural vibration of the dry structure. From an advanced numerical study it was found that hydroelastic effects are only important if the value of the ratio is less than 2. This criterion can help to decide either a hydroelastic analysis is required or the effect of hydroelasticity can be neglected. Furthermore, it is quite simple to apply practically, because the duration of the impact can be defined through application of many available fluid codes or even on the basis of analytical solutions since the rigid body water penetration has to be considered. A simple modal analysis of the structure can be performed through the use of finite element analysis in order to find the first period of the structural natural vibration. Finding both the impact duration and the period of vibration determines the ratio. The author hopes that this recommendation will find practical applications.

What does it mean if the value of the ratio is less than 2? It means that the slam duration should be shorter than double period of the structural vibration, in other words, either the structure has to be more flexible or the slam should be very short. The slam with short duration can take place when a quite large area of the structure abruptly comes into contact with the water. This occurs if the ship hull has a small deadrise angle or a small angle between the hull and the wave surface in a more general case. This is the situation in which the air entrapment can take place. It was found that entrapped air leads to a substantial reduction of impact loads, and therefore the structural response, for very small deadrise angles ($0° - 5°$). The entrapped air behaves as an effective cushion. For greater angles the effect of entrapped air is not important and can be neglected. The most dangerous case is observed for a two-degree deadrise angle when the air can escape the impact area. This makes the impact loads higher, which leads to more severe structural response. At the same time, for zero-angle the response is slightly less because more air is entrapped.

The effect of hydroelasticity is obviously a function of the structural flexibility. A decrease of the structural flexibility contributes to the effect of hydroelasticity. However it was found that this contribution is much less significant than could be expected. It was found for one of the 2D models that the increase of the structural stiffness by a factor of 15 (the moment of inertia of the bottom beams is increased 15 times) changed the reduction of the maximum deflection of the bottom due to the effect of hydroelasticity from 76% to 51% only. This finding can lead to the following practical conclusion: an increase of structural stiffness by introducing more material is not a universal solution when hydroelasticity is involved. Stiffer structures bend less. This makes the hydrodynamic pressure higher. The structure experiences greater loads. This causes more severe structural response.

The investigation of the effect of water compressibility showed that the water compressibility is not important for the structural response. However, this is a preliminary conclusion based on a model with a particular deadrise angle in which no hydroelasticity is taken into account. On the one hand, incompressible fluid model is more simple in comparison with compressible fluid model. Thus, the priority can be given to further development of incompressible fluid-structural models. On the other hand, incompressible fluid-structural model appears to be very unstable when the weak formulation is deployed (Section 2.3.6).

Most of theoretical finding of this thesis are based on 2D models. At the same time all practical situations are obviously three-dimensional. An additional series of calculations showed that the effect of three-dimensionality is significant. The basic difference between a 2D model and a 3D model is the fact that in a 3D fluid model the pressure wave spreads in three directions causing faster energy diffusion across the whole fluid volume. Thus, the hydrodynamic forces found from a 2D model are usually overestimated. However, the conclusions based on 2D models, are expected to remain valid because these are qualitative conclusions. Typically two 2D models are compared with each other, whether it is comparison of a hydroelastic model with a model where hydroelasticity is not considered, or this is investigation of effect of entrapped air. These are both 2D models, which means that they both can overestimate the hydrodynamic forces and, hence, the

structural response in comparison with 3D modeling. But the qualitative estimation of each particular effect within a 2D formulation remains valid. In other words 2D modeling is a very effective tool in the investigation of the different factors involved in the slamming problem. However if more detailed study is required a 3D modeling should be carried out.

In addition to the investigation of local structural response, global effects caused by slamming were numerically analyzed for a cruise ship suffering the aftbody slamming. It was surprising to find that the hydroelastic contribution of the hull girder to the reduction of impact loads and the structural response is twice as much as the contribution of the local stern structure directly subjected to the slamming loads. Further analysis showed that the ratio (according to the criterion introduced in this thesis) for the girder was 1 and for the local structure 7, meaning that the girder response is expected to be hydroelastic, while the hydroelastic contribution of the local structure is small. With respect to practical aspects it was found that the hydroelastic model gives 33% reduction of the global whipping bending moment in comparison with the traditional 2-step approach (without hydroelastic coupling). This reduction is significant since the whipping moment can correspond to 23% (in case of hydroelastic modelling) and 35% (in case no hydroelasticity) of the design wave bending moment.

**Conclusions**

1. The hydroelasticity contributes to a significant reduction of the structural responses in comparison with the traditional 2-step approach, where the loads are determined separately from the structural response, if the value of the ratio between the duration of the slamming impact and the first period of natural vibration of the dry structure is less than two.
2. The entrapped air between the structure and the water surface leads to a substantial reduction of impact loads, and therefore the structural response, for very small deadrise angles (typically $0° - 5°$).
3. A decrease of the structural flexibility contributes to the effect of hydroelasticity. However it was found that this contribution is much less significant than could be expected.
4. The effect of water compressibility was found not important for the structural response.
5. The effect of three-dimensionality was found significant.
6. Investigation of the global effects showed that the effect of hydroelasticity can be very important not only for local but also for global structural response.

**Recommendations for future research**

1. It would be desirable to consider a large number of different practical problems, where water impacts take place, in order to narrow those practical cases, where the effect of hydroelasticity plays an important role. The validity of criterion of importance of hydroelasticity introduced by the author should be verified by a larger number of practical examples.
2. A simple tool is required for design offices and shipping classification societies in order to estimate the effect of hydroelasticity. Only when hydroelasticity matters and an accurate prediction of loads and structural response is needed, then the decision to perform a fully hydroelastic analysis should be taken.
3. The majority of commercial software is either purely hydromechanical or focused on the structural analysis only. Not so much effort is required to combine the software in order to have a good tool for the treatment of hydroelastic problems. And this development would be desirable.
4. Unfortunately the strong formulation for hydroelastic coupling discussed in Section 1.5.2 is suitable for quite simple problems only, while the weak formulation is more flexible but less accurate. Further development of the strong formulation for a greater range of practical problems is required.
5. Today the modern computers are still not powerful enough for handling large hydroelastic models. But there are no doubts that the future developments will bring more possibilities. Then detailed 3D hydroelastic models should be developed and verified by full-scale measurements in order to give better insight in hydroelasticity of slamming problem.
6. Perhaps, at a later stage of the introduction of fully hydroelastic analysis for practical problems, a global integration of this analysis into major procedures including the global ship motion, determination of loads incorporated with stochastic analysis, and the structural response, should take place.

# ACKNOWLEGEMENTS

First of all, I would like to thank TNO and MARIN for their financial support of my project. Without this support the completion of this thesis would not be possible. I would like to express a special acknowledgement to TNO for the experimental data, which I used in this thesis for verification of the numerical results.

Furthermore I am grateful to MSC.Software Corporation for their software which I used working on this thesis, for the flexible software price policy for me, for their interest in my research, and quick on-line help.

My interest in hydroelasticity was initiated by Nikolai Maluzenko. His intention, a few years before I began to work on this thesis, was to study an underwater explosion. Shortly my interest was changed to slamming problem. However his enthusiasm inspired me and gave a great motivation to work on fluid-structure interaction problem. I wish to thank Nikolai Maluzenko for this and also for his help in Saint-Petersburg.

I would like to express my deepest acknowledgement to Valeri Postnov who has been a great teacher and supervisor for me, for his time and effort, for his enthusiasm and motivation, for showing me of what a real scientist should be. His great support and encouragement as a scientific supervisor helped me in my work and completion of this thesis.

Furthermore I am grateful to Jan Spoormaker for giving me an opportunity to come to TU Delft and first most important experiences in Holland, for his great support helping me in settling in a new environment. I would like to thank him for being my scientific supervisor during the first year in Holland. In spite of the fact that later I chose to work in another department, I have never lost contact with him always realizing that I can rely on his help.

I would like to express my acknowledgement to Bart Boon for accepting me as a PhD student with a completely new field of research for his department at his risk. I am grateful to him for his help and motivation.

I would like to express my gratitude to Jo Pinkster for his agreement to become my promoter after Bart Boon left the university. This made continuation of my research possible.

I am happy that during my PhD study I met Jay Bergquist who became a great friend of mine. This was and still is a really international friendship. He brought a lot of new experiences in my life. He helped me to find new great friends as well as important business contacts. His curiosity and desire to learn more about everything including the subject of this thesis gave me extra inspiration to work.

Two years ago my research received a second breath from Mirek Kaminski. Thanks to his great interest in my work. I am grateful to this huge impulse of enthusiasm and motivation which I received from him.

I am grateful to all my colleagues from the Ship Structures Laboratory for their help and support during my PhD study. Additionally I would like to thank Dineke Heersma, whom I was approaching with many practical questions and Co Vink for his in-depth comments on my publications and this thesis.

Furthermore I would like to thank all my friends just for being my friends, which makes my life happy and enjoyable.

I would like to thank Anton Heidweiller for his great friendship, for his ability to give a wise advice and his support.

I am grateful to Valerie Seitz, who once changed my life dramatically showing me a new world full of new incredible experiences making me to think about many things in a different way. I would also like to thank her for her help in designing of the cover of this book.

The photo of ship Victoriaborg on the front cover of this book was kindly presented by Wagenborg Shipping B.V.

Additionally I would like to thank Jeroen van der Cammen for his Dutch translations made for this book.

Finally, I would like to thank my parents not only for giving me a chance to exist in this world and growing me up, but also for their love, care and great support during my years in Holland. I dedicate this thesis to my mother and my father with all my gratitude.

# CURRICULUM VITAE

The author was born on April 16, 1972 in Leningrad, Russia. In 1989 he entered Leningrad Shipbuilding Institute (now named St. Petersburg State Marine Technical University) as his father did 28 years earlier. The author chose to study mechanical engineering with specializing in marine structures. Six years later, in 1995 the author received a diploma of engineer. During the two last years of his study (1994-1995), he additionally worked part-time in Krylov Shipbuilding Research Institute widening his practical experiences. However, considering the economical situation in Russia at the moment of graduation from the university the author had virtually no choice of finding of a suitable job related to his primary education. At the same time the author valued the knowledge received during 6 years of his study at the university. So the decision was taken to go on with scientific research. In 1995 he passed the entry examinations and became a PhD student at the same university choosing hydroelasticity for slamming problems as the subject of his research. But lack of possibilities and desire to learn more, discovering the world, made him take a chance to go abroad. In 1997 he agreed to take a research fellowship at Industrial Design Engineering Faculty of TU Delft. In spite of the fact that the project on investigation of mechanical properties of molded pulp packaging was quite far from the marine technology the author found the work interesting and full of new experiences. Combination of experimental research and numerical studies gave the author new practical knowledge. However, his inspiration by marine technology and desire to continue his former subject on hydroelasticity forced him to search for other possibilities. At the end of his research fellowship he found a PhD position at the Ship Structures Laboratory in TU Delft, the place where this thesis has been written...

# REFERENCES


1. Aksu S., Price W.G., and Temarel P., 1991, "A three-dimensional theory of ship slamming in irregular oblique seaways", Advances in Marine Structures -2. Elsevier Applied Science, pp. 208-229.

2. Aksu S., Price W.G., Suhrbier K.R. and Temarel P., 1993, "A comparative study of the dynamic behaviour of a fast patrol boat travelling in rough seas", Marine Structures, Vol. 6, pp. 421-441.

3. Alberts G.J.N., 2001, "Fluid-structure interaction as a result of Green water", Report on graduation project, Twente Institute of Mechanics.

4. Ann S.P., Lee H.S. and Lee S.K., 1995, "A computation of hydrodynamic forces by using-dimensional higher order panel method", The 6th International Symposium on Practical Design of Ships and Mobile Units", Vol. 1, pp. 382-393.

5. Arai M., and Miyauchi T., 1998, "Numerical study of the impact of water on cylindrical shells, considering fluid-structure interactions", The 7th International symposium on Practical Design of Ships and Mobile Units, (PRADS'98), The Netherlands.

6. Arai M., and Tasaki R., 1987, "A numerical study of water entrance of two-dimensional wedges – effect of gravity, spray generation and vertical load", The International Symposium on Practical Design of Ships and Mobile Units, Vol. 1, pp. 377-385.

7. Arai M., Cheng L.Y., and Inoue Y., 1994, "A computing method for the analysis of water impact of arbitrary shaped bodies", Journal of the Society of Naval Architects of Japan, Vol. 176, pp. 233-240.

8. Arai M., Cheng L.Y., and Inoue Y., 1995, "A computing method for the analysis of water impact of arbitrary shaped bodies (2nd Report)", Journal of the Society of Naval Architects of Japan, Vol. 177, pp. 91-99.

9. Arai M., Cheng L.Y., and Inoue Y., 1995, "Hydrodynamic impact loads on horizontal members of offshore structures", Proceedings of International Conference on Offshore Mechanics and Arctic Engineering, Vol. 1-A, pp. 199-206.

10. Arai M., Cheng L.Y., Inoue Y., and Miyauchi T., 1995, "Numerical study of water impact loads on catamaran with asymmetric hulls", Proceedings of International Conference on Fast Sea Transportation, Vol. 1, pp. 221-232.

11. Arai M., Cheng L.Y., Inoue Y., Miyauchi T., and Ishikawa M., 1995, "Numerical study of water impact loads on catamarans with asymmetric hulls", The International Symposium on Practical Design of Ships and Mobile Units, Vol. 1, pp. 672-683.

12. Armand J.L., and Cointe R., 1986, "Hydrodynamic impact analysis of a cylinder", International Conference on Offshore Mechanics and Arctic Engineering, pp. 250-256.

13. Bereznitski A. and Postnov V., 2001, "Hydroelastic model for bottom slamming", The 8th International symposium on Practical Design of Ships and Other Floating Structures, (PRADS-2001), September 16-21, Shanghai, China, Vol. 2, pp. 911-917.

14. Bereznitski A., 2000, "Fluid-Structure Interaction: Combination of MARC and a Self-Developed Code", Proceedings of the First Northern European Technology Conference, June 7-8, Manchester, UK.

15. Bereznitski A., 2001, "3D model for bottom slamming", 20th International Conference on Offshore Mechanics and Arctic Engineering (OMAE-2001), June 3-8, Rio de Janeiro, Brazil.

16. Bereznitski A., 2001, "Slamming: the role of Hydroelasticity", International Shipbuilding Progress, Vol. 48, no 4, pp. 333-351

17. Bereznitski A., Boon B., and Postnov V., 2001, "Hydroelastic formulation in order to achieve more accurate prediction of hydrodynamic loads", Proceedings of 11th International Offshore and Polar Engineering Conference, (ISOPE-2001), June 17-22, Stavanger, Norway, Vol. 4, pp. 337-342.

18. Bereznitski A., Boon B., Postnov V., 2000, "Influence of the ship structure flexibility on the hydrodynamic impact loads due to bottom slamming", Proceedings of the 7th International Marine Design Conference (IMDC-2000), May 21-24, Kyongju, Korea, pp. 697-705.

19. Bereznitski A., Boon B., Postnov V., 2000, "Numerical study of the hydroelastic effect on the impact loads due to bottom slamming on ship structure", Proceedings of ETCE/OMAE-2000 Joint Conference "Energy for the New Millennium", February 14-17, New Orleans, LA, USA.

20. Bereznitski A., Boon B., Postnov V., 2000, "The effect of hydroelasticity on the impact pressure due to bottom slamming on ship structure", Proceedings of 10th International Offshore and Polar Engineering Conference (ISOPE-2000), May 28-June 2, Seattle, WA, USA, Vol. 4, pp. 277-283.

21. Bereznitski A., Kaminski M., 2002, "Practical Implications of Hydroelasticity in Ship Design", Proceedings of 12th International Offshore and Polar Engineering Conference, (ISOPE-2001), May 26-31, Kitakyushu, Japan, Vol. 4, pp. 486-491.

22. Bereznitski A.V. and Postnov V.A., 1997, "Shock interaction of an elastic body with a fluid domain", //MORINTEH-97, Trans. of the Second International Conference on Marine Intellectual Technologies, St-Petersburg, Vol. 4, pp. 69-74, (in Russian).

23. Bereznitski A.V. and Postnov V.A., 2001, "Bottom slamming: is the effect of hydroelasticity important?", //MORINTECH-2001, Trans. of the Fourth International Conference and Exhibition on Marine Intellectual Technologies, September 20-22, Saint-Petersburg, Russia.

24. Bergquist J., 2001, "An investigation into the hydrodynamics of slamming on the bow flare of ships", Report on graduation project, Delft University of Technology.

25. Beukelman W., 1980, "Bottom impact pressures due to forced oscillation", International Shipbuilding Progress, Marine Technology Monthly, Vol. 27, No. 305, pp. 107-126.

26. Bishop R.E.D., and Price W.G., 1979, "Hydroelasticity of ships".

27. Brebbia C.A., Telles J.C.F., and Wrobel L.C., 1984, "Boundary Element Techniques", Berlin: Springer-Verlag.

28. Boytsov G.V, Paliy O.M., Postnov V.A., and Chuvikovski V.S., 1982, "Reference book on shipbuilding mechanics", Vol. 2, Sudostroeniye, St-Petersburg, (in Russian).

29. Chuang S.L., 1966, "Experiments on flat-bottom slamming", Journal of Ship Research, Vol. 10, No. 1, pp. 10-17.

30. Chuang S.L., 1967, "Experiments on slamming of wedge-shaped bodies", Journal of Ship Research, Vol. 11, No. 3, pp. 190-198.

31. Cointe R., 1989, "Two-dimensional water-solid impact", Journal of Offshore and Arctic Engineering, Vol. 111, pp. 109-114.

32. Colwell J.L., Datta I., and Rogers R., 1995, "Head seas slamming tests on a fast surface ship hull form series", RINA'95, Conference on Seakeeping and Weather.

33. Connor J.J., and Brebbia C.A., 1975, "Finite Element Techniques for Fluid Flow", London: Newnes-Butterworths.

34. Dambra R., Hoogeland M., and Vredeveldt A., 2000, "Drop Test Analysis of Flat Panels Using a Finite Element Hydro-Code", International Conference on Ship and Shipping Research.

35. Dambra R., Iaccarino R., and Porcari R., 2000, "The Role of Finite Element Technique in Ship Structural Design", Proceedings of the First South European Technological Meeting International Conference, Italy.

36. Datta I., 1986, "Measurement and analysis of model experiment data on bottom slamming", The 21st American Towing Tank Conference, pp. 345-352.

37. Dobrovol'skaya Z., 1968, "On some problems of similarity flow of fluid with a free surface", Journal of Fluid Mechanics, Vol. 36, pp. 805-829.

38. Du S.X., and Wu Y.S., 1998, "The effect of forward speed on the hydroelastic behaviour of ship structures", The International Symposium on Practical Design of Ships and Mobile Units, pp. 597-603.

39. Ershov N.F. and Shahverdy G.G., 1984, "The Finite Element Method in Problems of Hydrodynamics and Hydroelasticity", Sudostroeniye, Leningrad (in Russian).

40. Falch S., 1986, "A numerical study of slamming of two-dimensional bodies", Thesis, Norwegian University of Science and Technology.

41. Falch S., 1989, "Slamming of flat-bottomed bodies calculated with exact free surface boundary conditions", The 5th International Conference on Numerical Ship Hydrodynamics, pp. 251-267.

42. Faltinsen O.M., 1996, "Water impact and hydroelasticity", International Seminar on Hydroelasticity for Ship Structural Design, Genova.

43. Faltinsen O.M., 1997, "The effect of hydroelasticity on ship slamming", Phil. Trans. R. Soc. Lond. A(1997) 355, pp. 575-591.

44. Faltinsen O.M., 1998, "Hydroelasticity of high-speed vessels", Hydroelasticity in Marine Technology, Proceedings of the Second International Conference, pp. 1-13.

45. Faltinsen O.M., 1999, "Interpretation of full-scale tests of wetdeck slamming", International Conference on High-Performance Marine Vehicles, pp. 62-71

46. Faltinsen O.M., 1999, "Water entry of a wedge by orthotropic plate theory", Journal of Ship Research, Vol. 43, pp. 180-193.

47. Faltinsen O.M., 2001, "Hydroelastic slamming", Journal of Marine Science and Technology, Vol. 5, No. 2, pp. 49-65.

48. Faltinsen O.M., Kvalsvold J., and Aarsnes J.V., 1997, "Wave impact on a horizontal elastic plate", Journal of Marine Science and Technology, Vol. 2, No. 2, pp. 87-100.

49. Faulkner D., 1999, "Showing up the cracks", Offshore Engineer, January.

50. Getting to grips with green water, 2000, Offshore Engineer, April.

51. Greenhow M., 1987, "Wedge entry into initially calm water", Applied Ocean Research, Vol. 9, No. 4, pp. 214-223.

52. Greenhow M., 1988, "Water-entry and -exit of a horizontal circular cylinder", Applied Ocean Research, Vol. 10, No. 4, pp. 191-198.

53. Grigoriev V.D., 1989, "Numerical Solution of Unsteady Hydroelasticity Problems". PhD Thesis, Leningrad (in Russian).

54. Hansen P.F., 1994, "On combination of slamming- and wave-induced responses", Journal of Ship Research, Vol. 38, No. 2, pp. 104-114.

55. Hansen P.F., Jensen J.J., and Pedersen P.T., 1994, "Wave-induced springing and whipping of high-speed vessels", Hydroelasticity in Marine Technology, pp. 191-204.

56. Haugen E.M., Faltinsen O., and Aarsnes J.V., 1997, "Application of theoretical and experimental studies of wave impact to wetdeck slamming", Proceedings of the International Conference on Fast Sea Transportation, pp. 423-430.

57. Hayman B., Haug T., and Valsgard S., 1991, "Response of fast craft hull structures to slamming loads", Proceedings of the International Conference on Fast Sea Transportation, pp. 381-398.

58. Hermans A.J., 1998, "A boundary element method to describe the excitation of waves in a very large floating flexible platform", Hydroelasticity in Marine Technology, pp. 69-76.

59. Hermans A.J., 2000, "A boundary element method for the interaction of free surface waves with a very large floating flexible platform", Journal of Fluids and Structures, Vol. 14, No. 7, pp. 943-956.

60. Hermundstad O.A., Wu M.K., and Moan T., 1994, "Hydroelastic response analysis of a high speed monohull", Hydroelasticity in Marine Technology, pp. 245-259.

61. Howison S.D., Ockendon J.R., and Wilson S.K., 1991, "Incompressible water-entry problems at small deadrise angles", Journal of Fluid Mechanics, Vol. 222, pp. 215-230.

62. Hydrodynamic Impact on Displacement Ship Hulls, 1995, Ship Structure Committee, (SSC-385), USA.

63. ISO-2631-1, Mechanical vibration and shock – Evaluation of human exposure to whole-body vibrations – Part 1 – General requirements, 1997.

64. ISSC Committee I.2, 1997, "Loads", Proceedings of the 13th International Ship and Offshore Structures Congress (ISSC'97), Vol. 1.

65. ISSC Committee II.2, 1991, "Dynamic Load Effects", Proceedings of the 11th International Ship and Offshore Structures Congress (ISSC'91), Vol. 1.

66. Iwanowski B., Fujikubo M., and Yao T., 1992, "Numerical simulation of air flow beneath a rigid body falling on a deformable surface", Journal of the Society of Naval Architects of Japan, Vol. 172, pp. 465-475.

67. Iwanowski B., Fujikubo M., and Yao T., 1993, "Analysis of horizontal water impact of a rigid body with the air cushion effect", Journal of the Society of Naval Architects of Japan, Vol. 173, pp. 293-302.

68. Jong G., 2001, "Bow flare impact simulation on a 9000 t dwt general cargo class", Report on graduation project, Delft University of Technology.

69. Kaplan P., 1995, "Computer simulation/prediction of ship motions and loads in a seaway", RINA'95 Conference on Seakeeping and Weather, pp. 1-12.

70. Kaplan P., 1996, "A theoretical method for determining slam impact pressure distributions on ship sections", Proceedings of International Conference on Offshore Mechanics and Arctic Engineering, Vol. 1-A, pp. 113-119.

71. Kaplan P., Murray J.J., and Yu W.C., 1995, "Theoretical analysis of wave impact forces on platform deck structures", Proceedings of International Conference on Offshore Mechanics and Arctic Engineering, Vol. 1-A, pp. 189-198.

72. Kapsenberg G., and Brizzolara S., 1999, "Hydro-elastic effects of bow flare slamming on a fast monohull", Proceedings of the International Conference on Fast Sea Transportation, FAST'99, Seattle.

73. Korobkin A., 1992, "Blunt-body impact on a compressible liquid surface", Journal of Fluid Mechanics, Vol. 244, pp. 437-453.

74. Korobkin A., 1994, "Blunt-body impact on the free surface of a compressible liquid", Journal of Fluid Mechanics, Vol. 263, pp. 319-342.

75. Korobkin A., 1995, "Wave impact on the bow end of a catamaran wet deck", Journal of Ship Research, Vol. 39, No. 4, pp. 321-327.

76. Korobkin A., 1998, "Elastic response of catamaran wetdeck to liquid impact", Ocean Engineering, Vol. 25, No. 8, pp. 687-714.

77. Korobkin A., 1998, "Unsteady hydroelasticity of floating plates", Hydroelasticity in Marine Technology, pp. 109-117.

78. Kvalsvold J., and Faltinsen O.M., 1993, "Hydroelastic modelling of slamming against the wetdeck of a catamaran", Proceedings of the Second International Conference on Fast Sea Transportation, pp. 681-697.

79. Kvalsvold J., and Faltinsen O.M., 1994, "Slamming loads on wetdecks of multihull vessels", Hydroelasticity in Marine Technology, Proceedings of the First International Conference, 1994, pp. 205-220.

80. Kvalsvold J., Faltinsen O.M., and Aarsnes J.V., 1995, "Effect of structural elasticity on slamming against wetdecks of multihull vessels", The 6th International Symposium on Practical Design of Ships and Mobile Units", Vol. 1, pp. 684-699.

81. Lacey P., and Chen H., 1995, "Improved passage planning using weather forecasting, maneuvering guidance, and instrumentation feedback", Marine Technology, Vol. 32, No. 1, pp. 1-19.

82. Lacey P., and Edwards R., 1993, "ARCO tanker slamming study", Marine Technology, Vol. 30, No. 3, pp. 135-147.

83. Lewison G., and Maclean W.M., 1968, "On the cushioning of water impact by entrapped air", Journal of Ship Research, Vol. 12, No. 2, pp. 116-130.

84. Lundgren J., Cheung M.C., and Hutchison B.L., 1998, "Wave-induced motions and loads for a tanker. Calculations and model tests", The 7th International symposium on Practical Design of Ships and Other Floating Structures, PRADS'1998, pp. 503-511.

85. Mansour A., and d'Oliveira J.M., 1975, "Hull bending moment due to ship bottom slamming in regular waves", Journal of Ship Research, Vol. 19, No. 2, pp. 80-92.

86. Maskew B., Tidd D.M., and Fraser J.S., 1993, "Prediction of nonlinear hydrodynamic characteristics of complex vessels using a numerical time-domain approach", The 6th International Conference on Numerical Ship Hydrodynamics, pp. 591-611.

87. Mei X., Liu Y., and Yue D.K.P., 1999, "On the water impact of general two-dimensional sections", Applied Ocean Research, Vol. 21. pp. 1-15.

88. Motora S., Fujino M., and Sakurai K., 1982, "On the mechanism of the occurrence of wave impact on high speed boats", RINA'82, The 2nd Symposium on Small Fast Warships and Security Vessels.

89. MSC.DYTRAN, User's manual, version 2002, MSC.Software Corporation.

90. MSC.MARC, User's manual, version 2000, MSC.Software Corporation.

91. Nikolaidis E., and Kaplan P., 1992, "Combination of slamming and wave induced motion: a simulation study", International Conference on Offshore Mechanics and Arctic Engineering, OMAE-1992, pp. 351-358.

92. Ochi M.K., and Motter L.E., 1969, "Prediction of extreme values of impact pressure associated with ship slamming", Journal of Ship Research, Vol. 13, No. 2, pp. 85-91.

93. Ochi M.K., and Motter L.E., 1973, "Prediction of slamming characteristics and hull responses for ship design", SNAME, Transactions.

94. Ogilvie T.F., 1963, "Compressibility Effects on Ship Slamming", Schiffstechnik, Bd.10, Heft 53.

95. Okada S., and Sumi Y., 1998, "On the impact phenomenon of an elastic plate on a water surface in small attack angles", Hydroelasticity in Marine Technology, pp. 139-144.

96. Postnov V.A., and Volkov E.A, 1998, "Variational formulation of the structure-fluid interaction", Proceedings of the International Shipbuilding Conference, St. Petersburg, Russia.

97. Postnov V.A., Bereznitski A.V., 1998, "Impact interaction between ship's structures and liquid domain (2D problem)", Journal Applied Problems of Strength and Plasticity, Hi. Sch. Col., 1998, n 59, pp. 85-90, (Nizhny Novgorod State University, Russia), (in Russian).

98. Postnov V.A., Harhurim I. I., 1974, "Finite Element Method in the Calculation of Ship Constructions", Leningrad: Sudostroeniye (in Russian).

99. Price W.G., and Temarel P., 1994, "Prediction of wave induced responses, loads and stresses using hydroelasticity theory", Proceedings of the International Conference on Ship and Marine Research, Vol. 1.

100. Price W.G., Temarel P., and Keane A.J., 1994, "Hydroelastic analysis of a SWATH in waves", Hydroelasticity in Marine Technology.

101. Radev D., and Beukelman W., 1992, "Slamming on forced oscillating wedges at forward speed: Part I – test results", International Shipbuilding Progress, Marine Technology Quarterly, Vol. 39, No. 417, pp. 399-422.

102. Ramos J., and Soares C.G., 1998, "Vibratory response of ship hulls to wave impact loads", International Shipbuilding Progress, Vol. 45, N 441, pp. 71-87.

103. Rassinot P., and Mansour A.E., 1995, "Ship hull bottom slamming", International Conference on Offshore Mechanics and Arctic Engineering, Vol. 1-A, pp. 253-262.

104. Samuelides M., and Katsaounis G., 1997, "Experimental modelling of wetdeck slamming", Proceedings of the International Conference on Fast Sea Transportation, pp. 413-422.

105. Shahverdy G.G., 1993, "Impact Interaction of Ship Structures with Fluid", Sudostroeniye, St-Petersburg, (in Russian).

106. Shibue T., Ito A., and Nakayama E., 1994, "Structural response analysis of cylinders under water impact", Hydroelasticity in Marine Technology, pp. 221-228.

107. Soares C.G., 1989, "Transient response of ship hulls to wave impact", International Shipbuilding Progress, Vol. 36, No. 406, pp. 137-156.

108. Takemoto H., Miyamoto T., Hashizume Y., Oka S., and Ohsawa N., 1993, "Slamming impact loads and hull-girder response of a large high-speed craft in waves", Proceedings of the International Conference on Fast Sea Transportation, pp. 723-731.

109. Tanizawa K., 1998, "A time-domain simulation method for hydroelastic impact problem", Hydroelasticity in Marine Technology, pp. 119-127

110. Troesch A.W., and Kang C.G., 1986, "Hydrodynamic impact loads on three-dimensional bodies", The 16th Symposium on Naval Hydrodynamics, pp. 537-558.

111. Trosch A.W., and Kang C.G., 1998, "Evaluation of impact loads associated with flare slamming", The 13th Ship Technology and Research Symposium, 3rd International Marine Systems Design Conference, pp. 117-132.

112. Verhagen J.H.G., 1967, "The impact of a flat plate on a water surface", Journal of Ship Research, Vol. 11, No. 4, pp. 211-223.

113. Von Karman T., 1929, "The impact of seaplane floats during landing", NACA TN.

114. Vorus W.S., 1996, "A flat cylinder theory for vessel impact and steady planning resistance", Journal of Ship Research, Vol. 40, No. 2, pp. 89-106.

115. Vredeveldt A., Hoogeland M., and Janssen G., 2001, "Hydrodynamic impact response, a flexible view", International Conference on Fast Sea Transportation.

116. Wagner H., 1932, "Uber Stoss-und Gleitvorgange an der Oberflachte von Flussigkeiten. Zeitschrift fur Angewaendte Mathematik und Mechanik", 12(4), pp. 193-215.

117. Watanabe I., 1987, "Effects of the three-dimensionality of ship hull on the water impact pressure", Journal of the Society of Naval Architects of Japan, Vol. 162, pp. 163-174.

118. Watanabe I., 1987, "On hydrodynamic impact pressure acting upon flat bottomed ships", Naval Architecture and Ocean Engineering, Japan, Vol. 25, pp. 81-92.

119. Weems K., Zhang S., Lin W.M., Bennett J., and Shin Y.S., 1998, "Structural dynamic loading due to impact and whipping", The 7th International symposium on Practical Design of Ships and Other Floating Structures, PRADS'1998, pp. 79-85.

120. Wenyang D., and Yishan D., 1999, "Time-domain calculation of hydrodynamic forces on ships with large flare (part 1: two-dimensional case)", International Shipbuilding Progress, Marine Technology Quarterly, Vol. 46, No. 446, pp. 209-221.

121. Wenyang D., and Yishan D., 1999, "Time-domain calculation of hydrodynamic forces on ships with large flare (part 2: three-dimensional case)", International Shipbuilding Progress, Marine Technology Quarterly, Vol. 46, No. 446, pp. 223-233.

122. Witmer D.J., and Lewis J.W., 1995, "The BP oil tanker structural monitoring system", Marine Technology, Vol. 32, No. 4, pp. 277-296.

123. Wu M.K., Hermundstad O.A., and Moan T., 1993, "Hydroelastic analysis of ship hulls at high forward speed", International Conference on Fast Sea Transportation, pp. 699-710.

124. Xia J., and Wang Z., 1997, "Time-domain hydroelasticity theory of ships responding to waves", Journal of Ship Research, Vol. 41, No. 4, pp. 286-300.

125. Xia J., Wang Z., and Jensen J.J., 1998, "Non-linear wave loads and ship responses by a time-domain strip theory", Marine Structures, Vol. 11, pp. 101-123.

126. Xu L., Troesch A.W., and Peterson R., 1999, "Asymmetric hydrodynamic impact and dynamic response of vessels", Journal of Offshore Mechanics and Arctic Engineering, Vol. 121, pp. 83-88.

127. Xu L., Troesch A.W., and Vorus W.S., 1998, "Asymmetric vessel impact and planning hydrodynamics", Journal of Ship Research, Vol. 42, No. 3, pp. 187-198.

128. Yamamoto Y., Fujino M., Ohtsubo H., Fukasawa T., Iwai Y., Watanabe I., Ikeda H., Kumano A., and Kuroiwa T., 1984, "Disastrous damage of a bulk carrier due to Slamming", Naval Architecture and Ocean Engineering, Vol. 22, pp. 159-169.

129. Zhao R., and Faltinsen O., 1993, "Water entry of two-dimensional bodies", Journal of Fluid Mechanics, Vol. 246, pp. 593-612.